

JOINT INSTITUTE FOR AERONAUTICS AND ACOUSTICS

National Aeronautics and
Space Administration

Ames Research Center



Stanford University

JIAA TR 119

**DEVELOPMENT OF AN APPARATUS
FOR WIND TUNNEL DYNAMIC
EXPERIMENTS AT HIGH- α**

Nelson Pedreiro

*Department of Aeronautics and Astronautics
Stanford University
Stanford, CA 94305*

February 1997

Abstract

A unique experimental apparatus that allows a wind tunnel model two degrees of freedom has been designed and built. The apparatus was developed to investigate the use of new methods to augment aircraft control in the high angle of attack regime. The model support system provides a platform in which the roll-yaw coupling at high angles of attack can be studied in a controlled environment. Active cancellation of external effects is used to provide a system in which the dynamics are dominated by the aerodynamic loads acting on the wind tunnel model.

Acknowledgments

This work was supported by the Joint Institute for Aeronautics and Acoustics, between Stanford University and the NASA Ames Research Center. NASA Grant NCC 2-55.

Contents

Abstract	ii
Acknowledgments	iii
List of Figures	v
List of Tables	vii
List of Symbols	viii
1 Introduction	1
2 Wind Tunnel	3
3 Wind Tunnel Model	4
4 Air Injection System	5
5 Model Support System	7
5.1 Conceptual Design and Overall Configuration	7
5.2 Implementation of the Two Degrees of Freedom	11
5.3 Equations of Motion	14
5.4 Active Cancellation System	16
5.5 Sensor and Actuator Characteristics	19
5.5.1 Potentiometers	19
5.5.2 Accelerometers	22
5.5.3 Torque Sensor	24
5.5.4 Six-component Force-Torque Sensor	27
5.5.5 Torque Motor	29
6 Operation During Dynamic Experiments	32
7 Conclusions and Suggested Improvements	34
Appendix A - Geometry and Mass Properties of the Wind Tunnel Model	36
Appendix B - Servo Valve and Flowmeter	44
Appendix C - Model Support System Mechanical Design Drawings	52
Appendix D - Listing of Computer Program	104
References	109

List of Figures

Figure 1: Top view of the wind tunnel	3
Figure 2: Wind tunnel model used as baseline in the design of the apparatus	4
Figure 3: Closed loop control of the jet momentum coefficient, C_{μ}	6
Figure 4: The two degrees of freedom. Approximation to roll-yaw	8
Figure 5: Side view of test section and two degrees of freedom model support system	9
Figure 6: View of wind tunnel facilities and experimental apparatus	10
Figure 7: Implementation of rotation about the ϕ -axis	11
Figure 8: Implementation of rotation about the γ -axis	12
Figure 9: Concept and operation of the active cancellation loop	16
Figure 10: Measurement of angular acceleration $\ddot{\gamma}$ using two linear accelerometers	18
Figure 11: Dimensions of the potentiometer used for measurements of ϕ and γ	20
Figure 12: Calibration results for the measurement of the angle ϕ	21
Figure 13: Calibration results for the measurement of the angle γ	21
Figure 14: Systron Donner model 4310A-1-P116 linear servo accelerometer	22
Figure 15: Torque sensor mechanical component	24
Figure 16: Strain gage configuration and Wheatstone bridge used in the torque sensor	25
Figure 17: Torque sensor calibration results	26
Figure 18: Configuration of the six-component force-torque sensor	28
Figure 19: Torque motor static calibration	30
Figure 20: Torque caused by the cogging in the motor versus the 'yaw' shaft angle	31
Figure A.1: Geometry of the wind tunnel model and detail of blowing slot	39
Figure A.2: Detailed geometry for model configuration N6	40
Figure A.3: Detailed geometry for model configuration T6	41
Figure A.4: Detailed geometry for model configuration N7	42
Figure A.5: Detailed geometry for model configuration T7	43
Figure B.1: Servo valve design and configuration. From Wong [9]	47
Figure B.2: Alternative design for the servo valve rotor	48
Figure B.3: Flowmeter design and configuration	49

Figure B.4: Velocity profiles at the exit of the flowmeter calibration tube	50
Figure B.5: Flowmeter calibration results	51
Figure C.1: Roll system assembly drawing	54
Mechanical design drawings for the roll system components	55
Figure C.2: Yaw system assembly drawing	63
Mechanical design drawings for the yaw system components	64
Figure C.3: Active cancellation system assembly drawing	83
Figure C.4: Alternate position for accelerometers	84
Mechanical design drawings for the active cancellation system components	85

List of Tables

Table 1: Main parameters of the model support system	14
Table 2: Sensors and actuator used in the dynamic model support system	19
Table 3: Characteristics of MKV-F78SC203 potentiometer	20
Table 4: Characteristics of the Systron Donner 4310A-1-P116 linear servo accelerometer	23
Table 5: Maximum torque sensor errors due to cross-coupling	26
Table 6: Characteristics of the torque sensor	27
Table 7: Characteristics of the six-component force-torque sensor	29
Table 8: Characteristics of the S-4075-R-H00AA / DM-30 brushless servo system	29
Table A.1: Nomenclature used for the different wind tunnel model configurations	36
Table A.2: Main characteristics of the various wind tunnel model configurations	37
Table A.3: Mass and inertia properties of the various wind tunnel configurations	38

List of Symbols

b	wing span
C_{μ}	jet momentum coefficient, $\dot{m}_j V_j / q_{\infty} S_{ref}$
I_A	inertia of the suspension system about the γ -axis
I_M	model inertia in body frame
I_{ϕ}^R	inertia of the roll sub-system about the ϕ -axis
I_{γ}^S	inertia of the yaw sub-system about the γ -axis
g or g	acceleration of gravity
\dot{m}_j	jet mass flow rate
M_{ϕ}	moment about the ϕ -axis
M_{γ}	moment about the γ -axis
P	point defined by the intersection of the ϕ -axis and the γ -axis
p, q, r	roll, pitch and yaw rates respectively
q_{∞}	dynamic pressure, $\rho U^2/2$
S_{ref}	reference area, wing planform area
U	freestream velocity
V_j	air jet speed at the exit of the forebody slot
	wind tunnel model (body fixed) reference frame, centered at P
α	angle of attack
α_0	nominal incidence angle, equal to α when $\phi = \gamma = 0$
β	side slip angle
ϕ	first degree of freedom, roll
γ	second degree of freedom
ρ	air density

1 Introduction

The study of aircraft dynamics in the high angle of attack regime requires a description of the aerodynamics that includes both steady and transient effects. This involves modeling phenomena that are not completely understood such as separation and vortex breakdown. The main difficulties associated with flight at these regimes relate to vehicle control since flow separation results in decreased efficiency of conventional control surfaces and flow asymmetries result in the onset of lateral loads which cause departure from controlled flight. To address this problem various methods of active flow control have been suggested as a means to provide the necessary control augmentation [1-6,10,12]. For the most part the research in this area has consisted of characterizing the effects of various methods of flow control in the static loads acting on the vehicle and using this data, as an incremental effect, in simulations to demonstrate control augmentation. The problem with this approach is that either the transient effects are not incorporated in the model or at best they are approximated. There is also the issue of treating flow control devices as incremental effectors, *e.g.* assuming that stability derivatives of the vehicle are not a function of the actuation. Static data is sufficient to demonstrate that a certain device provides control authority, *i.e.* generates aerodynamic loads, but the issue of augmenting aircraft control is one of controllability and requires that the transient effects be taken into account. Given the difficulties in modeling the aerodynamics at these flight regimes a convincing proof of controllability can only be achieved through an experimental demonstration.

The Department of Aeronautics and Astronautics at Stanford University has been involved in research in the field of Active Flow Control for several years. In particular the use of pneumatic means of flow control have been studied extensively [6-16]. Most of this effort has been conducted under the Joint Institute for Aeronautics and Acoustics (JIAA). In the subject of control augmentation at high angles of attack the work of Wong [9] is set apart because besides aerodynamic modeling and dynamic simulations it entailed an experimental demonstration in which the roll motion of a delta wing was controlled using pneumatic means of flow control as the only actuator. The success of his

experiments created an interest in conducting an experiment in which a wind tunnel model would have two degrees of freedom allowing a more complete investigation of the lateral-directional dynamics at high angles of attack.

In this report the development of an experimental apparatus that allows a wind tunnel model two degrees of freedom is presented. A model support system was designed and built in which dynamic experiments can be conducted to study the roll-yaw coupling at high angles of attack. Active cancellation of external effects is used to provide a system in which the dynamics is dominated by the aerodynamic loads acting on the wind tunnel model. The main objective achieved with the development of the apparatus is that the aerodynamic phenomena can be characterized, including transient effects, and new control augmentation techniques can be verified experimentally in a controlled and repeatable environment. In this way the validity of assumptions regarding the modeling of the aerodynamics and how it is affected by the use of flow control devices can be determined.

In addition to describing the design and operation of the experimental apparatus this report contains detailed data on sensor and actuator calibration and on the geometry and mass and inertia properties of the two degrees of freedom model support system. In this way all of the information necessary to operate, maintain and modify the experimental apparatus is contained in this document.

2 Wind Tunnel

The two degrees of freedom apparatus was designed for use in the low speed wind tunnel of the Aeronautics and Astronautics Department at Stanford University. The top view of the closed circuit wind tunnel is shown in Figure 1. The maximum freestream speed at the center line of the test section is 60 m/sec. The air speed is controlled by a variable speed motor to which a variable pitch fan is attached. Screens are located upstream of the test section and reduce the mean turbulence level at the test section to approximately 0.1% [9]. Three independent measurements are available of the freestream air speed obtained from the difference in the static pressure from two stations in the contraction and from two Pitot static tubes located in the upstream portion of the test section.

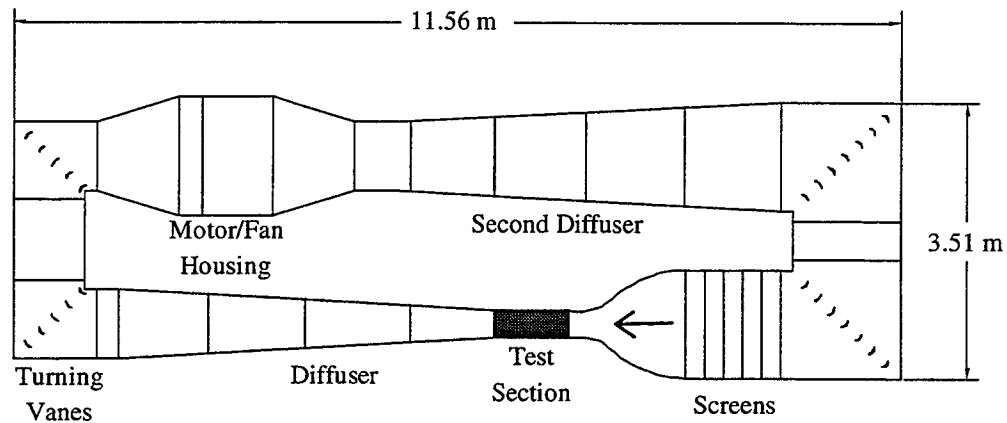


Figure 1: Top view of the wind tunnel.

Test section dimensions are: 0.45m X 0.45m X 0.91m, width, height and length respectively. It consists of a welded cast-iron frame. The bottom wall is made of sheet metal and top and side walls are made of plexiglass. The entire section is mounted on a cast-iron cart with castors and can be attached or removed from the rest of the wind tunnel. When in place, the test section is bolted to the exit of the tunnel contraction section.

3 Wind Tunnel Model

The development of the two degrees of freedom model support system occurred under the active flow control research initiative of the JIAA. As such a wind tunnel model consisting of a generic tailless fighter configuration and equipped with slots that allow the injection of air tangentially to the forebody was used as a baseline model in the development of the apparatus. This baseline model configuration, shown in Figure 2, has a sharp leading edge, 60 degree sweep angle delta wing, and a cone-cylinder fuselage¹. The model has no movable control surfaces and slots through which blowing is applied are located on both sides of the forebody. Air is provided to the forebody plena through flexible tubing that enters the model through the rear end of the fuselage.

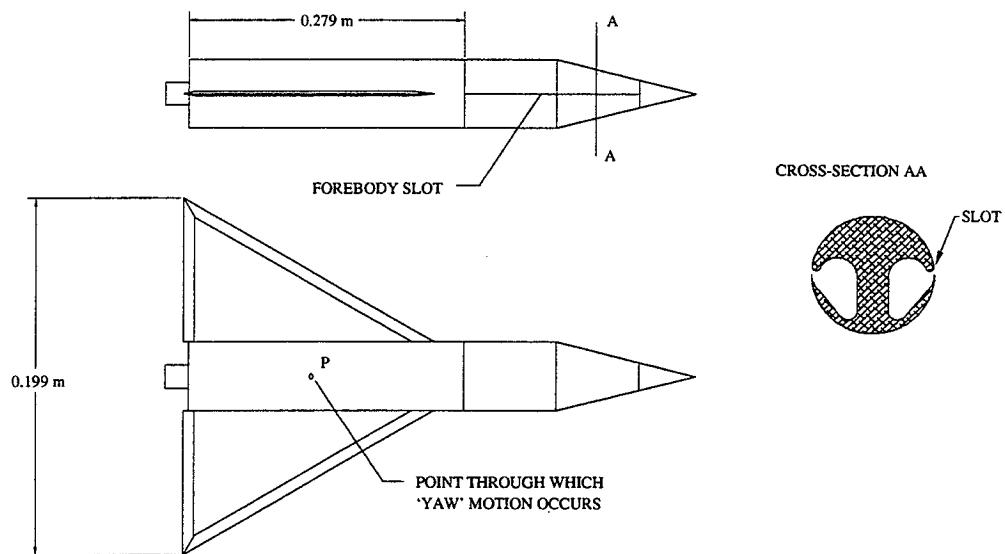


Figure 2: Wind tunnel model used as baseline in the design of the apparatus

Details on the dimensions of the model as well as the geometry of the slots are given in Appendix A. Mass, center of mass, and inertia properties of the model are also included as these quantities are required for the dynamic experiments. For completeness the characteristics of other available model configurations are also listed in the appendix.

¹ Designed by Dr. Zeki Celik (Research Associate, Aero/Astro Department, Stanford University); machined by Mr. Tom Hasler (Former Aero/Astro Machine Shop, Stanford University).

4 Air Injection System

The air injection system controls the amount of air that is injected through the forebody slots and consequently changes the flow and the aerodynamic loads acting on the model. An overall understanding of the air injection system is necessary because in the context of the research in Active Flow Control it operates in conjunction with the model suspension and is the only means of controlling the two degrees of freedom system since the model has no movable control surfaces.

The amount of air that is injected is quantified by the jet momentum coefficient, C_μ , defined as:

$$C_\mu \equiv \frac{\dot{m}_j V_j}{q_\infty S_{ref}} \quad (1)$$

where \dot{m}_j is the jet mass flow rate through the slot, V_j is the jet velocity at the exit of the plenum, q_∞ is the freestream dynamic pressure, and S_{ref} is the reference area (wing planform area).

Air is provided to the model through flexible tubing. Two servo-valves¹ are used to vary the amount of injected air on both plena independently. Specially designed flowmeters are used to measure the mass flow rate from which the jet momentum coefficient can be calculated. A closed loop control system is used to control the amount of air that is injected through each slot on the model. Figure 3 shows the block diagram for the closed loop control of C_μ . Feedforward is used to compensate for the non-linear characteristic of the valves and feedback control is used to generate adequate transient C_μ response and reject errors caused for example by pressure fluctuations on the source line. A detailed description of the servo valves and flowmeters is presented in Appendix B.

¹ Designed by Dr. Grant S. Wong [9]; machined by Mr. Tom Hasler (Former Aero/Astro Machine Shop).

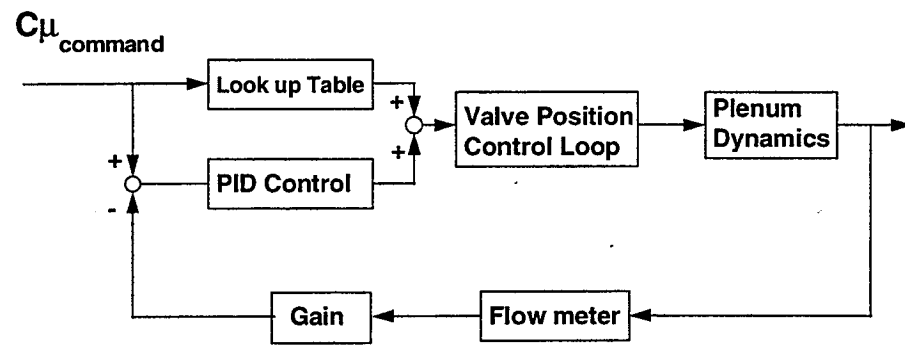


Figure 3: Closed loop control of the jet momentum coefficient, C_{μ} .

5 Model Support System

In this section the two degrees of freedom model support system is described. The objectives of designing and constructing such a suspension system are summarized and a discussion of the design approach is presented. The equations of motion for the two degrees of freedom system are included. Characteristics of the sensors and actuators used in the apparatus, as well as, parameters that characterize the support system are also presented. Detailed mechanical design drawings and assembly drawings are included in Appendix C.

5.1 Conceptual Design and Overall Configuration

The design of the apparatus was motivated by the need to conduct wind tunnel dynamic experiments to study aircraft control augmentation in the high angle of attack regime. Of particular interest was the use of pneumatic means of active flow control to improve the lateral-directional dynamics of the vehicle. To reach this goal an apparatus which allows the wind tunnel model two degrees of freedom was designed and built. The choice of degrees of freedom was determined by the particular interest in studying the roll-yaw coupling at high angles of attack and by implementation issues, such as: system complexity and cost, and compatibility with existing hardware.

The implemented degrees of freedom, ϕ and γ , are an approximation to roll and yaw. ϕ is a rotation about the longitudinal axis of the model and γ is a rotation about a perpendicular axis as illustrated in Figure 4. The approximation to roll-yaw is represented by relating $\dot{\phi}$ and $\dot{\gamma}$ to the roll, pitch and yaw rates, p , q , and r respectively:

$$\begin{aligned} p &= \dot{\phi} \\ q &= \dot{\gamma} \sin\phi \\ r &= \dot{\gamma} \cos\phi \end{aligned} \tag{2}$$

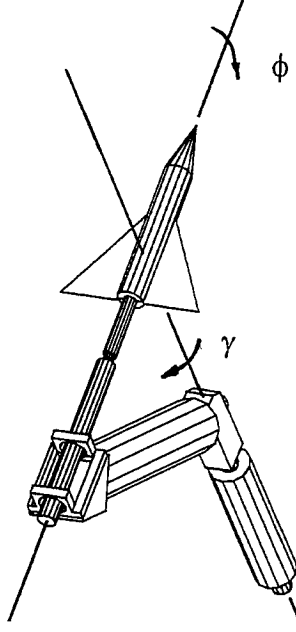


Figure 4: The two degrees of freedom. Approximation to roll-yaw.

The apparatus degrees of freedom, ϕ and γ , relate to the angle of attack, α , and the side slip angle, β , through the following expressions:

$$\begin{aligned}\cos\alpha \cos\beta &= \cos\alpha_0 \cos\gamma \\ \sin\beta &= \sin\alpha_0 \sin\phi - \cos\alpha_0 \sin\gamma \cos\phi \\ \sin\alpha \cos\beta &= \sin\alpha_0 \cos\phi + \cos\alpha_0 \sin\gamma \sin\phi\end{aligned}\tag{3}$$

where α_0 is used to represent the nominal incidence angle, *i.e.* the angle between the longitudinal axis of the model and the freestream velocity for $\phi=\gamma=0$.

Once the two degrees of freedom were defined the overall configuration of the apparatus was determined driven by the following guidelines:

- Apparatus interference with the flow in the test section should be minimal.
- The aerodynamic loads acting on the model should dominate the dynamics of the system.
- The apparatus stiffness should be selected so that aeroelastic effects can be neglected.

The resulting system is shown in Figure 5 mounted to the wind tunnel test section. The wind tunnel model is attached to a shaft (roll shaft) mounted on bearings which allows rotation about the longitudinal axis of the model. The roll shaft support is connect to a second shaft ('yaw' shaft), also mounted on bearings, through a mechanical arm which runs parallel to the bottom wall of the test section. Only part of the roll shaft enters the test section resulting in a clean aerodynamic configuration in which the test section blockage caused by the apparatus is approximately 1%. The diameter and wall thickness of the roll shaft and mechanical arm were determined to provide a stiff model supporting structure. Their dimensions based on the linear and angular deflections at the center of mass of the model caused by 1.2 times (design margin) the maximum expected aerodynamic loads acting on the model when the tunnel is run at its maximum speed.

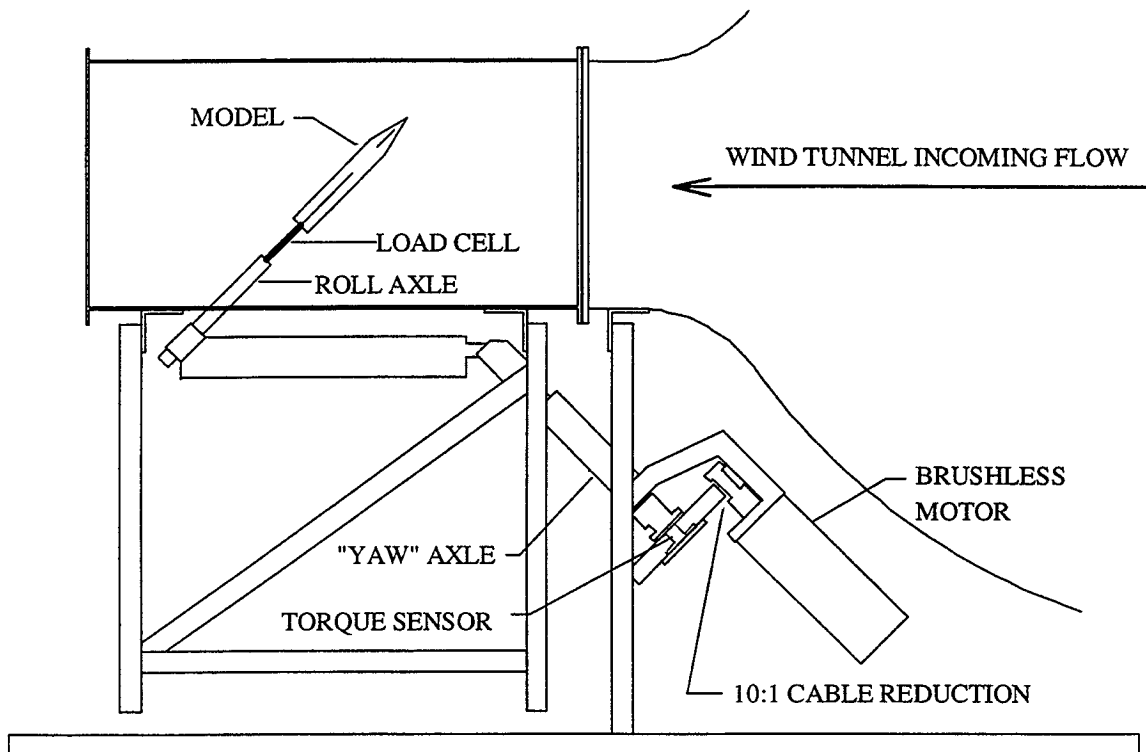


Figure 5: Side view of test section and two degrees of freedom model support system.

Experiments and simulations [15,16] indicated that the inertia and gravity restoring moment of the support system were large effects that dominated its dynamic behavior. To address this problem a system to provide active cancellation of these large external effects was designed and built. The active cancellation system has sensors that measure angular position and acceleration about the γ -axis from which a torque command is generated and sent to a motor connected to the 'yaw' shaft. The motor applies a torque to the 'yaw' shaft that cancels the torque due to gravity and inertia of the apparatus. A picture of the test section with a wind tunnel model mounted to the two degrees of freedom model support system is shown in Figure 6.

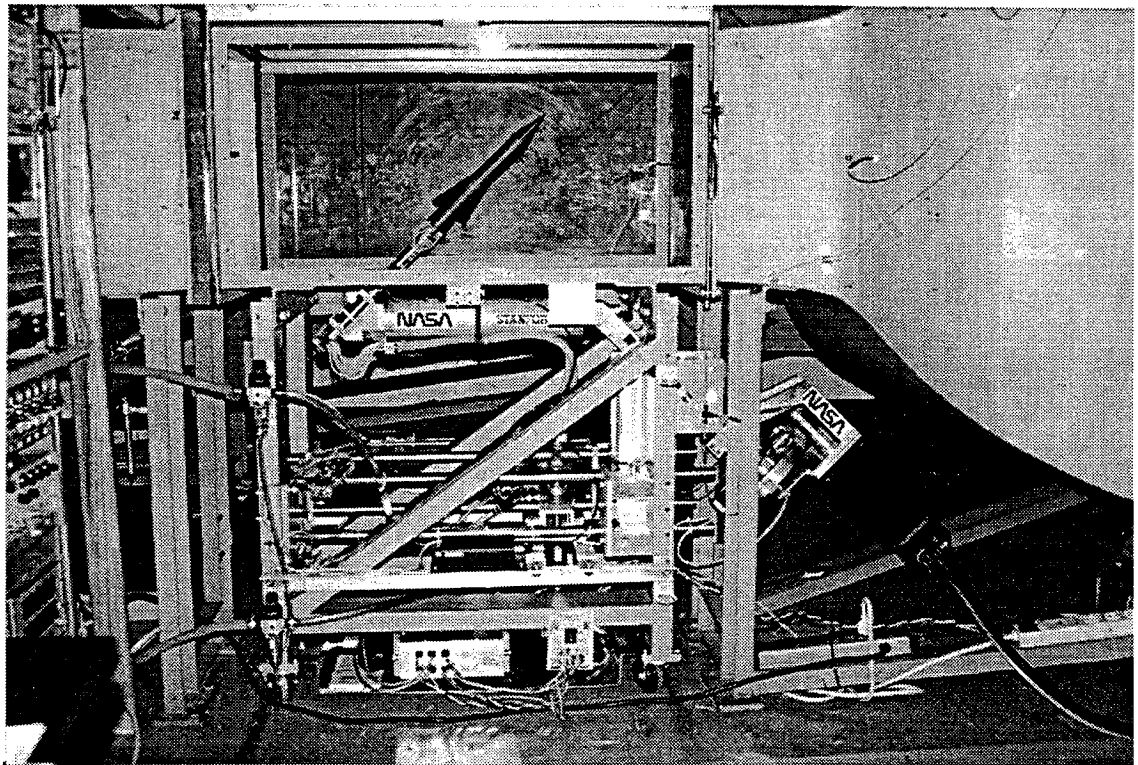


Figure 6: View of wind tunnel facilities and experimental apparatus.

Mechanical constraints limit the degrees of freedom to the following ranges: $|\phi| < 105$ degrees and $|\gamma| < 30$ degrees. It is possible to vary the nominal incidence angle, α_0 , in the range from 37 to 55 degrees. Provisions exist to lock each of the degrees of freedom independently at any position within the envelope of the apparatus. This feature is used during static experiments.

5.2 Implementation of the Two Degrees of Freedom

The main components of the roll system are shown in Figure 7. Also shown is the baseline wind tunnel model mounted to the system. All parts are made of aluminum 6061-T6 except for the roll shaft and the bearings which are made of steel. The model is mounted to the roll shaft through a six-component force-torque sensor¹ which provides static and dynamic measurements of the loads acting on the model. The roll shaft is mounted on precision bearings² to allow rotation about the longitudinal axis of the model. A low friction precision potentiometer³ is used to measure the roll angle. For the active flow control experiments it is necessary to provide pressurized air to the plena of the wind tunnel model. This is accomplished by routing the air supply tubing (eight 3/16 inch external diameter flexible tubes) through the interior of the roll shaft. The tubing enters the shaft at its end close to the potentiometer and emerges at the other end of the shaft where it is routed around the force-torque sensor and connected to special ports at the rear end of the model.

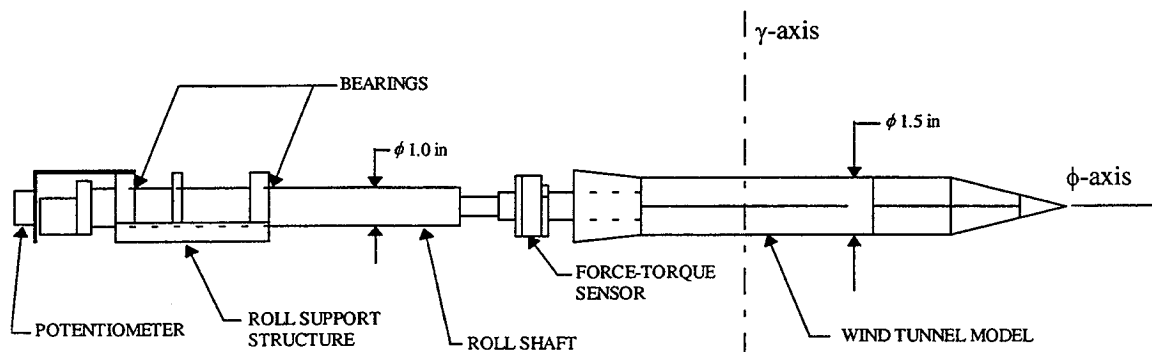


Figure 7: Implementation of rotation about the ϕ -axis.

¹ Mini 90N/4.2Nm. Serial #FT3253. Assurance Technologies, Inc. Garner, NC 27529.

² Kaydon KAA10CL4 ball bearing. Kaydon Corporation, Muskegon, Michigan 49443 USA.

³ Precision potentiometer MKV-F78S. Conductive plastic RESISTOFILM[®]. New England Instrument Company. Woonsocket, RI 02895-1129.

The inertia of the moving parts about the ϕ -axis excluding the model is labeled I_ϕ^R and is listed in Table 1. It includes contributions from the roll shaft, bearings, collars, fixtures, potentiometer and air supply tubing. Disturbance torques about the ϕ -axis are caused by the friction on the bearings and potentiometer and springiness of the air supply tubing. Stiction does not occur because the unsteady aerodynamics at high angles of attack has a dither like effect on the system. Experiments showed that the moment due to friction could be represented by:

$$M_\phi^F = -C_F \dot{\phi} \quad (4)$$

where C_F is a constant determined experimentally and is listed in Table 1. The moment due to the springiness of the air supply tubing, M_ϕ^T , depends on the configuration used for the tubing. For the configuration shown in Figure 6 this moment is less than 0.002 Nm for $|\gamma| < 35$ degrees [16].

Figure 8 illustrates the implementation of the second degree of freedom, γ . For completeness the roll system and the active cancellation system are also shown in the figure. Rotation about the γ -axis is made possible by a mechanical assembly consisting of two co-axial shafts connected through bearings¹. The inner shaft can rotate while the outer shaft is fixed to the test section. The roll-yaw connecting structure is mounted to the inner shaft and can rotate about the γ -axis. In the figure the location of the bearings and of the torque sensor used to connect the yaw shaft to the active cancellation system are indicated by shaded areas.

¹ BERG Ball Bearings - #B1-21 - UNSHIELDED

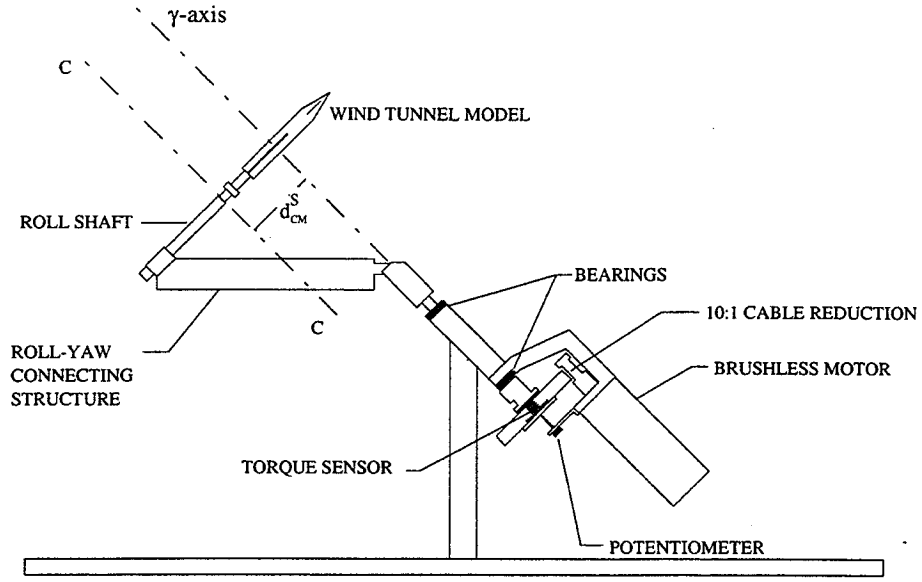


Figure 8: Implementation of rotation about the γ -axis.

Given the geometry and mass distribution of the supporting structure a gravity restoring moment exists about the γ -axis which is given by:

$$M_{\gamma}^G|_S = -m_s g d_{CM}^S \sin(\gamma) \quad (5)$$

where the quantities in the equation refer to a system S formed by the moving parts of the support system about the γ -axis, *i.e.* m_s is the mass of the moving parts of the support system and does not include the model and d_{CM}^S is the distance from the center of mass of S to the γ -axis. In the equation g represents the acceleration of gravity. In Figure 8 the center of mass of S is at some point on line CC . Measured values for m_s and d_{CM}^S as well as for the inertia of the support system about the γ -axis, I_{γ}^S , are given in Table 1. A potentiometer, identical to the one used to measure the roll angle, is used to provide a measure of the second degree of freedom γ .

The moment about the γ -axis due to friction in the bearings and potentiometer, M_γ^F , is given by:

$$M_\gamma^F = -D_F \dot{\gamma} \quad (6)$$

where the constant D_F was determined experimentally and is listed in Table 1.

Characteristic	Value	Units
I_ϕ^R	$(8.4 \pm 0.5) \times 10^{-5}$	Kg m^2
m_s	3.91 ± 0.01	Kg
d_{CM}^S	$(119.6 \pm 0.8) \times 10^{-3}$	m
I_γ^S	$(155.8 \pm 1.0) \times 10^{-3}$	Kg m^2
C_F	$(1.1 \pm 0.3) \times 10^{-3}$	Nm sec
D_F	$(8.5 \pm 2.6) \times 10^{-3}$	Nm sec

Table 1: Main parameters of the model support system.

5.3 Equations of Motion

The equations of motion of the two degrees of freedom system are:

$$\begin{aligned}
 I_{M_x} \ddot{\phi} + (I_{M_z} - I_{M_y}) \sin \phi \cos \phi \dot{\gamma}^2 + I_{M_{xz}} \cos \phi \ddot{\gamma} &= M_\phi \\
 (I_A + I_{M_y} \sin^2 \phi + I_{M_z} \cos^2 \phi) \ddot{\gamma} + (I_{M_y} - I_{M_z}) 2 \sin \phi \cos \phi \dot{\phi} \dot{\gamma} \\
 + I_{M_{xz}} (\ddot{\phi} \cos \phi - \dot{\phi}^2 \sin \phi) &= M_\gamma
 \end{aligned} \quad (7)$$

where I_M is represents the inertia characteristics of the model with respect to a body-fixed frame $(XYZ)_M$ centered at point P, the intersection of the ϕ and γ axis, with X oriented along the longitudinal axis of the model, Z in the vertical plane of symmetry of the model oriented towards the pressure side and Y given by the cross-product: $Z \times X$. I_A is

the inertia of the support about the γ -axis including the inertia of the motor times N^2 , where $N:1$ is the reduction ratio between the 'yaw' shaft and the motor shaft. M_ϕ is the moment acting about the longitudinal axis of the model, ϕ -axis, and M_γ is the moment about the γ -axis.

As discussed in Section 5.1 an objective in designing the apparatus was that the dynamic properties of the support system should not dominate the dynamic response of the model. One of the effects of the apparatus is represented on left hand side of Equation 7 by a term proportional to the inertia of the support system. Because this inertia is much larger than the inertia of the model (50 times larger than the inertia of the baseline model in yaw) this term dominates the response about the γ -axis and degenerates the dynamics of the system. Other effects of the apparatus can be identified by a closer examination of the right hand side of Equations 7. Expressions for the moments about the ϕ and γ axis can be written as:

$$\begin{aligned} M_\phi &= M_\phi^A + M_\phi^T + M_\phi^F \\ M_\gamma &= M_\gamma^A + M_\gamma^T + M_\gamma^F + M_\gamma^G \end{aligned} \quad (8)$$

where superscripts A, T, F and G indicate the origin of the moments: Aerodynamic, Tubing, Friction and Gravity respectively. It is seen that the springiness of the air supply tubing and the friction from the bearings and potentiometer affect both the motion about the ϕ and γ axis, and a gravity restoring moment affects the motion about the γ -axis only. Experiments demonstrated that the effects of the tubing and friction are small when compared to the aerodynamic loads [11,16], *i.e.* these effects do not dominate the dynamic response of the system. Moreover these effects are known, *e.g.* Equations 4 and 6, and can be accounted for if necessary. For these reasons neither the friction nor the spring effects are canceled about the ϕ -axis and the friction moment is not canceled about the γ -axis. On the other hand, cancellation of the gravity restoring moment and inertia of the apparatus was necessary as these are large effects that dominate the response of the

system about the γ -axis. The concept for the active system designed and built to cancel these effects was presented in Section 5.1 and a detailed description of this system given in the next section.

5.4 Active Cancellation System

The active cancellation system uses measurements of the angle γ and the angular acceleration $\ddot{\gamma}$ to compute the torque that should be applied to the γ -shaft to cancel the moments due to inertia, gravity and tube springiness about the γ -axis. This computed torque is sent to a torque closed loop control system which consists of an electric brushless motor¹ connected to the 'yaw' shaft through a 10:1 cable reduction² and a specially designed torque sensor that provides a precise measure of the torque applied to the system. The logic for the torque control loop consists of a notch filter³ and is implemented in a micro computer equipped with A/D and D/A converters. The computer program is written in C and its listing is given in Appendix D. Figure 9 illustrates the operation of the active cancellation system in block diagram form.

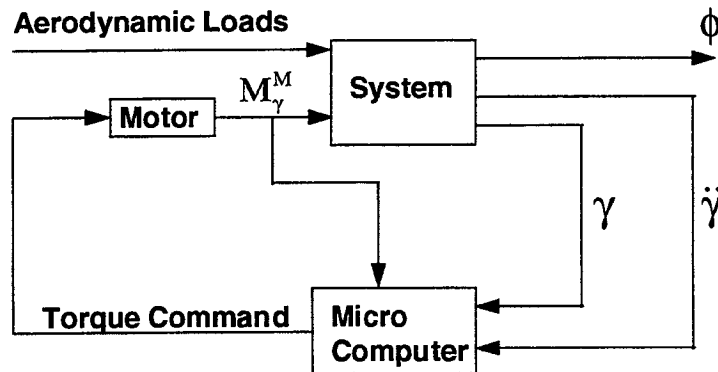


Figure 9: Concept and operation of the active cancellation loop.

¹ Electro-Craft Brushless Servo System: DM-30 drive, S-4075-R-H00AA motor. Reliance Motion Control, Inc. Eden Prairie, MN 55344.

² A simulation of the natural motion of the model free from any effect of the apparatus and for the tunnel running at maximum speed was used to calculate the torque required from the motor. This result indicated that a reduction was necessary to provide enough torque to cancel the inertia of the apparatus. A cable reduction was selected because of its linear characteristics and smoothness.

³ The notch filter was required to stabilize the lowest resonance mode of the structure at 33 Hz.

The torque commanded to the motor is given by:

$$M_{\gamma}^{M_c} \equiv I_A \hat{\ddot{\gamma}} + K_T^{\gamma} \hat{\dot{\gamma}} + K_G \sin \hat{\gamma} \quad (9)$$

where $\hat{\gamma}$ and $\hat{\ddot{\gamma}}$ are estimates of the angle γ and the angular acceleration $\ddot{\gamma}$. Using M_{error} to represent the errors in the torque control loop the actual torque applied to the shaft can be written as:

$$M_{\gamma}^M \equiv M_{\gamma}^{M_c} + M_{\text{error}} \quad (10)$$

Substituting the various expressions for the moments into Equation 7, and adding to the moment about the γ -axis the torque due to the motor results:

$$\begin{aligned} I_{M_x} \ddot{\phi} + (I_{M_z} - I_{M_y}) \sin \phi \cos \phi \dot{\gamma}^2 + I_{M_{xz}} \cos \phi \ddot{\gamma} &= M_{\phi}^A - C_F \dot{\phi} - K_T^{\phi} \phi \\ I_A (\ddot{\gamma} - \hat{\ddot{\gamma}}) + (I_{M_y} \sin^2 \phi + I_{M_z} \cos^2 \phi) \ddot{\gamma} + (I_{M_y} - I_{M_z}) 2 \sin \phi \cos \phi \dot{\phi} \dot{\gamma} \\ + I_{M_{xz}} (\ddot{\phi} \cos \phi - \dot{\phi}^2 \sin \phi) &= M_{\gamma}^A - D_F \dot{\gamma} - K_T^{\gamma} (\dot{\gamma} - \hat{\dot{\gamma}}) - K_G (\sin \gamma - \sin \hat{\gamma}) + M_{\text{error}} \end{aligned} \quad (11)$$

The angle γ is measured directly through the use of a potentiometer. This measured value, γ_m , is used as the estimate for γ , *i.e.* $\hat{\gamma} \equiv \gamma_m$. Two high precision linear accelerometers¹ are mounted to the γ -axle. When $\gamma=0$ they are located in the vertical plane that contains the γ -axis and are mounted at equal distances in opposite sides of the γ -axle as shown in Figure 10. Adding the signals from the two accelerometers cancels the effect of specific weight and provides a signal that is proportional to $\ddot{\gamma}$. This measurement of the angular acceleration, $\ddot{\gamma}_m$, is accurate to 0.01 rad/sec² and is used as the estimate value for that quantity, *i.e.* $\hat{\ddot{\gamma}} \equiv \ddot{\gamma}_m$. In this way the torque required to cancel

¹ Systron Donner 4310A-1-P116 Linear Servo Accelerometer. Systron Donner Company. Inertial Division. Concord, CA 94518.

the external effects is computed according to Equation 9, using the measurements for γ and $\ddot{\gamma}$ as their estimates.

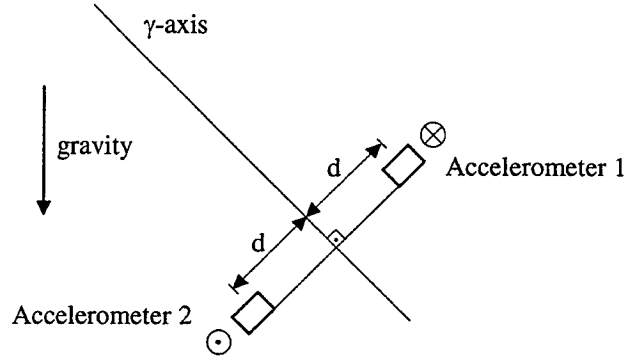


Figure 10: Measurement of angular acceleration $\ddot{\gamma}$ using two linear accelerometers.

The cancellation is not perfect due to limitations of the actual implementation. Errors occur in the torque closed loop control and in the measurements of γ and $\ddot{\gamma}$. To access the performance of the cancellation loop the error between the commanded torque, as given by Equation 9, and the actual torque measured during the natural motion of the system was compared to the unsteady aerodynamic moment about the γ -axis, M_γ^A [16]. The torque due to errors in the cancellation loop resulted as large as 14% of the aerodynamic moment, mostly due to a lightly damped resonant mode at approximately 33 Hz. This indicates that although the aerodynamics is the main factor determining the motion of the system the errors in the cancellation loop need to be included if an accurate description of the system dynamics is sought. The main reason for the large errors in the cancellation loop is the large inertia of the support system¹ which requires the application of a large torque to the γ -axis. This means that even a small percentage error in the applied torque translates into a significant moment as compared to the aerodynamic loads. For these reasons when using the equations of motion for the two degrees of freedom system either the moment applied by the motor should be explicitly included or the cancellation error should be treated as a disturbance.

¹ The inertia of the support about the γ -axis is approximately 50 times the inertia of the model in yaw.

5.5 Sensor and Actuator Characteristics

As discussed in the previous sections the dynamic model support system includes various sensors and an actuator which form an integral part of the apparatus and are required for it to function properly. These sensors and actuator are listed in Table 2 with a description of their functionality. A discussion of each of these devices is presented in the following sections including their physical characteristics and calibration.

Application	Sensor / Actuator
Measurement of the two degrees of freedom, ϕ and γ	ECONOPOT [®] Precision potentiometer MKV-F78SC103. Conductive plastic RESISTOFILM [®] . New England Instrument Company. Woonsocket, RI 02895-1129.
Measurement of the angular acceleration, $\ddot{\gamma}$	Systron Donner 4310A-1-P116 Linear Servo Accelerometer. Systron Donner Company. Inertial Division. Concord, CA 94518.
Measurement of the torque applied to the γ -axle	Custom designed torque sensor.
Measurement of the loads acting on the model	Mini 90N/4.2Nm. Serial #FT3253. Assurance Technologies, Inc. Garner, NC 27529.
Torque cancellation	Electro-Craft [®] Brushless Servo System: DM-30 drive, S-4075-R-H00AA motor. Reliance Motion Control, Inc. Enden Prairie, MN 55344.

Table 2: Sensors and actuator used in the dynamic model support system.

5.5.1 Potentiometers

Precision potentiometers are used to measure the two degrees of freedom ϕ and γ by measuring the roll and ‘yaw’ shaft angles. The selected sensor is a 10 K Ω low friction potentiometer, model MKV-F78SC103, manufactured by New England Instrument Company [17]. Its main characteristics are summarized in Table 3. A drawing of the sensor with its dimensions is shown in Figure 11.

Parameter	Value
Total resistance	10 K Ω
Linearity	0.25 %
Theoretical electrical travel	340 deg.
Output smoothness	0.15 %
Life expectancy	20 x 10 ⁶ cycles
Resolution	essentially infinite
Power rating	1 Watt at 70°C
Insulation resistance	1000 Megohms min. at 500 VDC
Dielectric withstanding voltage	750 Volts RMS
Standard torque	0.5 oz.-in. max.
Operating temperature	-65°C to +125°C

Table 3: Characteristics of the MKV-F78SC103 potentiometer.

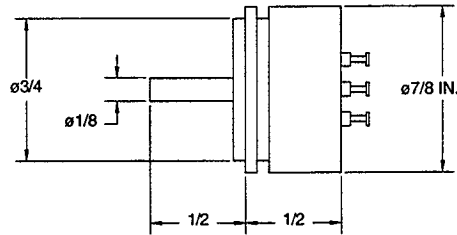


Figure 11: Dimensions of the potentiometer used for measurements of ϕ and γ .

Calibrations were performed for the measurements of the angles ϕ and γ obtained using the potentiometers connected to the proper excitation circuitry. The calibration procedure consisted of mounting the potentiometer to an aluminum plate and connecting a compass to its shaft. Data were recorded for the compass readings versus the potentiometer output in Volts for various angles and a least squares fit was used to determine the gain from output voltage to angle. Calibration results for the measurement of ϕ and γ are shown in Figures 12 and 13 respectively. The plots show both the experimental data and the result of the least squares fit.

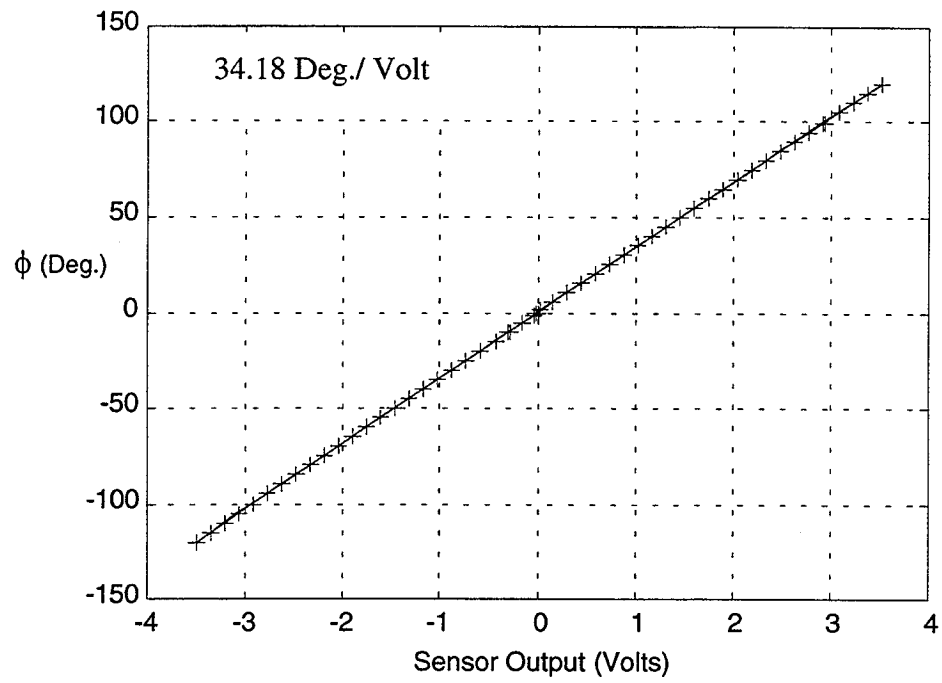


Figure 12: Calibration results for the measurement of the angle ϕ .

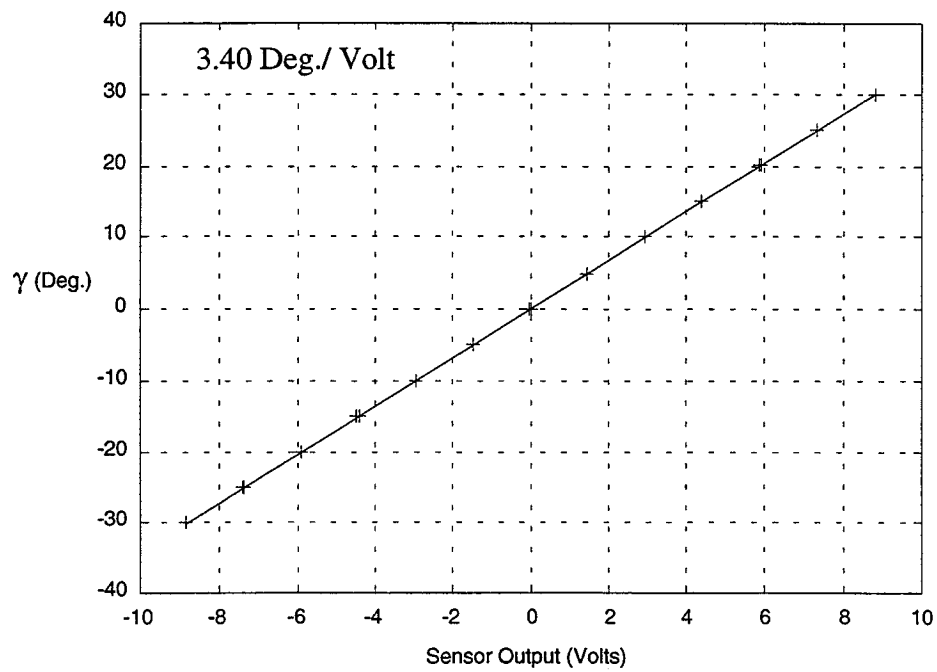


Figure 13: Calibration results for the measurement of the angle γ .

5.5.2 Accelerometers

The measurement of the angular acceleration about the γ -axis is obtained by adding the output of two linear accelerometers arranged as described in Section 5.4. Two identical high accuracy linear servo accelerometers, model 4310A-1-P116, manufactured by Systron Donner Inertial Division are used in the apparatus. The dimensions and configuration of the accelerometers are shown in Figure 14. Physical properties and accuracy parameters are summarized in Table 4.

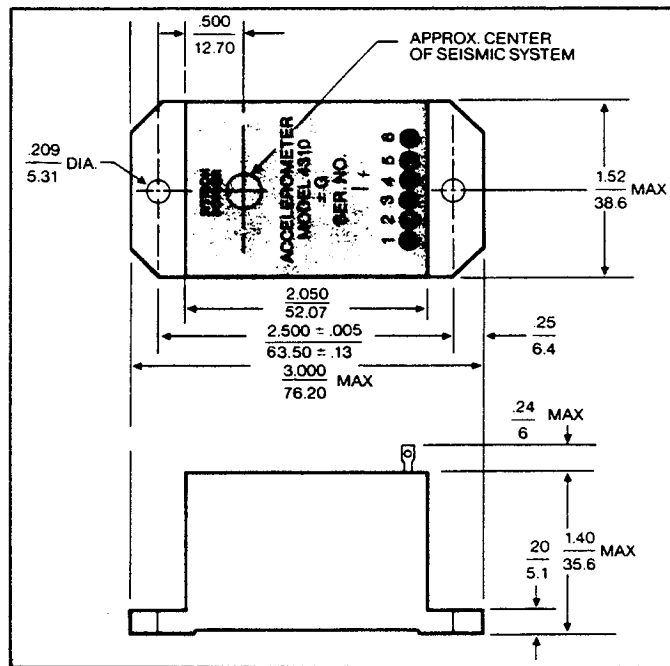


Figure 14: Systron Donner model 4310A-1-P116 linear servo accelerometer.

Parameter	Value
Range	$\pm 1.0 \text{ g}$
Input power	$\pm 15 \text{ VDC}$ at 10 mA max.
Voltage output	$\pm 7.5 \text{ VDC}$ full scale
Output Impedance	5 K Ω
Output current	3 mA full range
Electrical connections	6 solder terminals
Case alignment (each axis)	< 1 deg. to true sensitive axis
Weight	128 grams
Temperature range	-40°C to 93°C operating
Non-linearity	< 0.05% of full range
Hysteresis and non-repeatability	< 0.02% of full range
Resolution	< 0.001% of full range
Zero output (null)	< 0.05% of full range
Temp. coeff. of null	< 0.0018% per °C
Output noise	< 0.0075 VRMS
Cross-axis sensitivity	< 0.002 g / g
Scale factor	< 0.018% per °C
Natural frequency	50-250 Hz
Damping ratio at 22°C	0.7 \pm 0.1 (standard)

Table 4: Characteristics of the Systron Donner 4310A-1-P116 linear servo accelerometer.

The angular acceleration $\ddot{\gamma}$ is proportional to the sum of the output signals from the two linear accelerometers. The center of each accelerometer seismic system is located at 2.85 inches from the γ -axis and the calibration for the filtered output of each of the accelerometers resulted equal to 4.16 Volt/g. Using this results the gain between the sensor output (sum of the outputs from each accelerometer) and the angular acceleration $\ddot{\gamma}$ is 16.29 (rad/sec²)/Volt. To verify this result the motor of the active cancellation system was used to impart a harmonic motion to the ‘yaw’ system and data was recorded for the time histories of the outputs of the accelerometers and potentiometer. The signal of the potentiometer was processed (differentiated twice and smoothed) to generate a measure of the angular acceleration which was compared to the measurement of $\ddot{\gamma}$ from the accelerometers. This procedure was repeated for various frequencies of the harmonic

Semiconductor strain gages¹ are used to provide a large dynamic range on the torque measurement. Four gages are bonded, one at each surface of the square section at 45 degree angle, and connected to form a Wheatstone bridge, Figure 16. In the figure a, b, c and d represent the four strain gages and R their resistance, E_{IN} and E_{OUT} are the excitation and the output voltages respectively. An excitation voltage equal to 5 Volts is used and the output signal, E_{OUT} , is multiplied by a gain of 20 to provide a signal range of approximately ± 8 Volts in the operational region of the sensor.

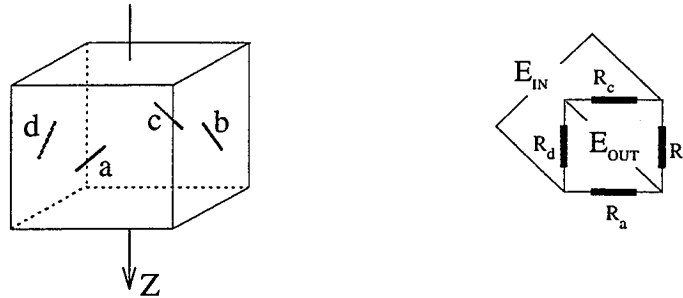


Figure 16: Strain gage configuration and Wheatstone bridge used in the torque sensor.

The sensor was designed to measure torque about the Z axis, T_z (shown in Figure 15), and to first order the sensor output is proportional to T_z . Data from calibration experiments and a least squares algorithm were used to determine the constant of proportionality. The results of the calibration and of the parameter fit are shown in Figure 17.

¹ Kulite semiconductor strain gages S/UDP-350-160 [18]. Kulite Semiconductor Products, Inc. Leonia, New Jersey 07605, USA.

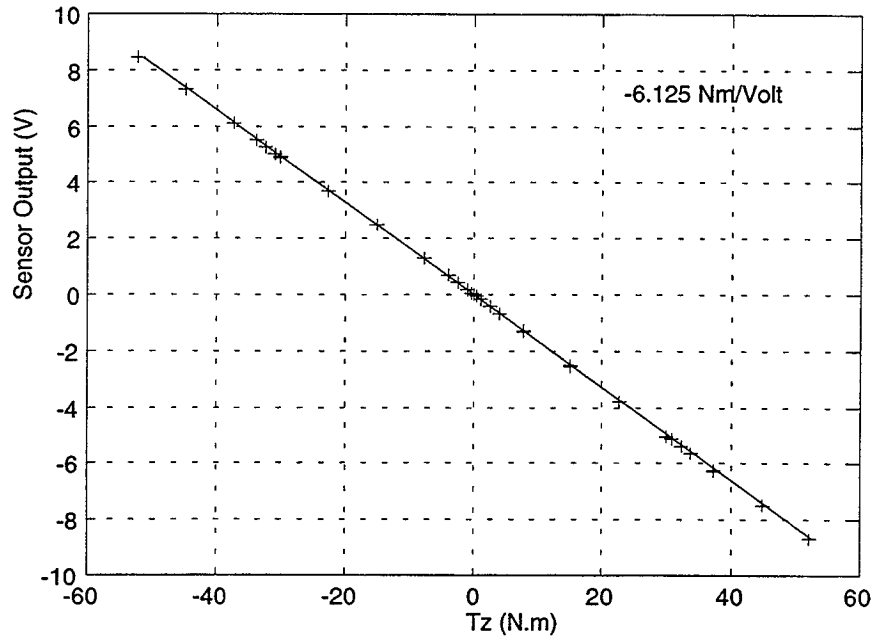


Figure 17: Torque sensor calibration results.

Because the sensor is subjected to forces and torques about the other two axis a calibration was conducted to determine the cross-coupling. The results of this calibration are summarized in Table 5, where the maximum errors in the sensor output caused by each of the other load components acting on the sensor are given. In the table subscripts X, Y and Z indicate the orientation (according to Figure 15) of the force and torque vectors \mathbf{F} and \mathbf{T} respectively. The total maximum error is approximately 1 % and is not compensated for.

Load Component Acting on Sensor	Sensor Output Error
\mathbf{F}_x	0.04 %
\mathbf{F}_y	0.82 %
\mathbf{F}_z	≈ 0
\mathbf{T}_x	0.01 %
\mathbf{T}_y	0.24 %

Table 5: Maximum torque sensor errors due to cross-coupling.

The main characteristics of the torque sensor are summarized in Table 6.

Parameter	Value
Operational range	± 50 Nm
Linearity	1.1 %
Maximum load	± 210 Nm
Resolution	essentially infinite
Stiffness about the Z axis	2.015×10^4 Nm/rad
Excitation voltage	5 VDC
Maximum input voltage	5.9 VDC
Power rating	0.1 Watt

Table 6: Characteristics of the torque sensor.

5.5.4 Six-Component Force-Torque Sensor

A six component force-torque torque sensor¹ connects the wind tunnel model to the roll shaft and is used to provide static and dynamic measurements of the loads acting on the model. The sensor used is a standard model manufactured by Assurance Technologies, Inc. and comes calibrated from the factory with electronics and cables. For this application a custom calibration was conducted to adapt this off-the-shelf item to the range of loads to be measured in the wind tunnel. The configuration and dimensions of the sensor are shown in Figure 18.

¹ Mini 90N/4.2Nm. Serial #FT3253. Assurance Technologies, Inc. Garner, NC 27529. USA.

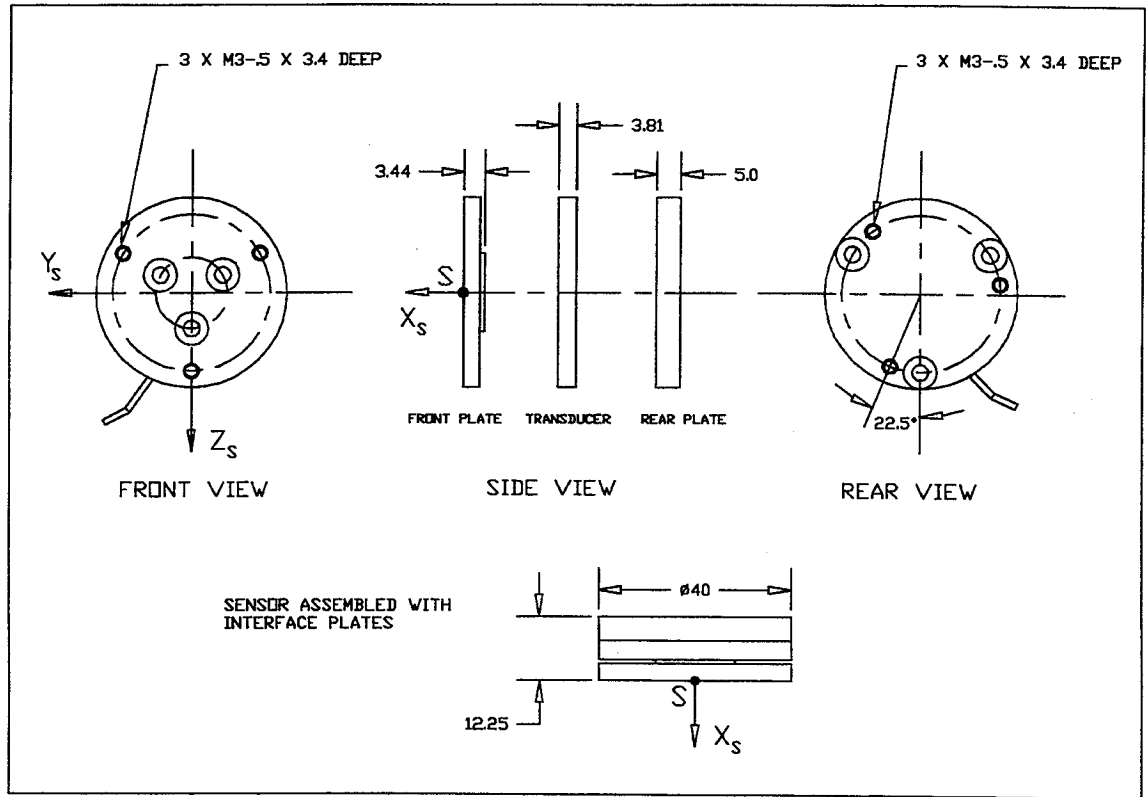


Figure 18: Configuration of the six-component force-torque sensor.

The sensor was evaluated by conducting an independent calibration which showed that, with exception of the axial force component, its measurements are accurate. The problem with the axial force component, force along X_s , is that the resolution is not adequate for the range of loads typical of the wind tunnel experiments. In spite of this fact this sensor was selected because the axial force component is not essential in the study of the lateral-directional dynamics of the system and because of the sensor low cost and the short lead time for delivery. The sensor maximum operational load and resolution are listed in Table 7, for each force-torque component with respect to reference frame $X_s Y_s Z_s$, defined in Figure 18, centered at point S on the sensor. More detailed data on the six-component sensor can be obtained from reference [19].

Force-Torque Component	Range	Resolution
Forces along Y_s and Z_s	± 90 N	0.045 N
Force along X_s	± 90 N	0.135 N
Moments about X_s , Y_s and Z_s	± 4.2 Nm	0.0011 Nm

Table 7: Characteristics of the six-component force-torque sensor.

5.5.5 Torque Motor

A servo system, consisting of a brushless motor and its drive, is used to provide the necessary actuation for the active cancellation described in Section 5.4 and is simply referred to as the torque motor. A low inertia brushless motor, model S-4075-R-H00AA, and a digital drive, model DM-30, both manufactured by Reliance Motion Control, Inc., are used to apply the necessary torque to the ‘yaw’ shaft. The main characteristics of the servo system are summarized in Table 8.

Parameter	Value
Rotor moment of inertia	0.00068 Kg m ²
Damping	0.068 Nm/Krpm
Friction torque	0.14 Nm
Max. continuous operating speed	3000 rpm
Continuous stall torque	10.2 Nm
Peak torque (at 25°C)	19.7 Nm
Sine wave torque constant (at 25°C)	0.74 Nm/A
Square wave torque constant (at 25°C)	0.81 Nm/A
Voltage constant	90 V/Krpm
Motor shipping weight	14.1 Kg
Motor envelope ¹ (approximate)	121 x 121 x 324 mm
Motor shaft	19 mm DIA. x 50 mm

Table 8: Characteristics of the S-4075-R-H00AA / DM-30 brushless servo system.

¹ See reference [20] for detailed dimensions.

Calibration tests were conducted to characterize the motor. The results are shown in next two figures. Figure 19 contains the calibration data for the motor static torque versus the input voltage to the motor. This data was obtained by restraining the 'yaw' shaft, applying a voltage command to the motor and measuring the output signal from the torque sensor. The overall response is fairly linear but the curve presents a change in slope in the region where the input voltage is between -0.2 and $+0.2$ Volts. The solid line shown in the plot corresponds to a gain of 21.428 Nm/Volt and represents a least squares fit to the data. On Figure 20 the torque due to motor cogging is shown as a function of the 'yaw' shaft angle, γ . This torque is repeatable but the data has to be recorded again every time the system is taken apart to account for the relative angular displacement between the motor shaft angle and the 'yaw' shaft angle.

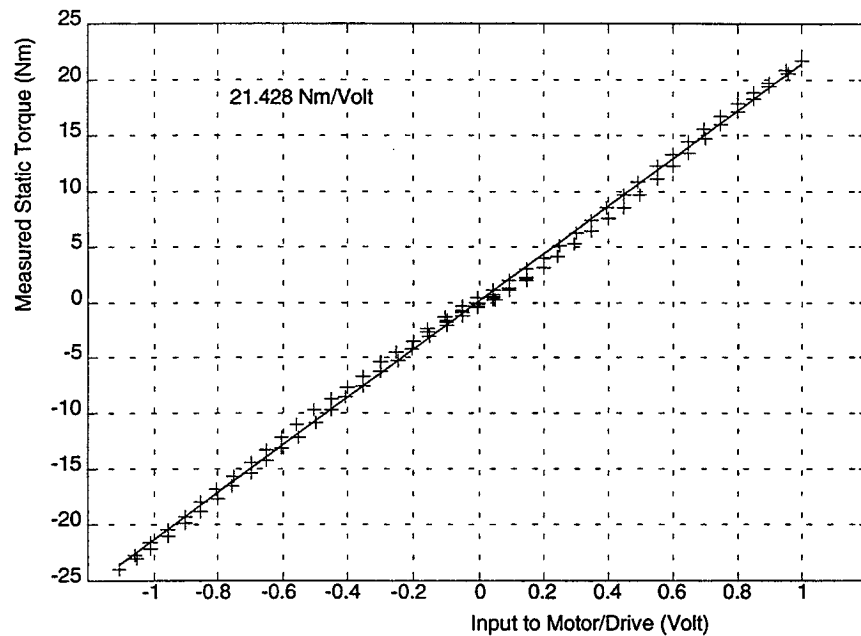


Figure 19: Torque motor static calibration.

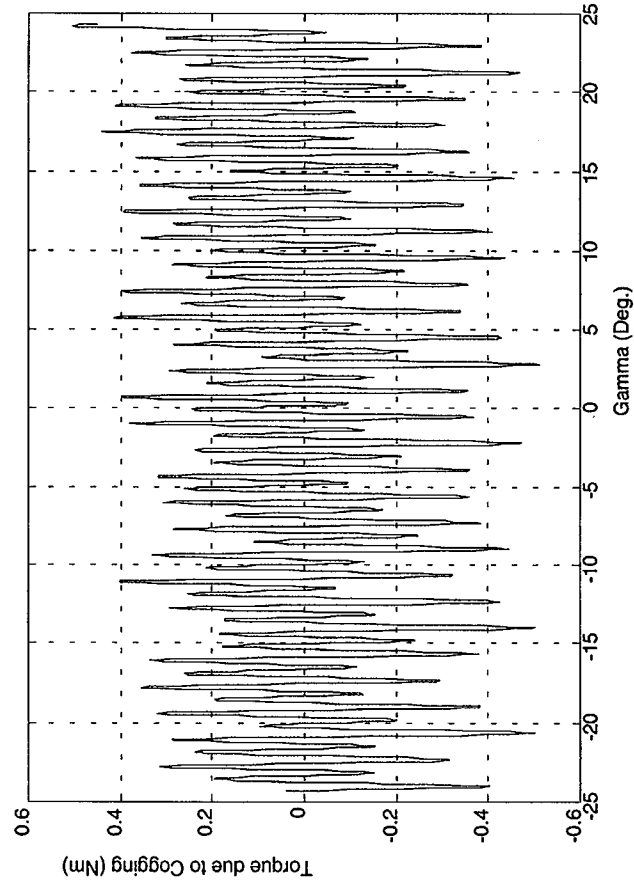


Figure 20: Torque caused by the cogging in the motor versus the 'yaw' shaft angle.

6 Operation During Dynamic Experiments

The operation of the two degrees of freedom apparatus during dynamic experiments requires the use of one computer equipped with A/D and D/A converters to control the active cancellation loop. Inputs to the A/D converter are: the torque from the torque sensor (used as feedback for the inner torque control loop), the 'yaw' shaft angle γ , and the angular acceleration $\ddot{\gamma}$. As described in Section 5.4 the signal from the torque sensor is used as feedback for the inner torque control loop, and the signals for γ and $\ddot{\gamma}$ are used to command the higher level cancellation loop. The output of the D/A converter is a current command sent to the brushless servo system used to apply a torque to the 'yaw' shaft. In general a second computer is used for data acquisition, *e.g.* loads acting on the wind tunnel model, and in the case where active flow control is required a third computer is used to control the servo valves and implement the air injection closed loop control¹. Currently three IBM-PC compatible micro computers, equipped with A/D - D/A cards², are used to perform these tasks. The programs are written in C³ and make use of real time assembly routines⁴ to interface to the A/D - D/A converters.

Use of the apparatus to conduct dynamic experiments is relatively simple but care should be taken because the cancellation system can apply large torques to the model supporting structure and the structure could collide with the mechanical stops that limit the motion about the γ -axis causing damage to the system. For this reason safety devices were implemented both mechanically and in the control software. Stops containing cushion material are used to stop the motion before the hard limits are reached. Use of this safety device decreases the range of motion about the γ axis from ± 30 degrees to approximately ± 23 degrees. Also a portable switch, that can be conveniently at hand at all times during the dynamic experiments, is implemented and allows for fast manual turn-off of the input

¹ The air injection system is discussed in Section 4.

² DT-2821 - Analog and digital I/O board. Data Translation, Inc., 100 Locke Drive, Marlboro, MA 01752-1192 USA.

³ Turbo C by Borland International, 4585 Scotts Valley Drive, Scotts Valley, CA 95066.

⁴ Real time I/O subroutines written by Marc Ullman while a student in the Aerospace Robotics Laboratory - Stanford University.

to the motor. Safety clauses were added to the software and do not allow more than a certain voltage to be sent as input to the servo system. The software is written in a way that when it is started the system cancels 0% of the external effects, *i.e.* no cancellation occurs, the user can then gradually increase this percentage by using the keyboard, in this way any instabilities or offsets can be identified at a low torque level.

7 Conclusions and Suggested Improvements

A unique experimental apparatus has been designed and built that allows a wind tunnel model two degrees of freedom. The model support system operates in the high angle of attack regime and its degrees of freedom are an approximation to roll and yaw. An active system is used to cancel effects of the apparatus resulting in a system with dynamics dominated by the aerodynamic loads acting on the wind tunnel model.

The apparatus was build to support the active flow control research conducted by the Joint Institute of Aeronautics and Acoustics between Stanford University and NASA Ames Research Center. The system provides a platform to which various wind tunnel models can be mounted and their lateral-directional dynamics (roll-yaw coupling) investigated in a controlled and repeatable environment.

The value and versatility of the apparatus have been demonstrated by its use in the investigation of the dynamics of a delta wing body combination at 45 degrees nominal incidence angle [11,14,15,16]. In those investigations the two degrees of freedom model support system was used as follows: 1) To characterize the flow over the wind tunnel model at 45 degrees angle of attack subjected to transient effects caused by the motion of the model and the application of forebody tangential blowing. 2) To determine the natural motion the system. 3) To demonstrate a closed loop control approach that used forebody tangential blowing as the only actuator to control the roll-yaw motion of the system.

Following are suggestions that the author believes would improve the performance of the existing apparatus:

- *Use of feedforward in the torque control loop.* Currently the torque closed loop control uses feedback logic only. The performance of this control loop can be improved by the use of feedforward in conjunction with feedback. In this way the gain of the feedback loop can probably be reduced and the damping of the closed

loop torque response increased. In addition the non-linearities identified in the motor¹ response can be used to generate a feedforward torque command which would improve the torque loop even further. These are relatively simple to implement improvements requiring mainly software changes.

- *Reduction of the apparatus inertia.* Reducing the inertia of the apparatus about the γ axis would provide a reduction in the required cancellation torque and would increase the first resonance frequency of the structure as a consequence the error in the torque loop would be reduced. Because of the modular characteristic of the design, a roll system which is connected to a 'yaw' system, it is possible to reduce the inertia by modifying the roll-yaw connecting structure only. A more efficient design of this structure would require characterizing the spectra of the loads to which the apparatus is subjected (defined by the unsteady aerodynamics in the operational envelope of the apparatus) and possibly the use of composite materials.

¹ Section 5.5.5.

A Geometry and Mass Properties of the Wind Tunnel Model

In this section the characteristics of four wind tunnel model configurations are presented. The general form of the model is shown in Figure A.1. The model consists of a cone-cylinder fuselage to which wings of different plan-forms as well as vertical fins can be mounted. The different configurations correspond to the possible combinations of delta wings of 60 and 70 degrees sweep angle and the optional use of a vertical fin. The nomenclature used to indicate each of the configurations is given in Table A.1.

Wind Tunnel Model Configurations	
Name	Description
N6	60 deg wing sweep angle <u>no</u> vertical fin
T6	60 deg wing sweep angle and vertical fin
N7	70 deg wing sweep angle and <u>no</u> vertical fin
T7	70 deg wing sweep angle and vertical fin

Table A.1: Nomenclature used for the different wind tunnel model configurations.

Figure A.1 includes a cross section of the forebody showing the geometry of the blowing slots. On the cylindrical portion of the forebody the slot has constant width given by $w_{cyl}/D = 0.0087$, where $D = 1.5$ inches is the diameter of the fuselage. On the conical portion of the forebody the slot is tapered, its maximum width is equal to w_{cyl}/D at the junction of the cylindrical and conical sections and its minimum width is $w_{min}/D = 0.0062$ at a station located 0.3 inches from the tip of the conical forebody.

The main characteristics the four wind tunnel model configurations are summarized in Table A.2. The detailed geometry is presented in Figures A.2 through A.5 at the end of this section. Point P, shown in the figures, is defined as the point along the longitudinal axis of the model through which the model rotates in 'yaw', *i.e.* the intersection of the ϕ -axis with the γ -axis.

The model is built from Aluminum 6061-T6 and anodized black. The tip of the forebody can be removed and besides the conical tip shown in the drawings a blunt tip consisting of a semi-sphere with a 0.3 inch radius is available. The reference area, S_{ref} , is the area of the wing plan form obtained by extending the leading and trailing edges of the wing. The mean aerodynamic chord shown in the table is defined as

$$MAC = \frac{1}{S_{ref}} \int_{-b/2}^{b/2} c^2(y) dy \quad (A.1)$$

where b is the wing span and $c(y)$ is the local chord. In Table A.2 the positions of the center of mass and of point P refer to the position along the longitudinal axis of the model and are given as a percentage of the mean aerodynamic chord, MAC.

Characteristics	Model Configuration			
	N6	T6	N7	T7
conical forebody semi-apex angle (deg)	14	14	14	14
wing sweep angle, Λ (deg)	60	60	70	70
wing span, b (in)	7.82	7.82	5.50	5.50
wing plan form area, S_{ref} (in ²)	26.46	26.46	20.68	20.68
wing aspect ratio, $AR = b^2/S_{ref}$	2.31	2.31	1.46	1.46
mean aerodynamic chord, MAC (in)	4.51	4.51	5.01	5.01
spanwise location of MAC (in)	1.30	1.30	0.92	0.92
position of center of mass (% of MAC)	18 %	21 %	24 %	27 %
position of point P (% of MAC)	38 %	38 %	44 %	44 %
model plan form area (in ²)	31.54	31.54	25.19	25.19
tunnel blockage at $\alpha_o = 45$ deg	9 %	9 %	7 %	7%
tunnel blockage at $\alpha_o = 90$ deg	12 %	12 %	10 %	10 %

Table A.2: Main characteristics of the various wind tunnel model configurations.

The mass, center of mass and inertia¹ properties for the four configurations are given in Table A.3. Center of mass and inertia are with respect to a reference frame XYZ oriented as shown in Figure A.1. Superscripts CM and P are used to indicate that a quantity is referred to frame XYZ with origin at the center of mass or at point P respectively. In the table, X_{CM}^P , Y_{CM}^P and Z_{CM}^P are the components of the position vector from point P to the center of mass of the model, CM.

Inertia Properties	Model Configuration			
	N6	T6	N7	T7
mass (± 0.0001 Kg)	0.6708	0.6913	0.6420	0.6625
X_{CM}^P ($\pm 0.03 \times 10^{-2}$ m)	2.27×10^{-2}	1.94×10^{-2}	2.48×10^{-2}	2.13×10^{-2}
Y_{CM}^P (m)	0	0	0	0
Z_{CM}^P ($\pm 0.05 \times 10^{-4}$ m)	≈ 0	-5.97×10^{-4}	≈ 0	-6.22×10^{-4}
I_{XX}^{CM} ($\pm 0.15 \times 10^{-4}$ Kg m ²)	2.70×10^{-4}	3.05×10^{-4}	1.76×10^{-4}	2.12×10^{-4}
I_{YY}^{CM} ($\pm 0.05 \times 10^{-3}$ Kg m ²)	2.88×10^{-3}	3.25×10^{-3}	2.79×10^{-3}	3.10×10^{-3}
I_{ZZ}^{CM} ($\pm 0.02 \times 10^{-3}$ Kg m ²)	3.02×10^{-3}	3.19×10^{-3}	2.83×10^{-3}	3.09×10^{-3}
I_{XY}^{CM} (Kg m ²)	0	0	0	0
I_{XZ}^{CM} ($\pm 0.1 \times 10^{-5}$ Kg m ²)	≈ 0	-9.0×10^{-5}	≈ 0	-9.1×10^{-5}
I_{YZ}^{CM} (Kg m ²)	0	0	0	0
I_{XX}^P ($\pm 0.15 \times 10^{-4}$ Kg m ²)	2.70×10^{-4}	3.06×10^{-4}	1.76×10^{-4}	2.12×10^{-4}
I_{YY}^P ($\pm 0.05 \times 10^{-3}$ Kg m ²)	3.24×10^{-3}	3.45×10^{-3}	3.19×10^{-3}	3.40×10^{-3}
I_{ZZ}^P ($\pm 0.02 \times 10^{-3}$ Kg m ²)	3.34×10^{-3}	3.51×10^{-3}	3.22×10^{-3}	3.39×10^{-3}
I_{XY}^P (Kg m ²)	0	0	0	0
I_{XZ}^P ($\pm 0.1 \times 10^{-5}$ Kg m ²)	≈ 0	-7.5×10^{-5}	≈ 0	-7.5×10^{-5}
I_{YZ}^P (Kg m ²)	0	0	0	0

Table A.3: Mass and inertia properties of the various wind tunnel model configurations.

¹ Moments of inertia were measured using a torsional pendulum [21].

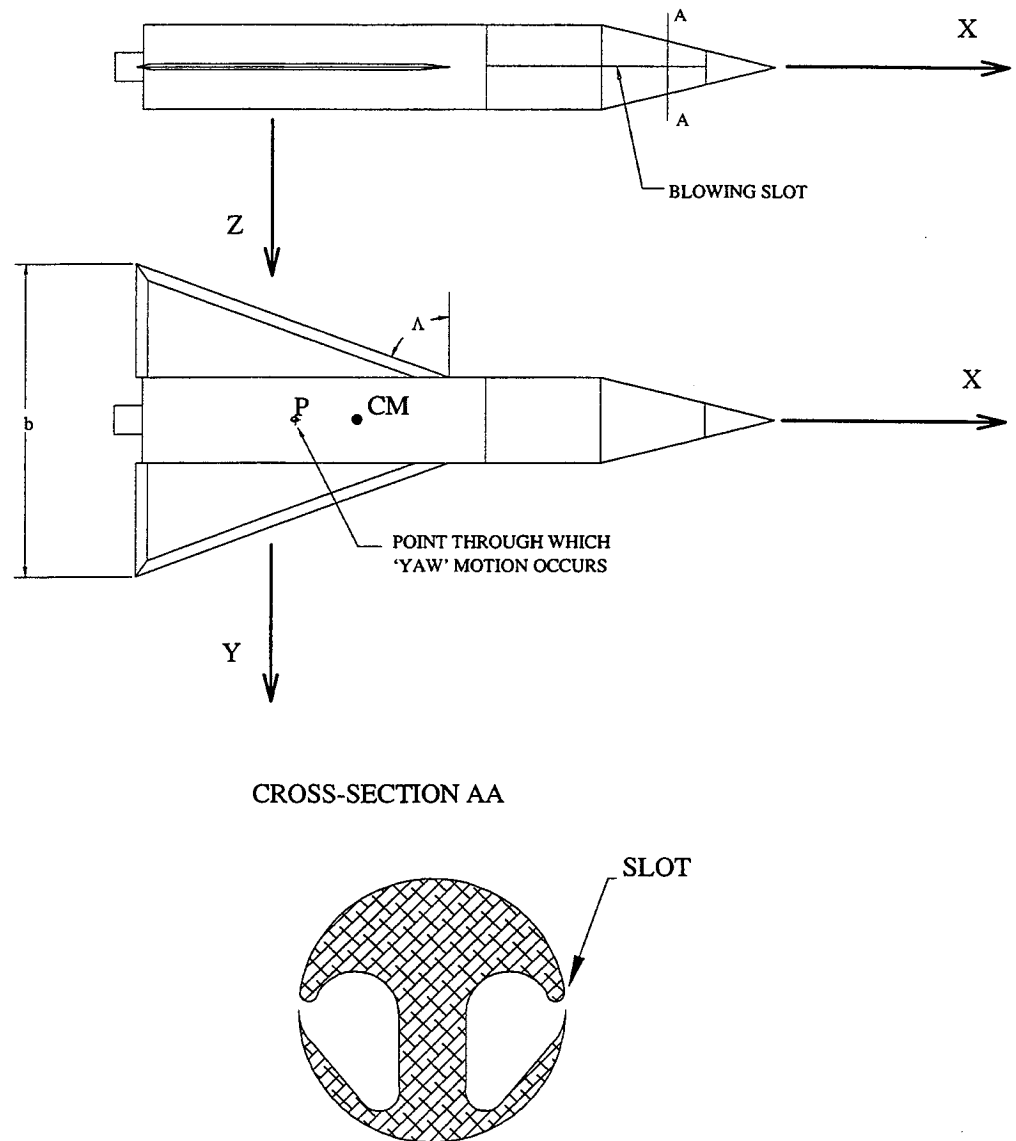


Figure A.1: Geometry of the wind tunnel model and detail of blowing slot.

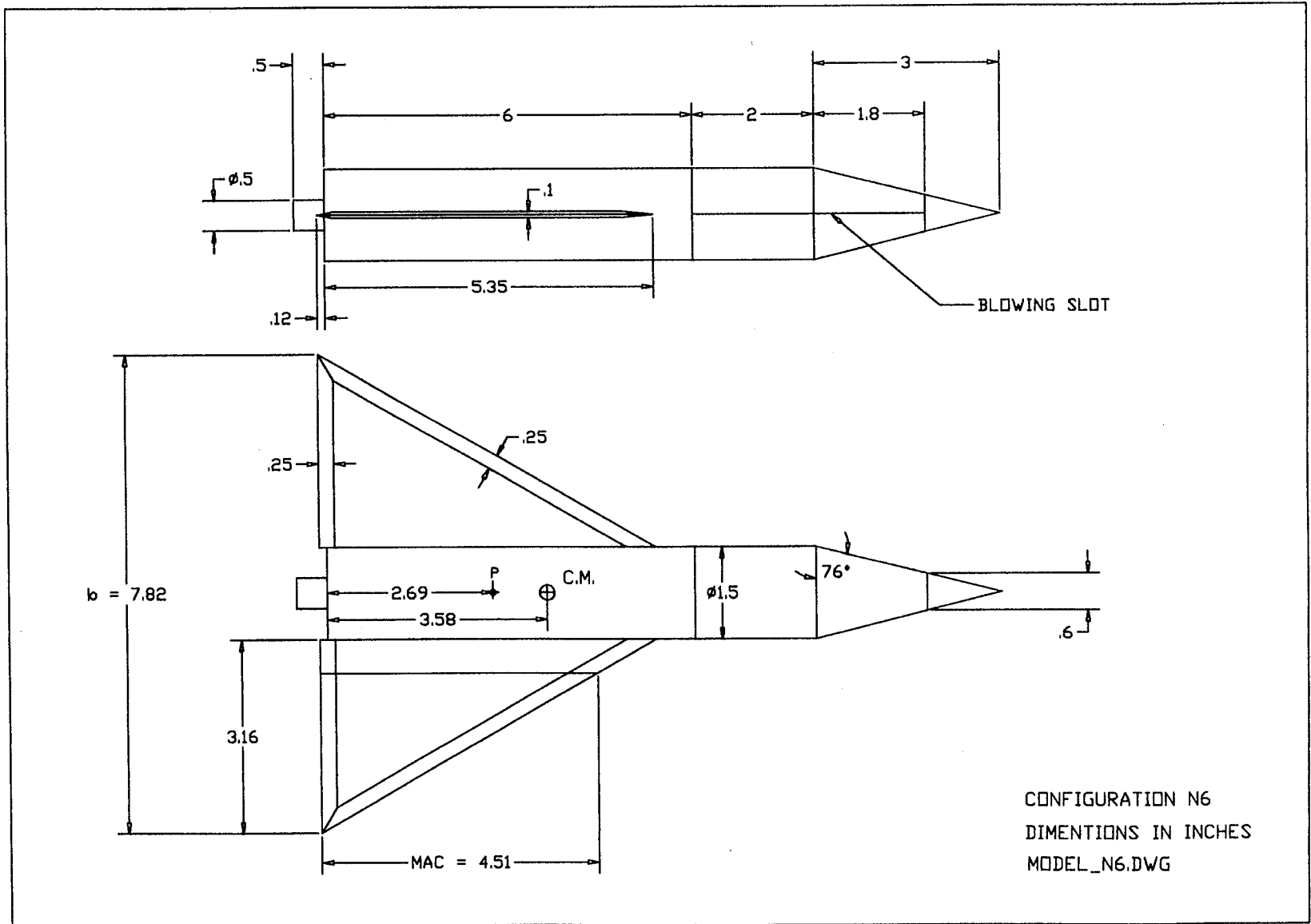
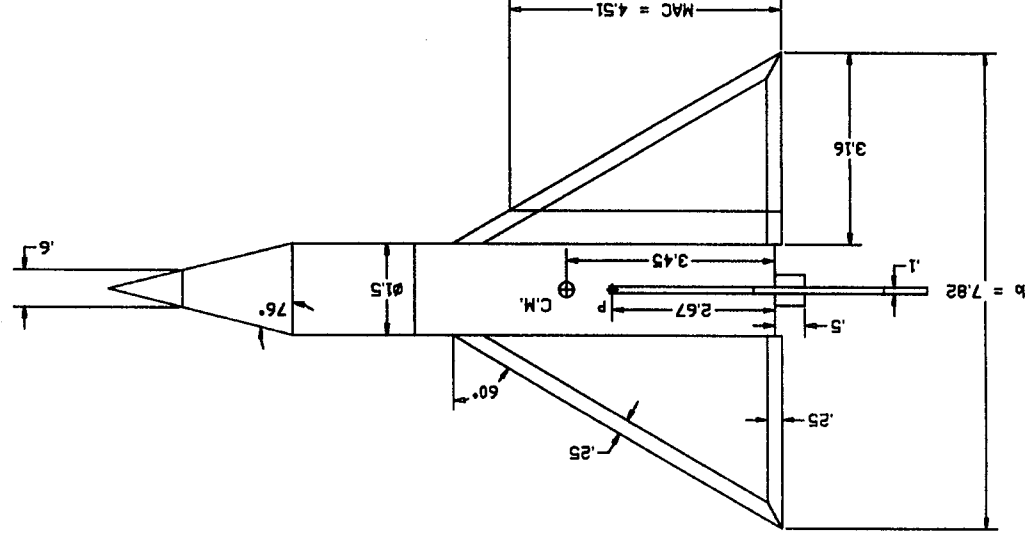
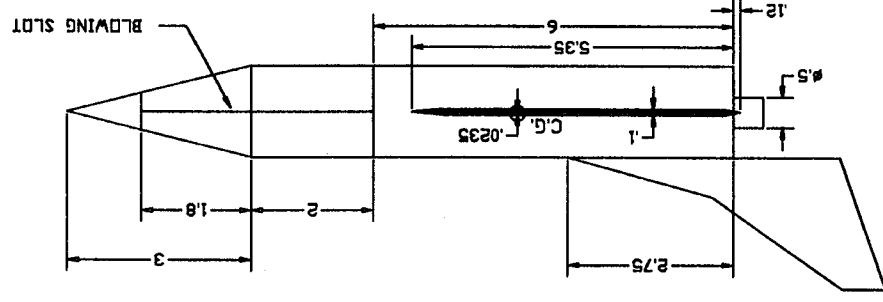
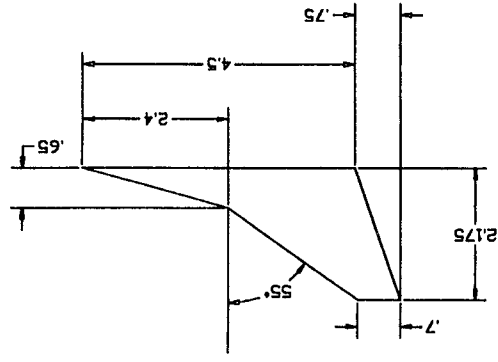


Figure A.2: Detailed geometry for model configuration N6



CONFIGURATION T6
DIMENSIONS IN INCHES
MODEL_T6.DWG

Figure A.3: Detailed geometry for model configuration T6

MODEL_T7.DWG
DIMENSIONS IN INCHES
CONFIGURATION T7

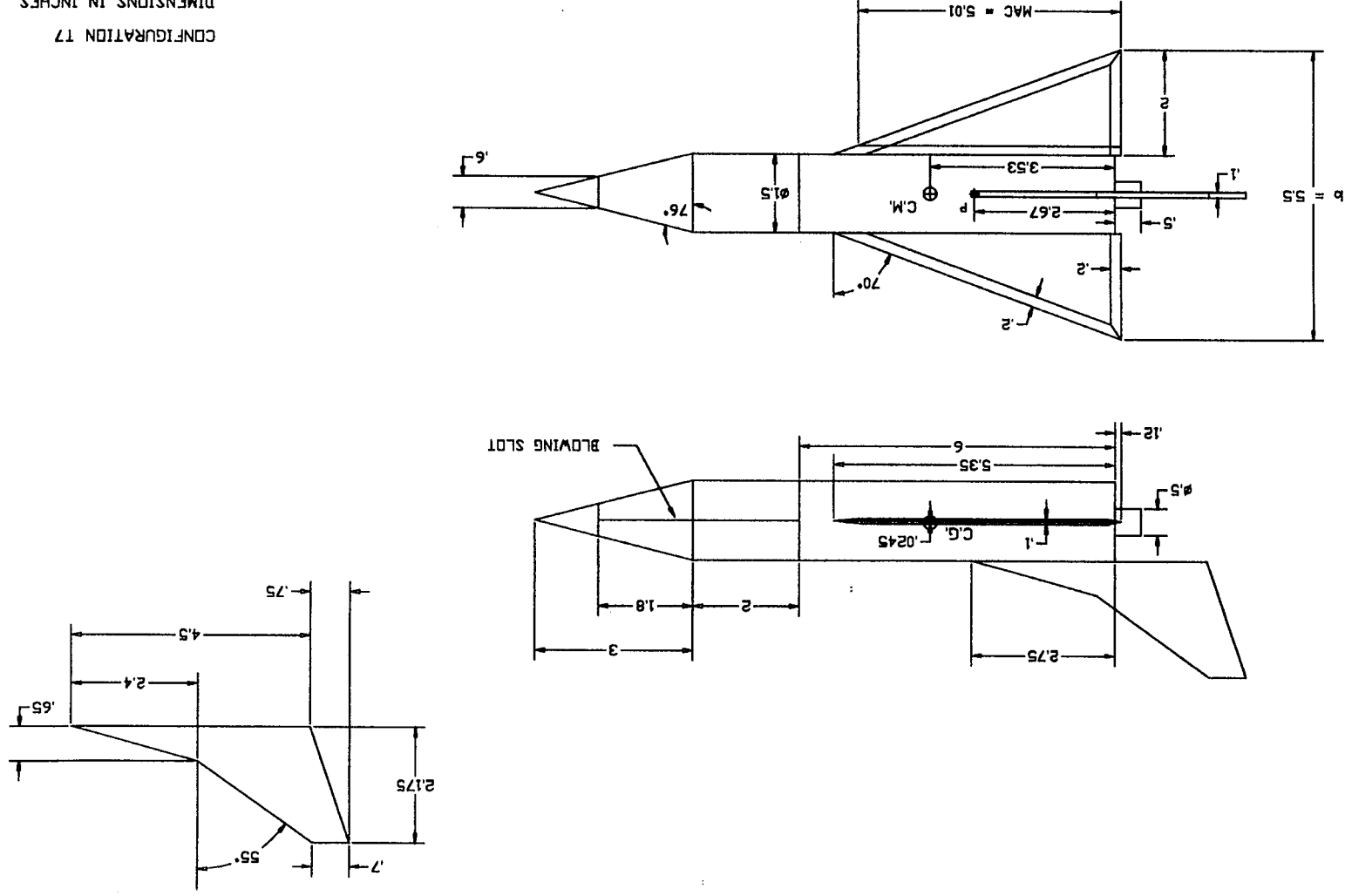


Figure A.5: Detailed geometry for model configuration T7

B Servo Valve and Flowmeter

Drawings of the servo valves¹ are shown in Figure B.1. The valve stator and rotor have cut outs and as the angle of the rotor varies so does the area available for the passage of air. A brushless motor is connected to the rotor shaft and a potentiometer is used measure the valve angle. A closed loop control logic is implemented through an analog circuit to control the rotor angular position [9]. The servo valve, as designed, presents a small leakage and a second rotor, shown in Figure B.2, was designed and built to minimize the leakage.

Two specially designed flowmeters² have been built to allow the direct measurement of jet momentum coefficient, C_μ . The design, shown in Figure B.3, uses a miniature pressure transducer³ to measure the dynamic pressure, p_F^o , at a point at the center line of the flowmeter, from which the jet momentum coefficient is obtained. The dynamic pressure p_F^o is given by:

$$p_F^o = \frac{1}{2} \rho_F^o V_F^{o2} \quad (B.1)$$

where ρ_F^o and V_F^o are respectively the air density and the air speed at the center line of the flowmeter. The mass flow rate, \dot{m} , can be written as:

$$\dot{m} = \int_{A_F} \rho_F V_F dA = \lambda_F \rho_F^o A_F V_F^o \quad (B.2)$$

¹ Servo valves designed by Dr. Grant S. Wong [9]. Machined by Mr. Tom Hasler (former Aero/Astro Machine Shop, Stanford University).

² Designed and built by the author.

³ Kulite Miniature IS[®] Silicon Diaphragm Pressure Transducer - XCS-093 Series. Kulite Semiconductor Products, Inc. Leonia, NJ 07605.

where A_F is the cross-sectional area of the flowmeter, and λ_F is a constant ($0 < \lambda_F < 1$) that depend on the velocity profile at the flowmeter cross-section where the pressure measurement is taken. λ_F is determined experimentally during the calibration of the flowmeter. From Equations B.1 and B.2 the following expression results for the mass flow rate.

$$\dot{m} = \lambda_F A_F \sqrt{2 \rho_F^\circ p_F^\circ} \quad (B.3)$$

The mass flow rates through the flowmeter and through the exit of the forebody slot are the same:

$$\rho_j A_j V_j = \lambda_F \rho_F^\circ A_F V_F^\circ \quad (B.4)$$

where subscript j is used to indicate that a quantity refers to the air jet at the exit of the forebody slot. Recalling the definition of C_μ , from Section 4, and using Equations B.3 and B.4 results:

$$C_\mu \cong 2\lambda_F \frac{A_F^2}{A_j q_\infty S_{ref}} p_d^\circ \quad (B.5)$$

where the approximation in the equation is due to the assumption made that the air density inside the flowmeter and at the jet exit are the same. This assumption is reasonable as the flowmeter is built such that $A_F \approx A_j$.

Flowmeter Calibration

The following procedure was used to calibrate the flowmeters: A tube, 0.548 inch internal diameter and 3 feet long, was attached to the exit of the flowmeter and the air velocity profile was determined at the exit of the tube using a miniature Pitot tube mounted to a traversing table. The velocity profiles were numerically integrated to

generate the mass flow rates which were then used in conjunction with the output of the flowmeters to perform the calibration.

Some of the velocity profiles obtained in one of the experiments are shown in Figure B.4, for various mass flow rates. It is assumed that the output of the flowmeter is proportional to the dynamic pressure p_F° , *i.e.*

$$\vartheta_F = k_v p_F^\circ \quad (\text{B.6})$$

where ϑ_F is the output of the flowmeter in Volts and k_v is the constant of proportionality. Equations B.3 and B.6 show that the mass flow rate is proportional to the square root of the output of the flowmeter:

$$\dot{m} = \lambda_F A_F \sqrt{\frac{2\rho_F}{k_v}} \sqrt{\vartheta_F} = C_F \sqrt{\vartheta_F} \quad (\text{B.7})$$

In Figure B.5 the mass flow rates obtained through the integration of the velocity profiles are plotted against the square root of the output of the flowmeter. Also shown is the result obtained with the least squares fit used to determine the constant C_F . This result together with Equations B.3 and B.6 show that the jet momentum coefficient is proportional to the output of the flowmeter.

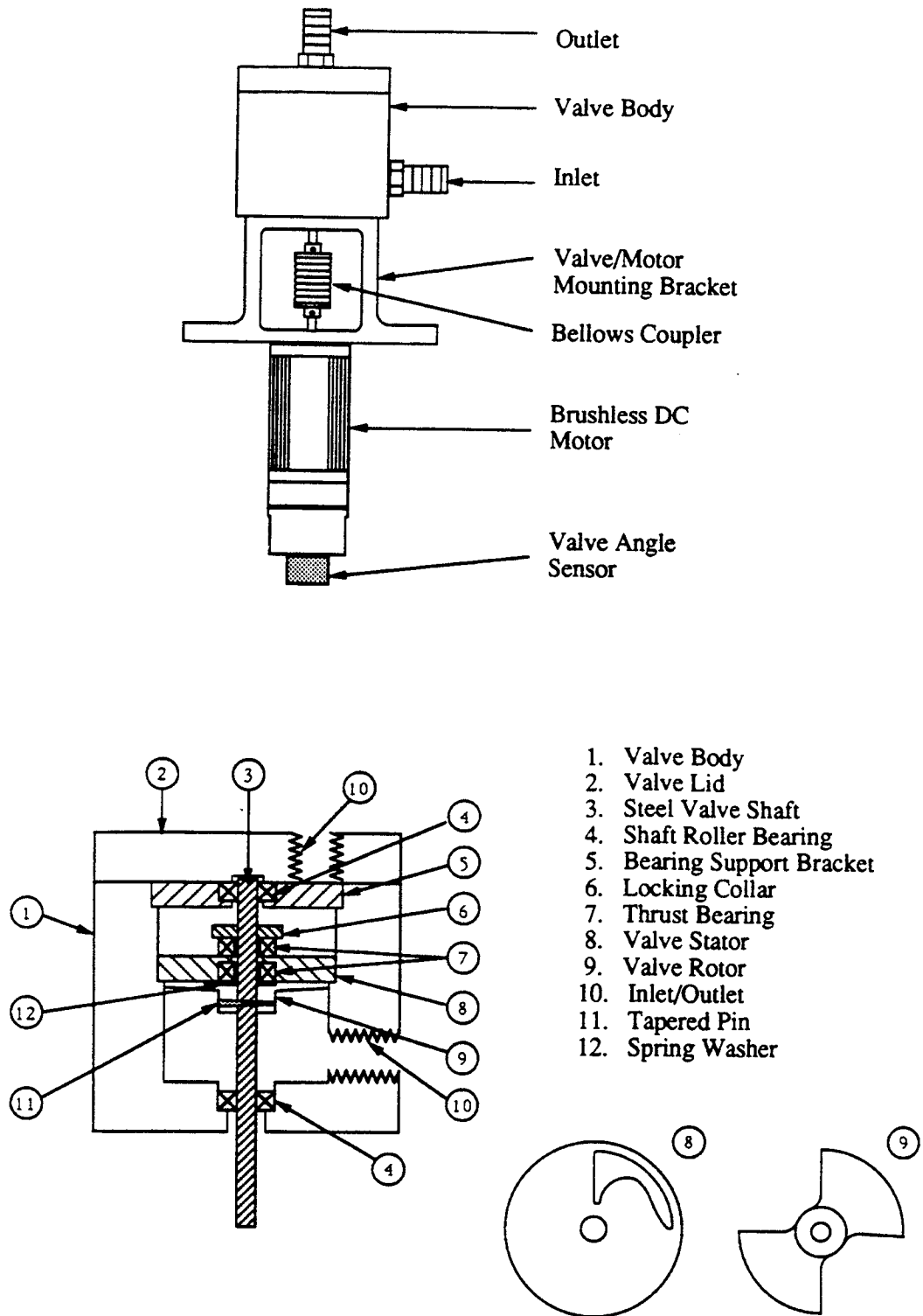
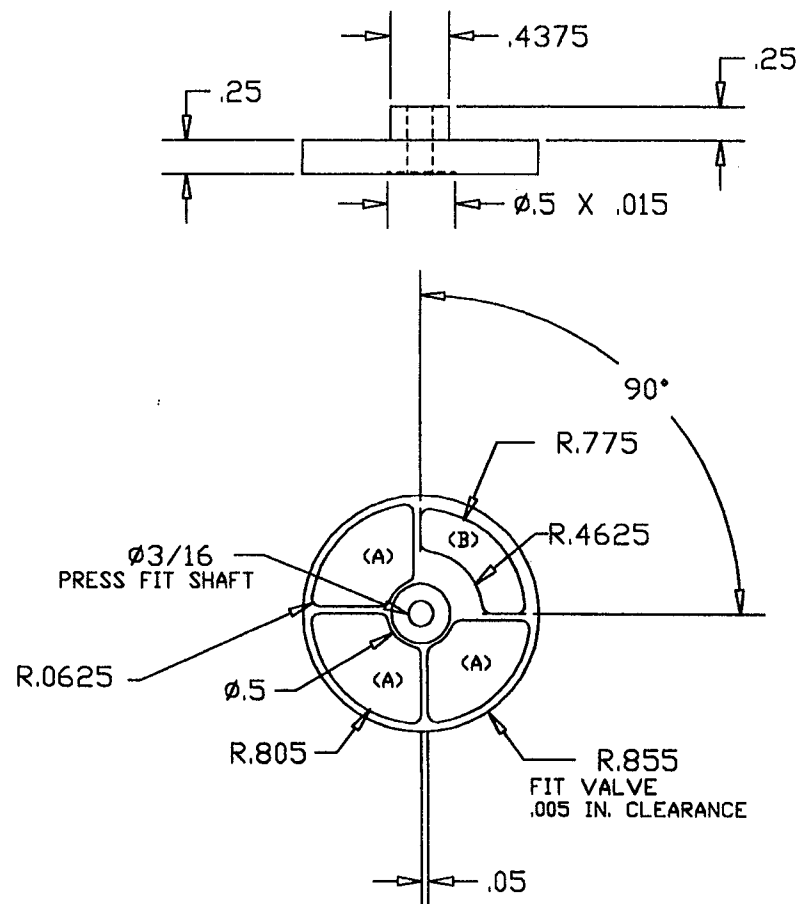


Figure B.1: Servo valve design and configuration. From Wong [9].

Figure B.2: Alternative design for the servo valve rotor.



VALVE_RT.DWG

NOTES:

1. ALUMINUM 6061-T6
2. DIMENSIONS IN INCHES
3. QUANTITY = 2
4. SHOULD FIT VALVE
5. PART IS TO BE MOUNTED ON A GIVEN SHAFT USING A TAPERED PIN

(A) .1937 DEEP

(B) THRU

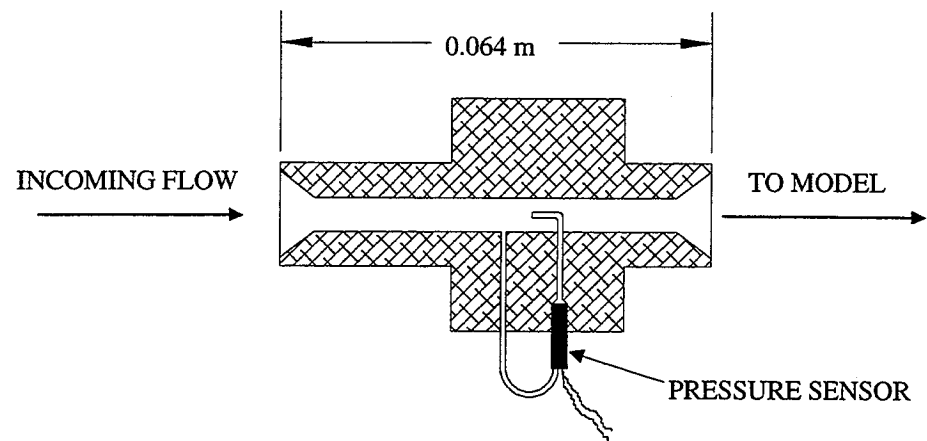


Figure B.3: Flowmeter design and configuration.

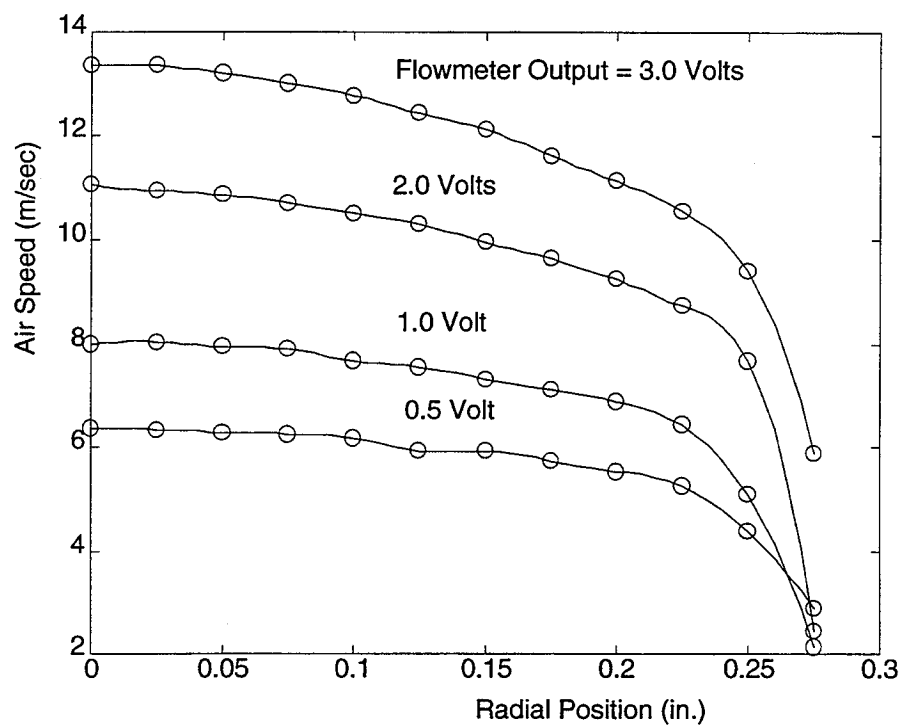


Figure B.4: Velocity profiles at the exit of flowmeter calibration tube.

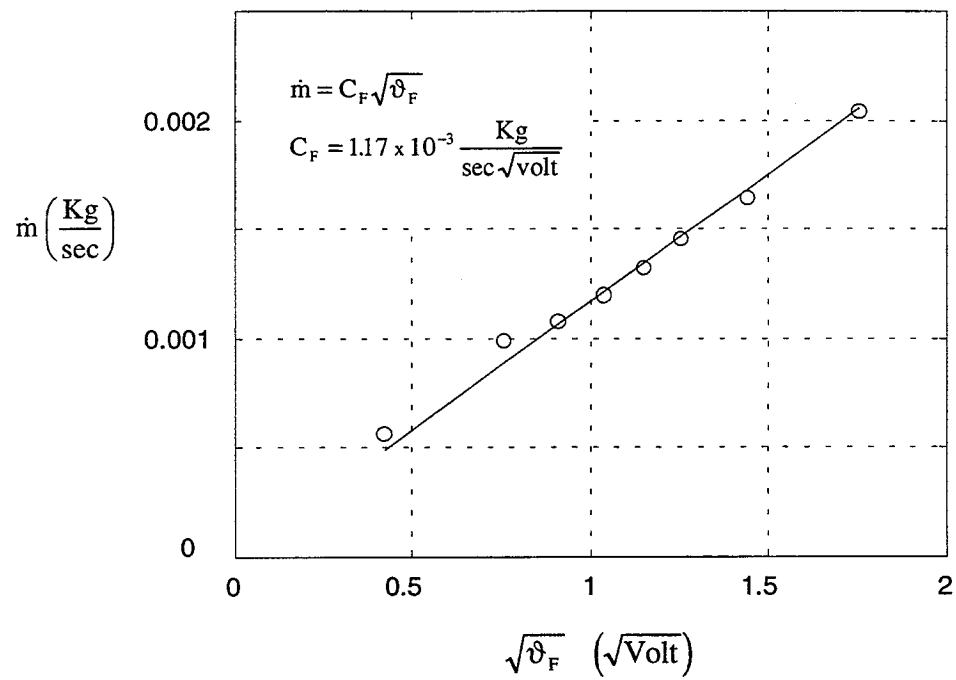


Figure B.5: Flowmeter calibration results.

C Model Support System Mechanical Design Drawings

The mechanical design drawings for the components that form the model support system are presented in the following pages. The drawings are divided in three groups according to the sub-system to which they belong. Drawings for the roll sub-system are presented first, followed by drawings for the yaw and for the active cancellation sub-systems. Unless otherwise specified dimensions are in inches and angles in degrees.

It is assumed that the reader who is interested in the detailed design has access to the apparatus and therefore the assembly of the various parts to form the complete system should not pose a problem, nonetheless a few assembly drawings are included to indicate how the various parts fit together.

C.1 Roll Sub-system

The mechanical components of the roll sub-system are identified on the assembly drawing presented in Figure C.1. A wind tunnel model is shown in the drawing to indicate how it is mounted to the roll system.

The roll shaft is mounted to the roll support structure through precision bearings¹, and held in place by two collars as shown in the figure. Part ENDPLT2A, the 6-component force-torque sensor, and part ENDPLT2B are used to connect the wind tunnel model to the roll shaft. Part ROLLEND connects the shaft of the potentiometer to the roll shaft.

The air supply tubing are not shown in the drawing. The tubing are routed from the yaw sub-system to the interior of the roll shaft through part ROLLEND, they emerge at the other end of the roll shaft at the section where the shaft diameter changes from 1 to 0.5 inches and are connected to special ports at the rear end of the model. Part ROLLOCK is used to constrain the motion of the roll shaft at a desired roll angle during static experiments.

It is possible to mount a motor² to the roll system for the purposes of driving the roll motion or canceling external effects such as the friction from the bearings and potentiometer and disturbances from the air supply tubing. The detailed drawings for parts MTRFXA and MTRFXB which are used to mount the motor to the roll system are included.

¹ Kaydon KAA10CL4 ball bearing. Kaydon Corporation, Muskegon, Michigan 49443 USA.

² Elcom 3111 WDG#4. Pittman Motors, Harleysville, PA 19438-003 USA.

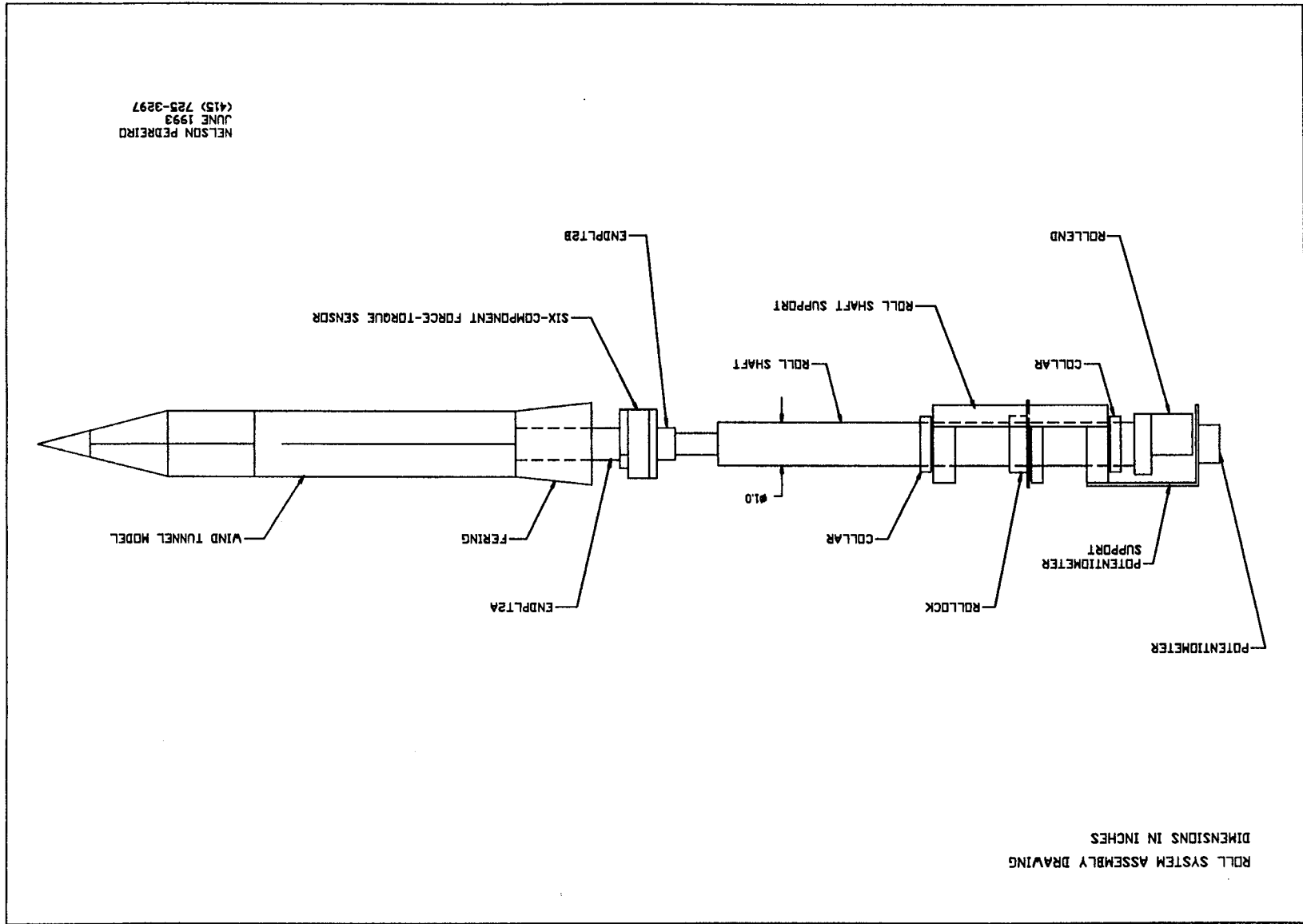
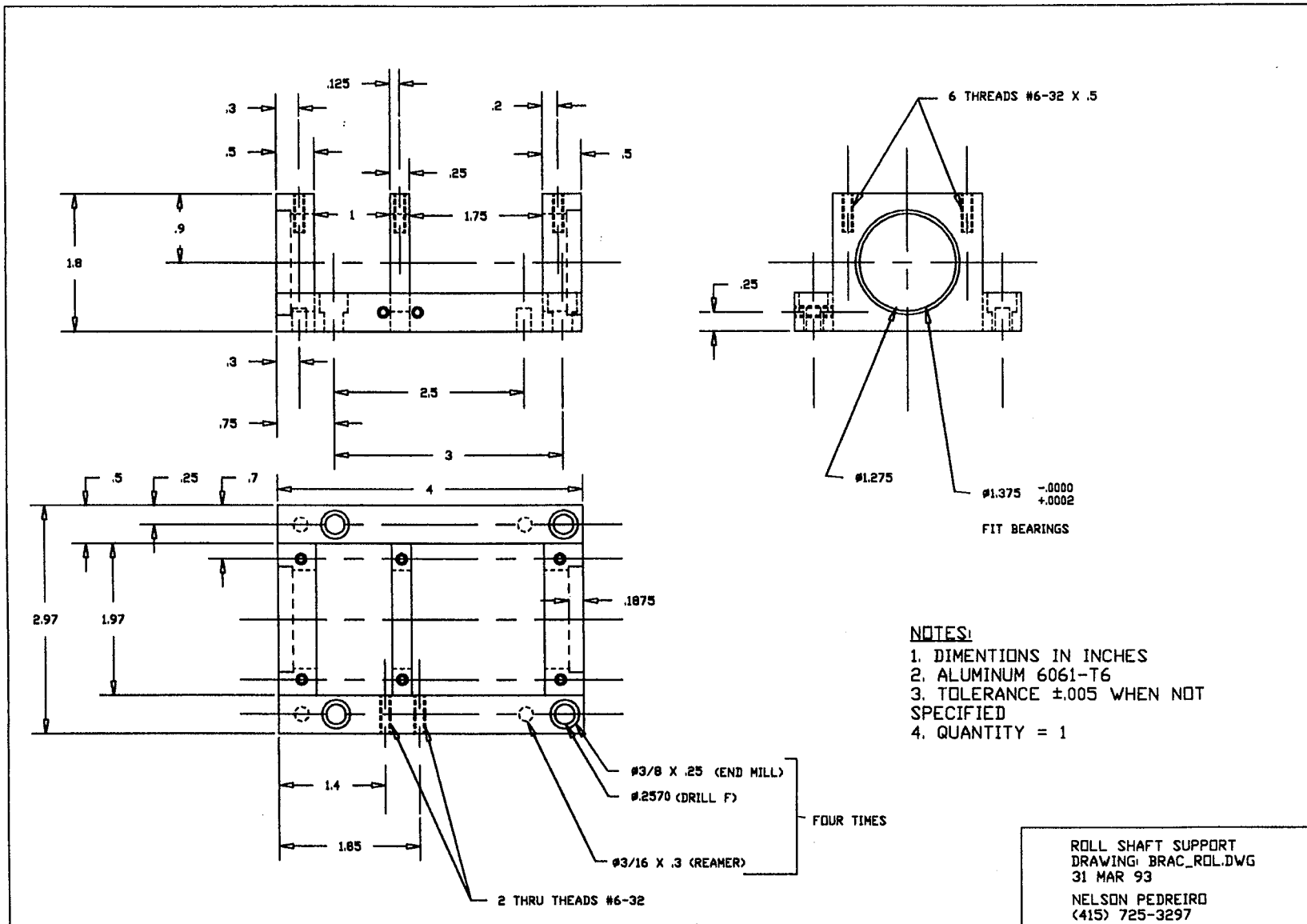


Figure C.1: Roll system assembly drawing.

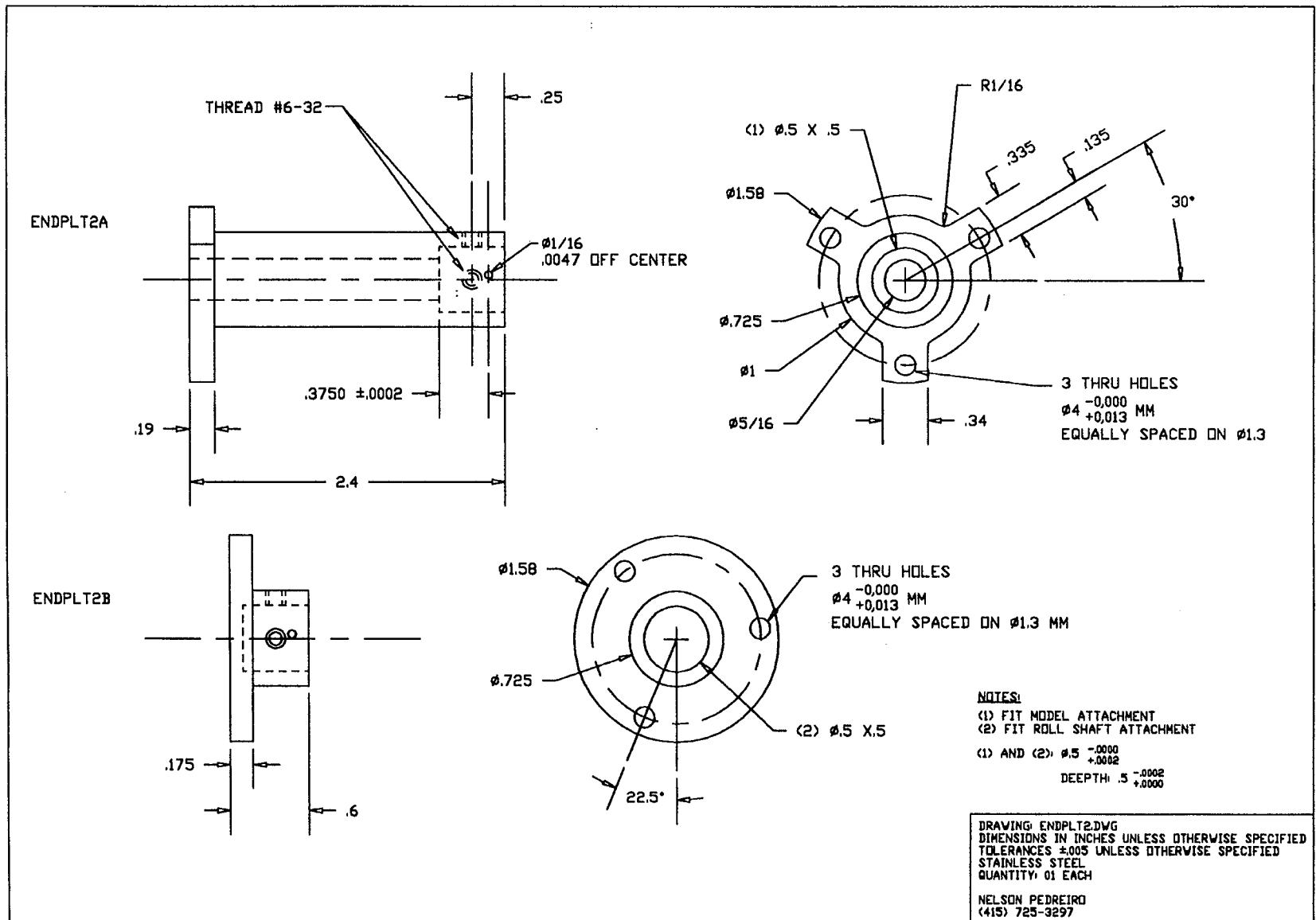




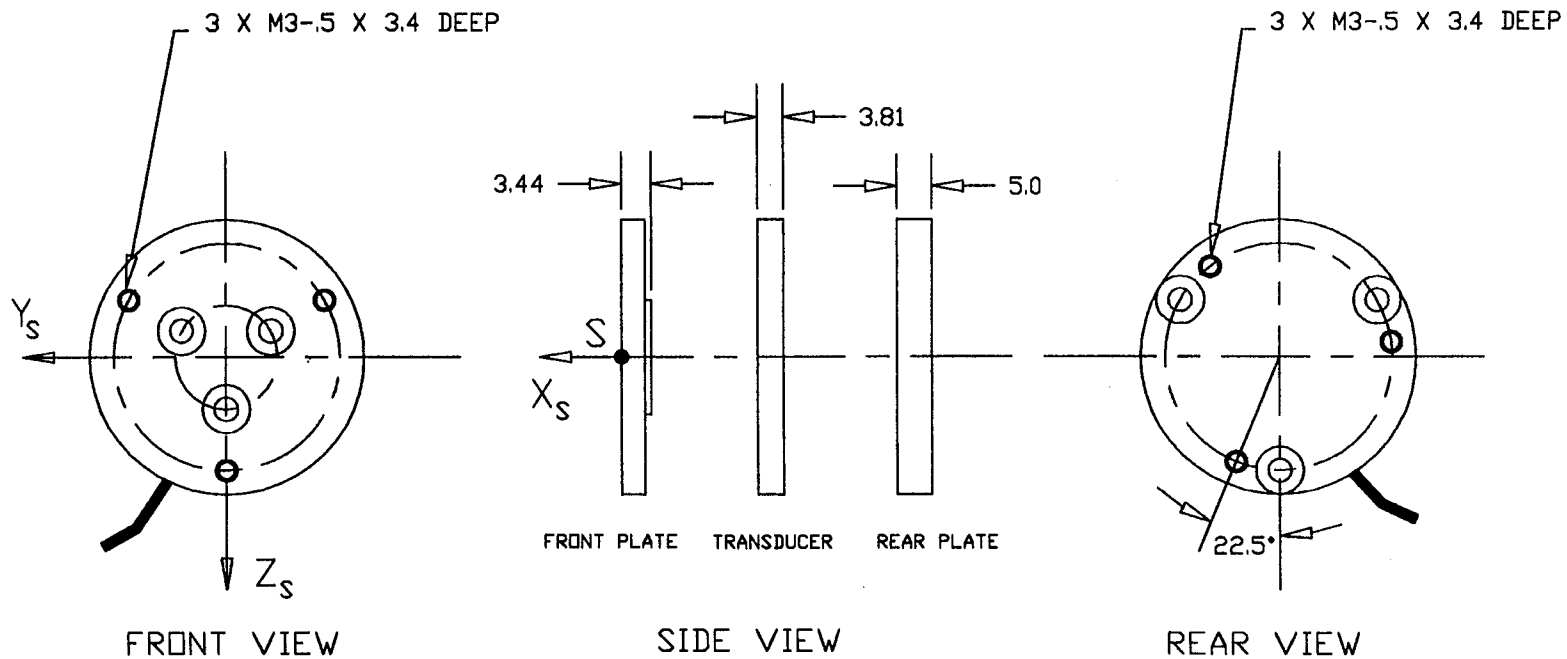
NOTES:

- NOTES:**
1. DIMENSIONS IN INCHES
2. STAINLESS STEEL - 304
3. TOLERANCE $\pm .005$ WHEN NOT SPECIFIED
4. QUANTITY = 1

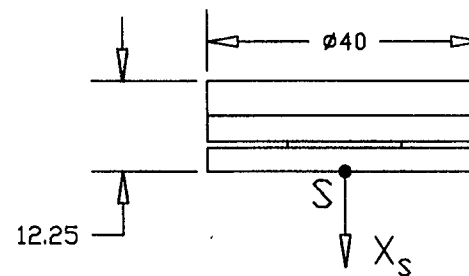
SHAFT TOLERANCES FOR FITTING THE BEARINGS ARE: $-.0000$
 $+.0002$

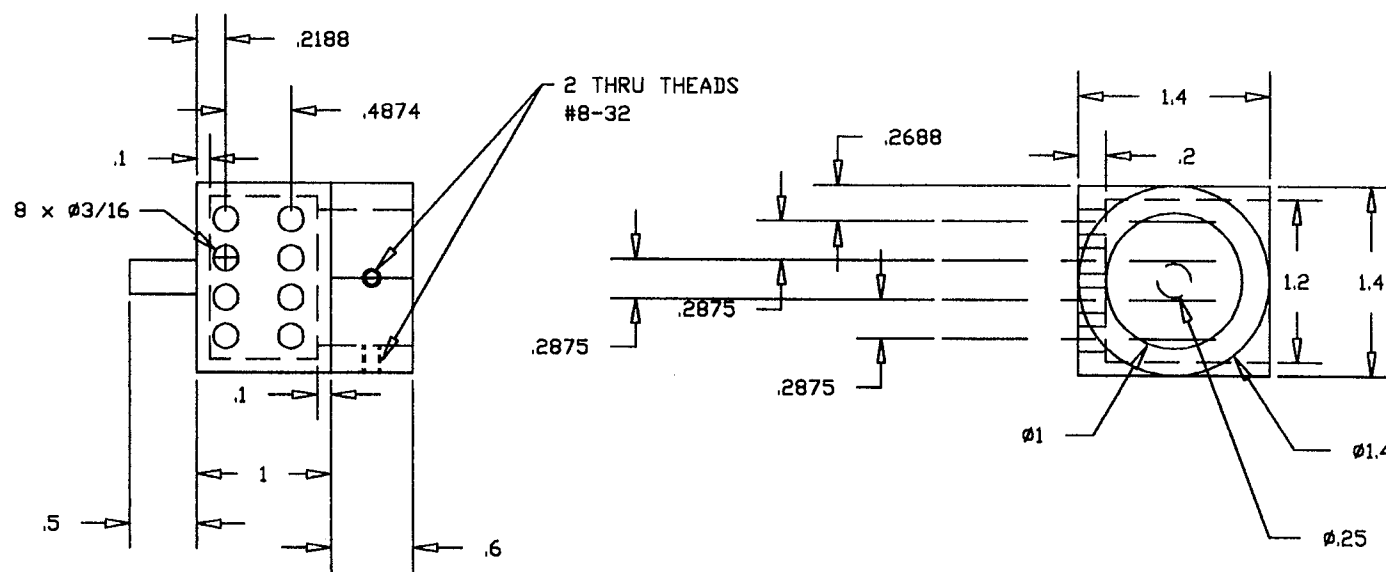


SIX-COMPONENT FORCE-TORQUE SENSOR MANUFACTURED BY ASSURANCE TECHNOLOGIES, INC.
 MODEL - MINI 90N/4.2Nm



SENSOR ASSEMBLED WITH
 INTERFACE PLATES





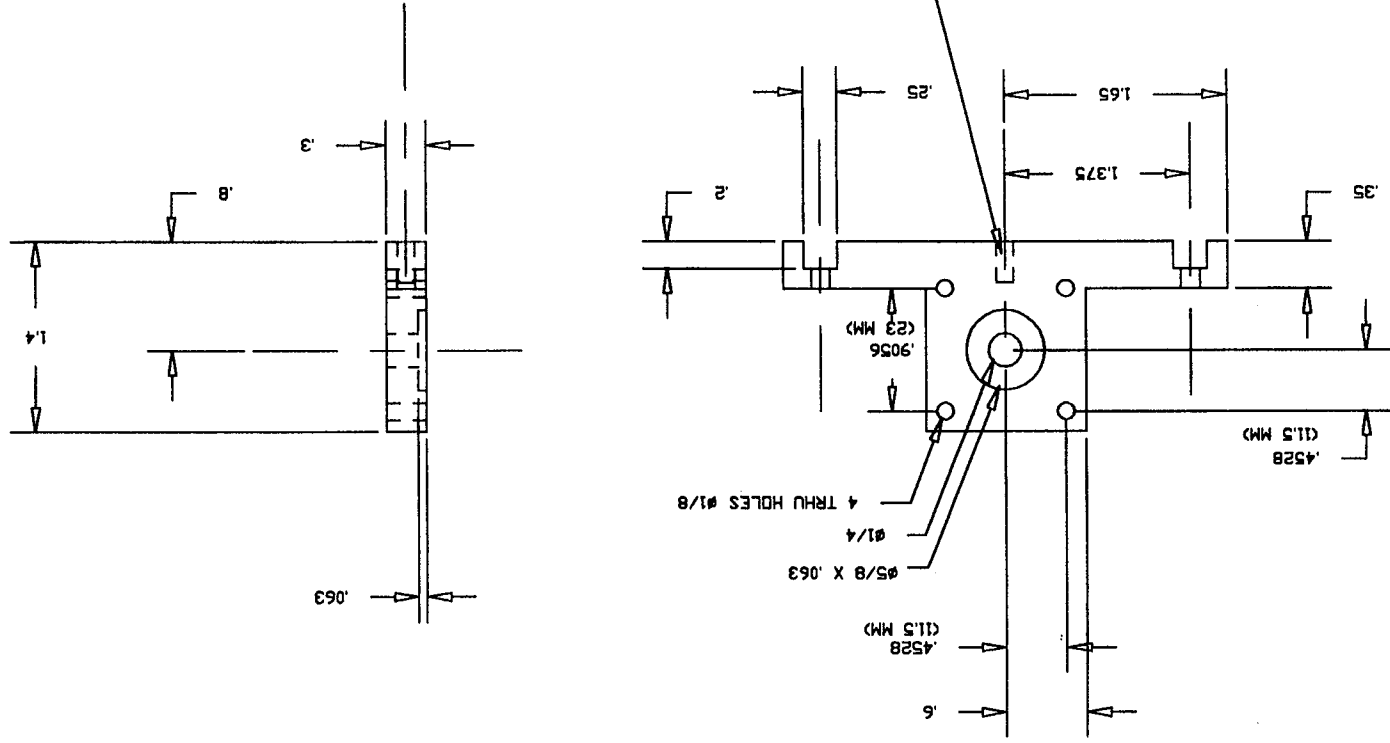
NOTES:

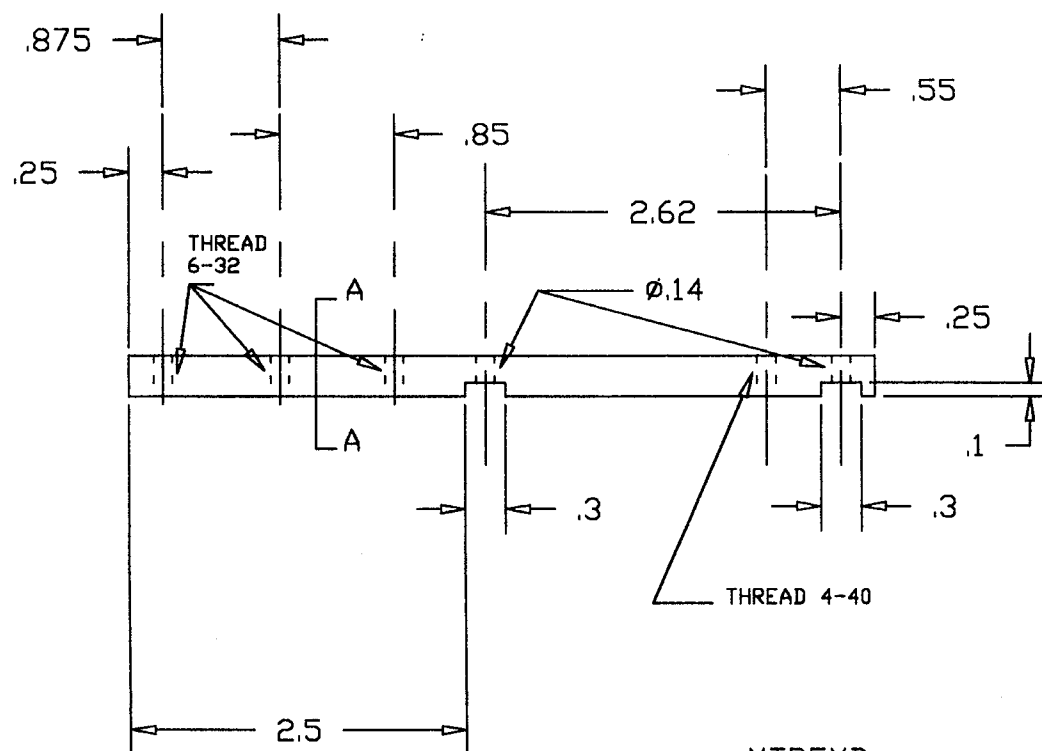
1. DIMENSIONS IN INCHES
2. ALUMINUM 6061-T6
3. TOLERANCE $\pm .005$ UNLESS OTHERWISE SPECIFIED
4. QUANTITY: 1

ROLLEND
DRAWING: ROLL_END.DWG
02 APR 93

NELSON PEDREIRO
(415) 725-3297

DRAWING: MOTORFIX.DWG





MTRFXB

DRAWING: ROLL3.DWG

NOTES:

1. DIMENSIONS IN INCHES
2. ALUMINUM - 6061-T6
3. TOLERANCE $\pm .005$ IN. IF NOT SPECIFIED
4. QUANTITY = 2

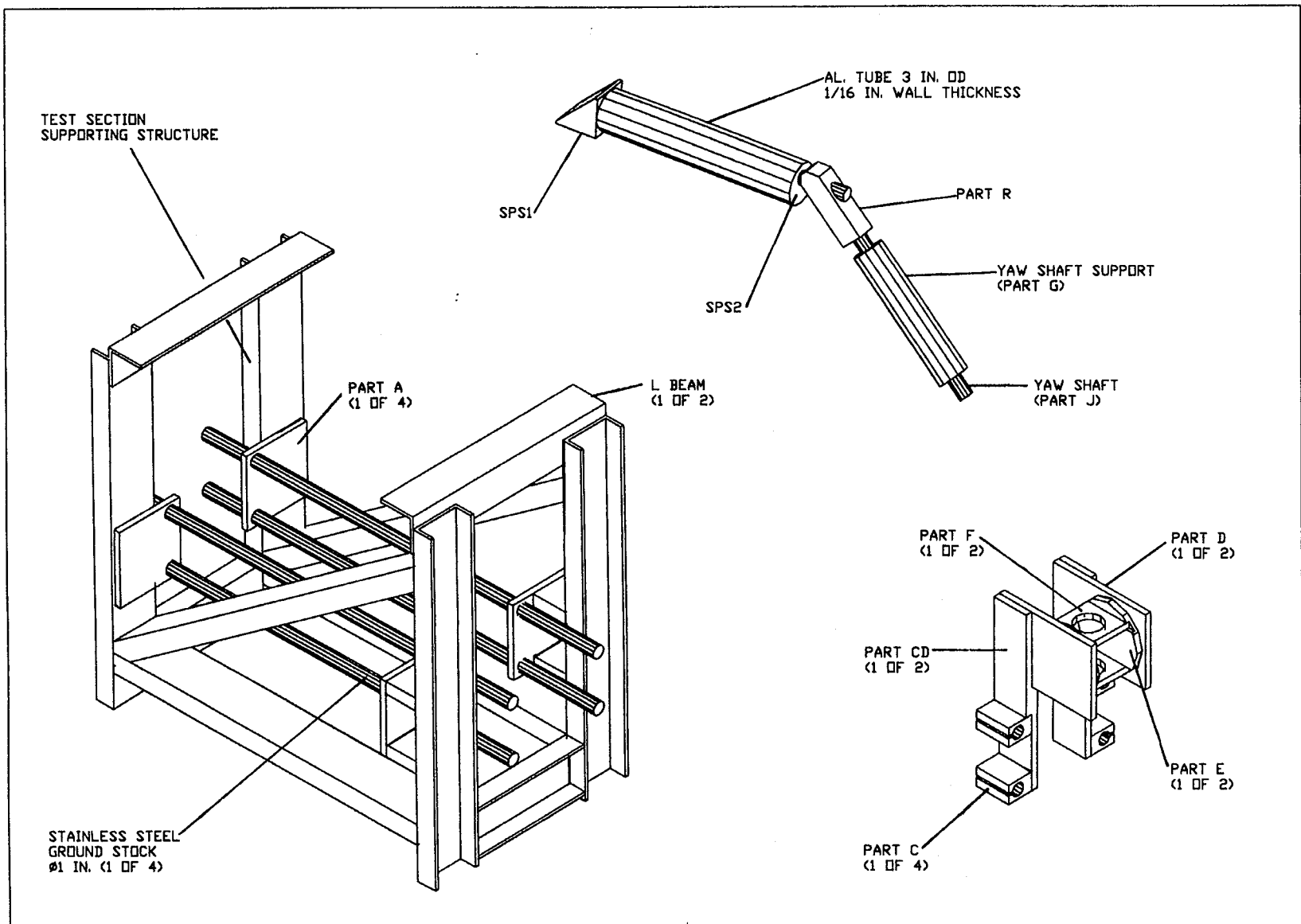
C.2 Yaw Sub-system

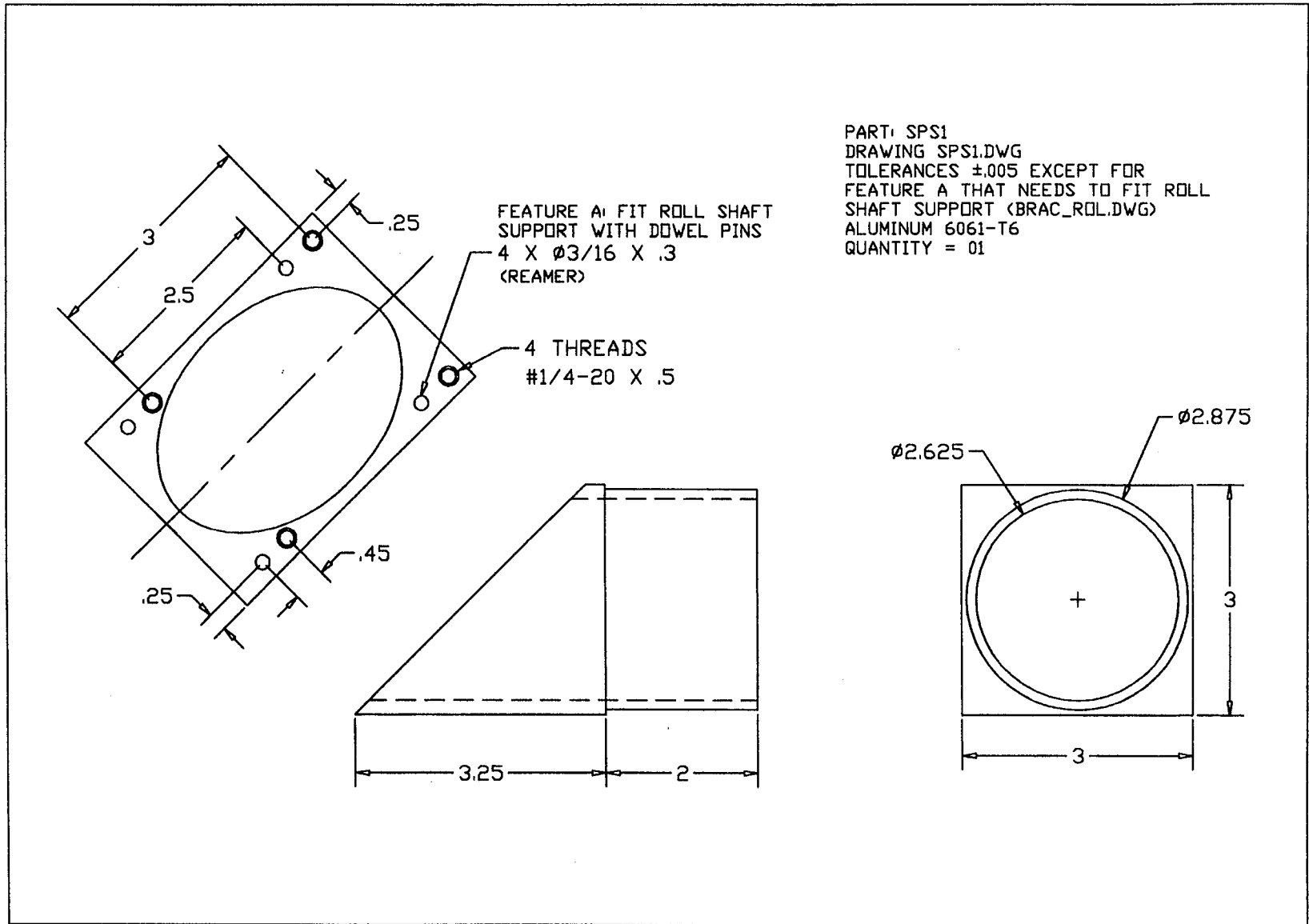
Assembly drawings are presented in Figure C.2 for the main components of the yaw subsystem. Parts SPS1 and SPS2 are welded to a 20.2 inch long aluminum tube with 3 inch external diameter and 1/16 inch wall thickness, the resulting part is used to connect the roll sub-system to the yaw shaft trough part R. Rotation about the γ or 'yaw' axis is obtained by mounting the yaw shaft to a co-axial aluminum structure, the yaw shaft support, through the use of bearings¹. The yaw shaft support is mounted to part F which with parts C, CD, E, and D form an assembly that is mounted to the test section supporting structure. The test section is bolted to the two L- beams shown in the figure, it has a cut on the bottom wall to allow the entrance of the roll shaft in the test section.

Parts C can slide on the four parallel stainless steel ground stock to allow adjustment of the position of the whole system along the longitudinal axis of the test section. The yaw shaft support, part G, can be fixed to part F at any position within a certain range to allow for the adjustment of the distance between the wind tunnel model and the bottom wall of the test section. Parts E are mounted to parts D through the use of shoulder screws and allow for adjustment of the incidence angle in the range from 35 to 55 degrees.

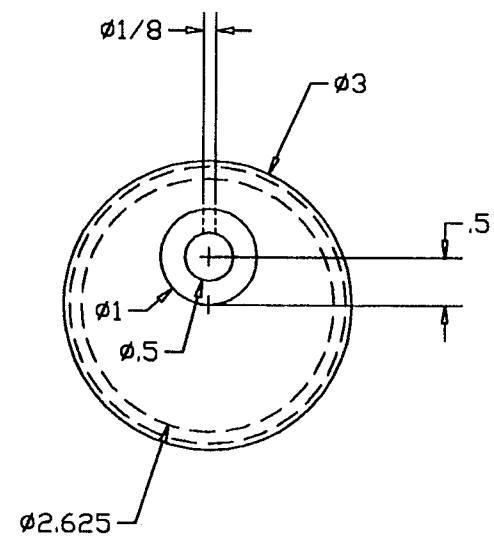
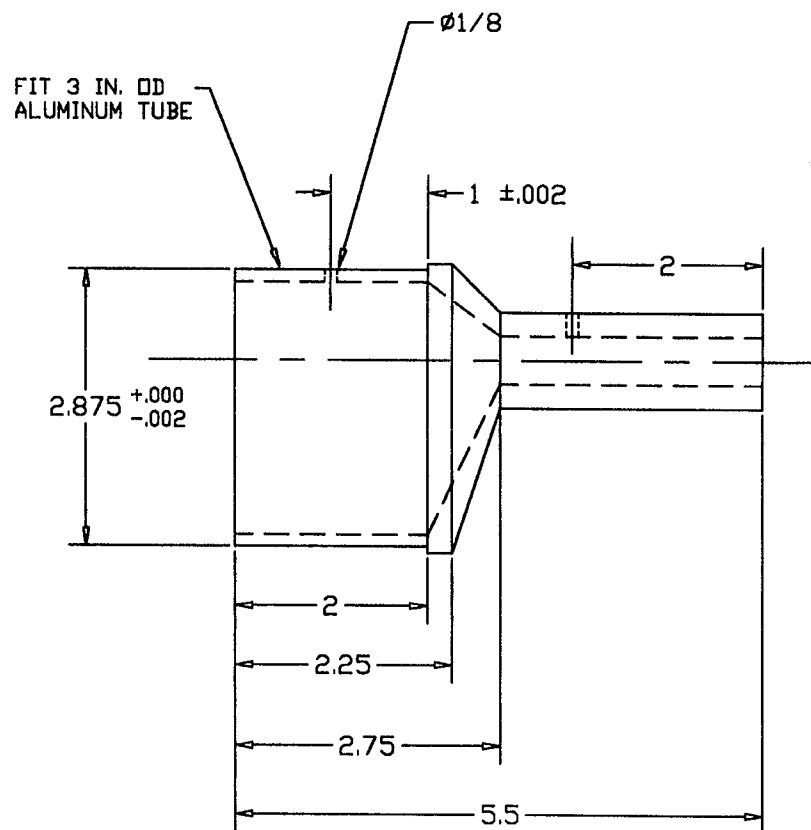
¹ BERG Ball Bearings - #B1-21 - UNSHIELDED.

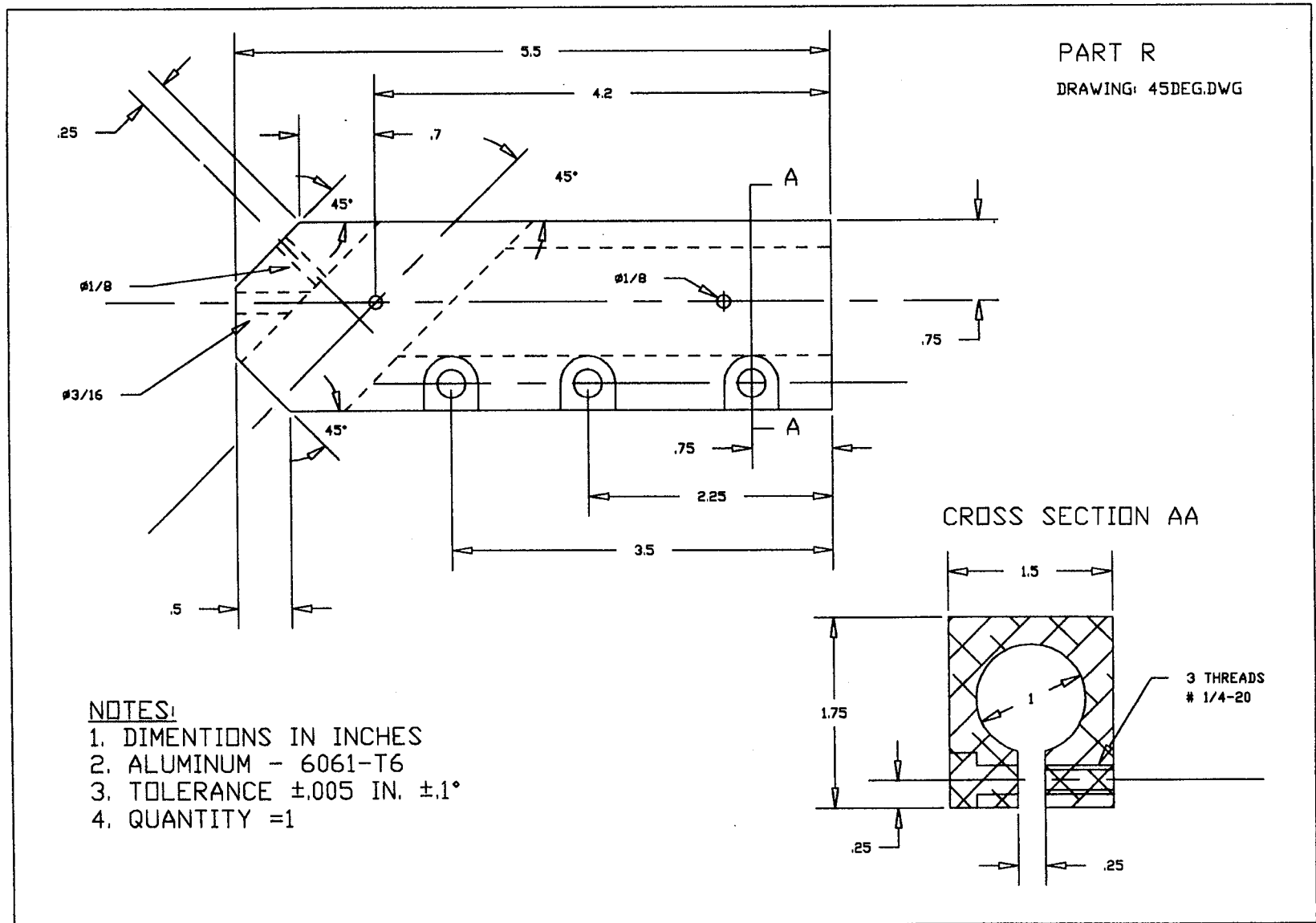
Figure C.2: Yaw system assembly drawing.





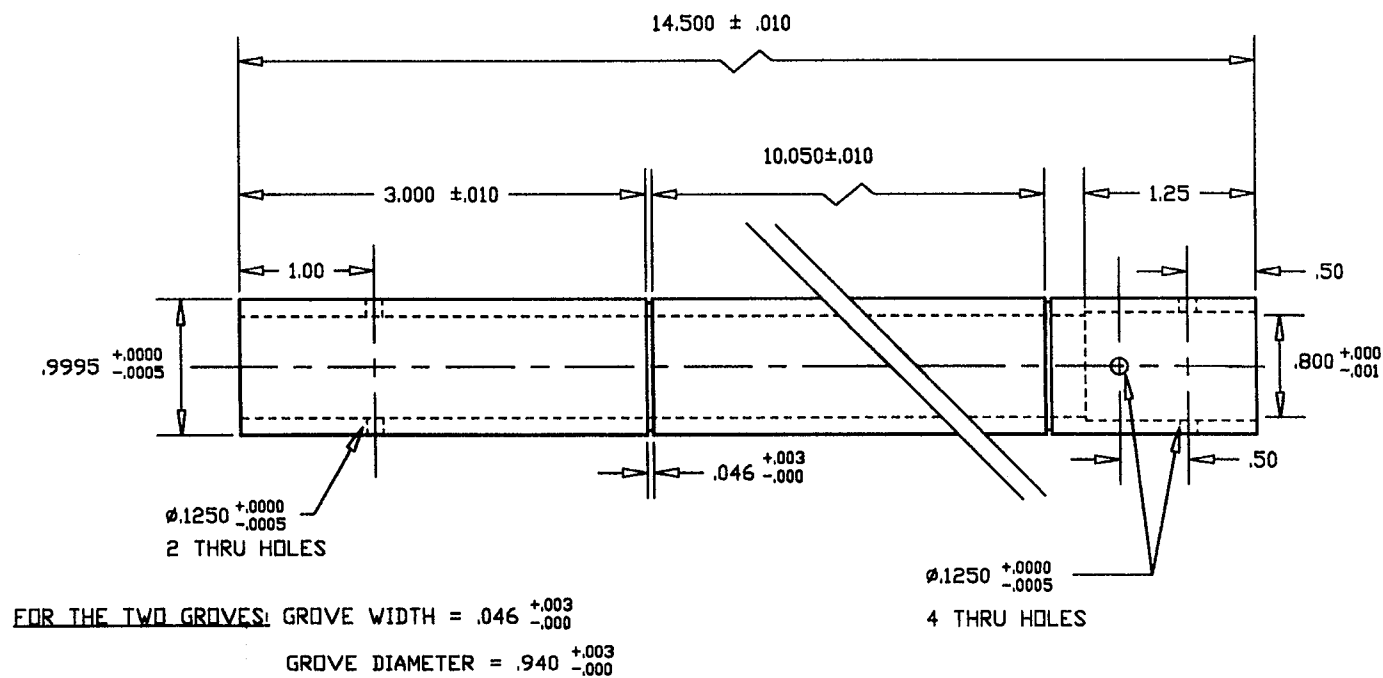
PART: SPS2
DRAWING SPS2.DWG
TOLERANCES ±.005 IF NOT SPECIFIED
ALUMINUM 6061-T6
QUANTITY = 01





NOTES:

1. DIMENSIONS IN INCHES
2. STAINLESS STEEL TUBE - CENTERLESS GROUND
3. WALL THICKNESS 1/8 IN.
4. QUANTITY 1
5. SEE DRAWING J02 FOR DETAILS OF PART BETWEEN GROVES

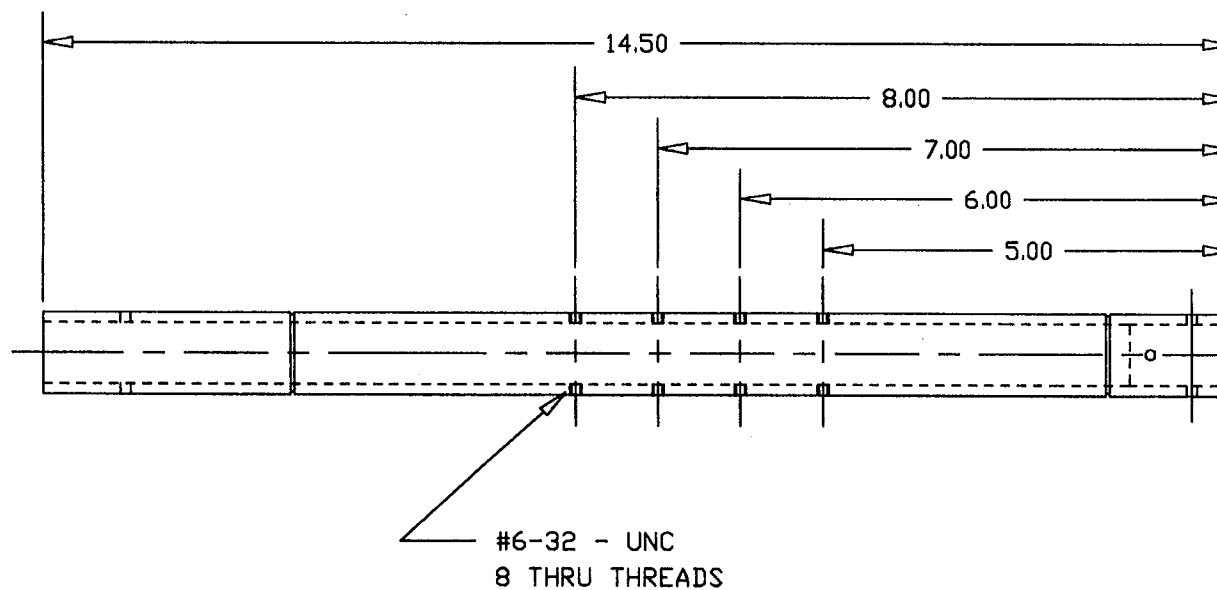


PART J
 J01
 SCALE 1:1

NOTES:

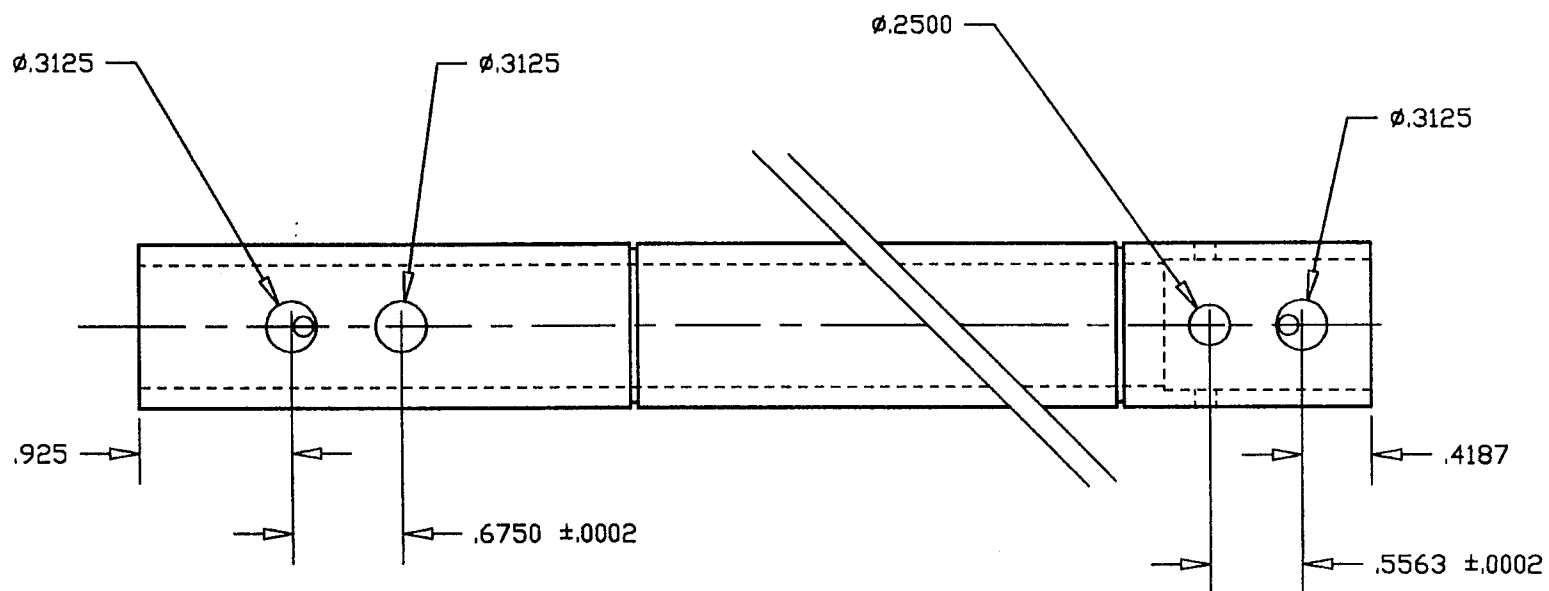
1. DIMENSIONS IN INCHES
2. STAINLESS STEEL TUBE - CENTERLESS GROUND
3. WALL THICKNESS 1/8 IN.
4. QUANTITY 1

OVERALL VIEW



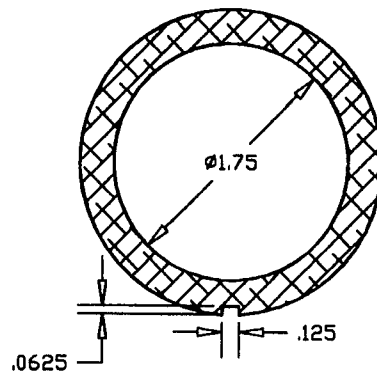
PART J
J02
SCALE 1/2

THIS SHAFT HAS $\phi 1/8$ HOLES AS SHOWN
 HOLES WITH $\phi 1/4$ AND $\phi 5/16$ FOR DOWEL PINS ARE
 TO BE ADDED AS SHOWN



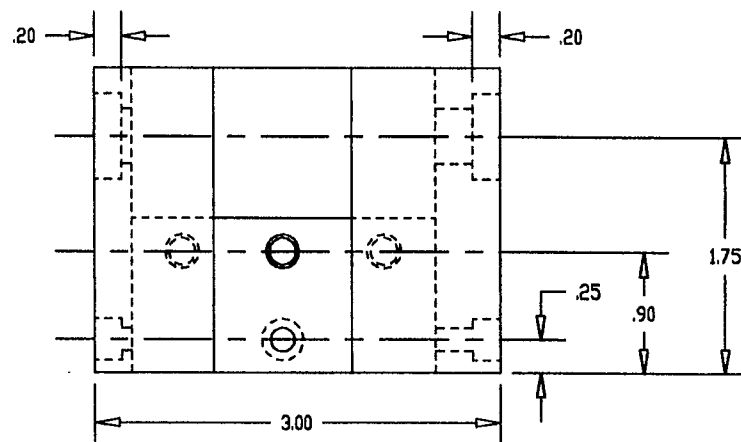
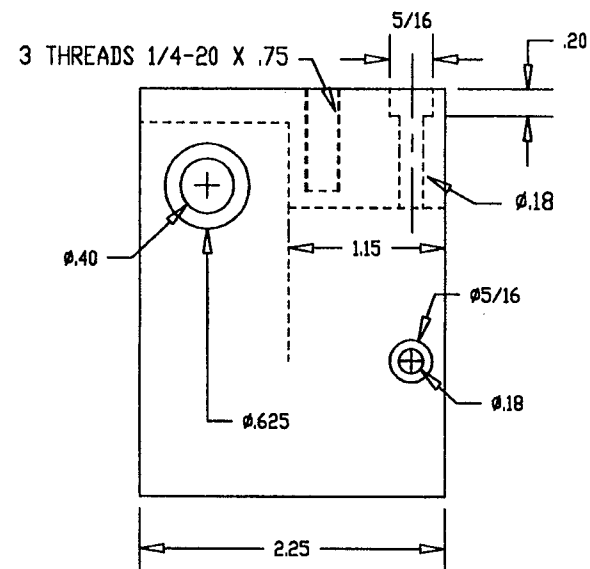
MODIFIED AS OF 05JAN94
 DRAWING: YAWSYS6M
 NELSON PEDREIRO (415) 725-3297

PART J
 DIMENSIONS IN INCHES
 SCALE 1:1



- NOTES:**
1. DIMENTIONS IN INCHES
 2. AL. 6061-T6 TUBE, WALL THICKNESS 1/4 IN.
 3. TOLERANCE ± 0.10 IN. IF NOT SPECIFIED
 4. QUANTITY = 1

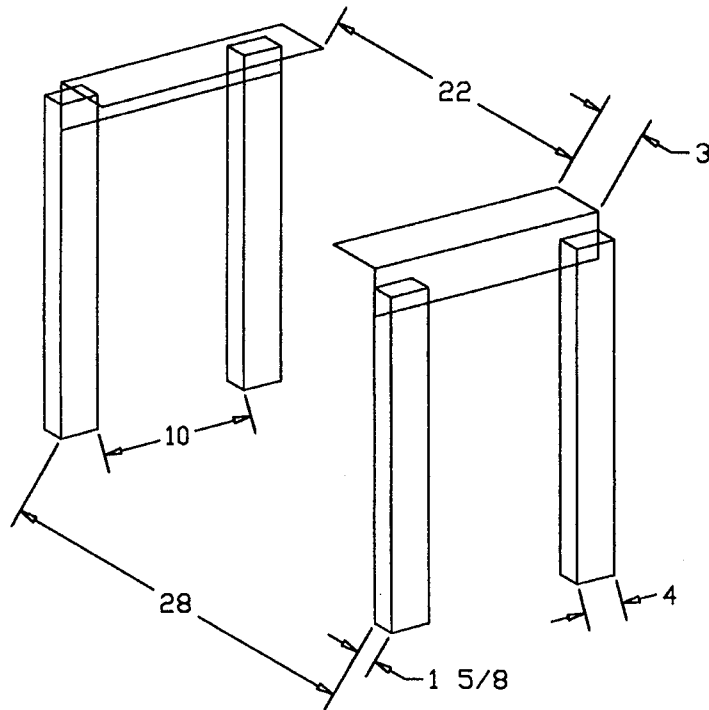
PART G
G01
SCALE 1/2



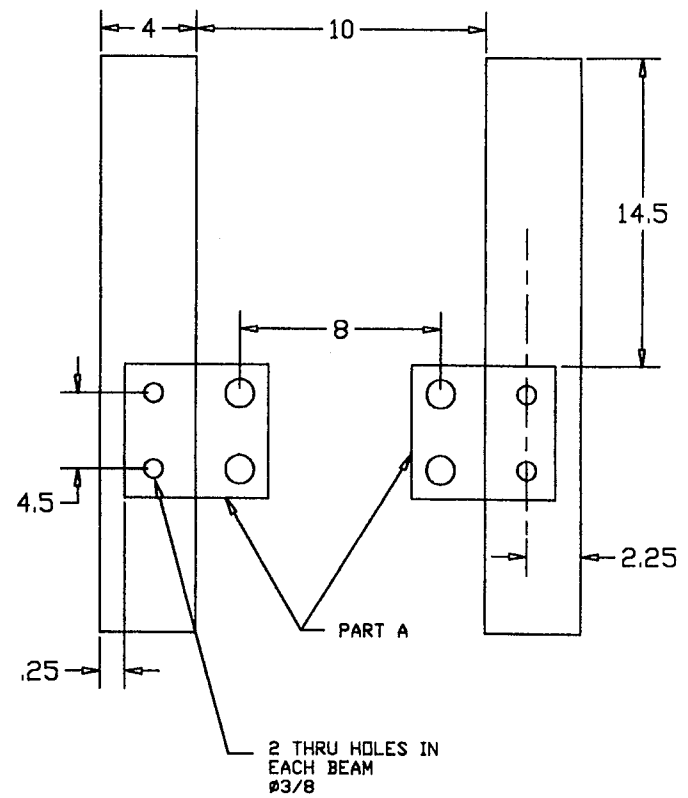
1. DIMENSIONS IN INCHES
2. ALUMINUM - 6061 - T6
3. TOLERANCE $\pm .005$ WHEN NOT SPECIFIED
4. QUANTITY = 1

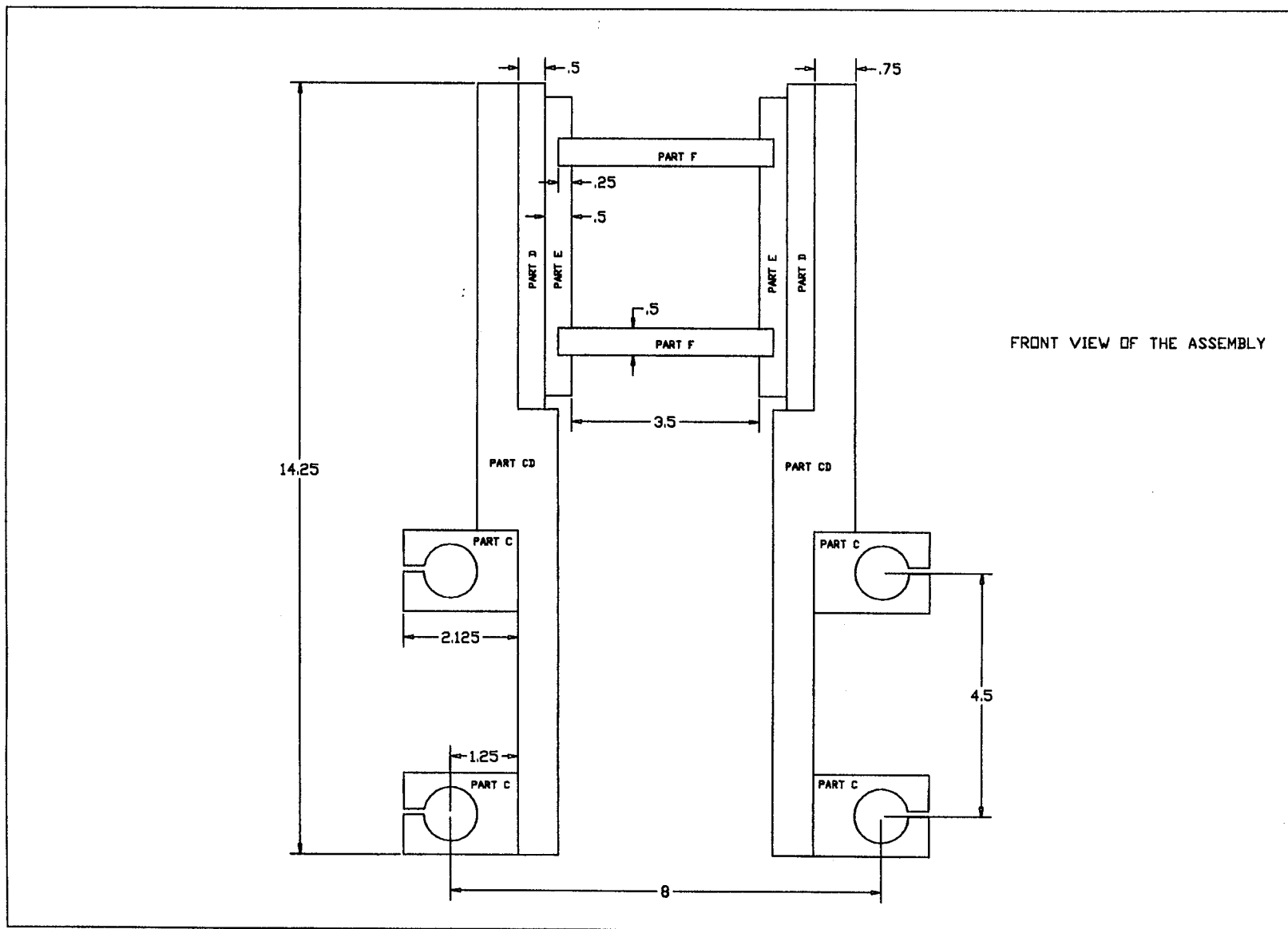
PART G1
G11

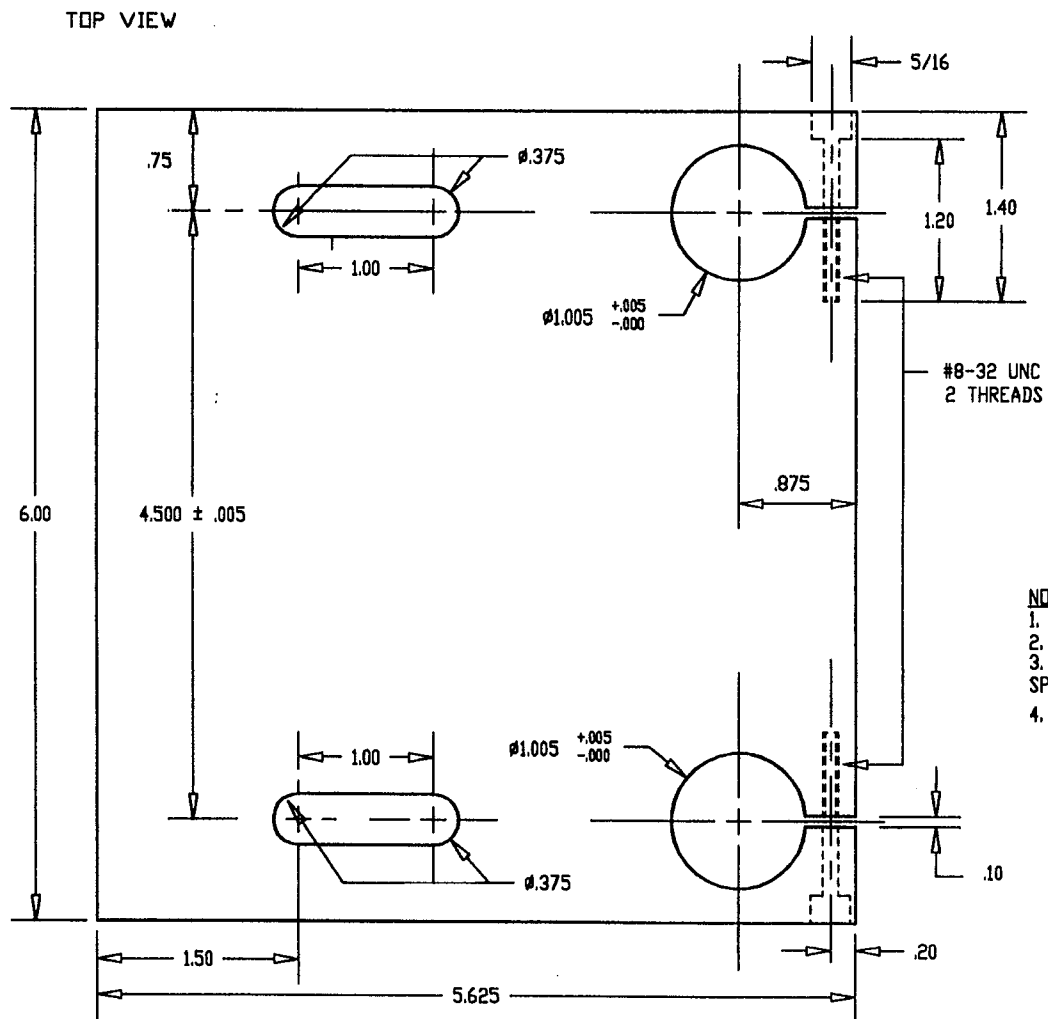
DIMENSIONS OF THE TEST SECTION SUPPORT
 DIMENSIONS ARE IN INCHES
 DRAWING IS NOT TO SCALE



FRONT VIEW OF THE SUPPORT
 DETAILS ON ATTACHEMENT OF PART A
 DRAWING NOT SCALE
 DIMENSIONS IN INCHES



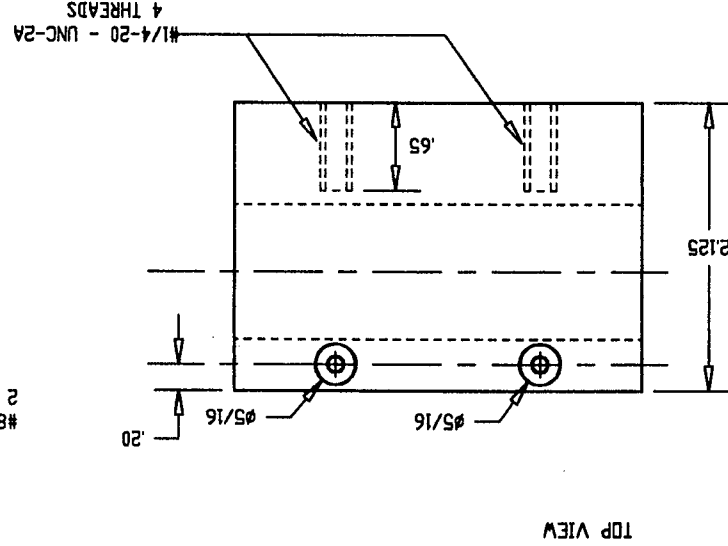
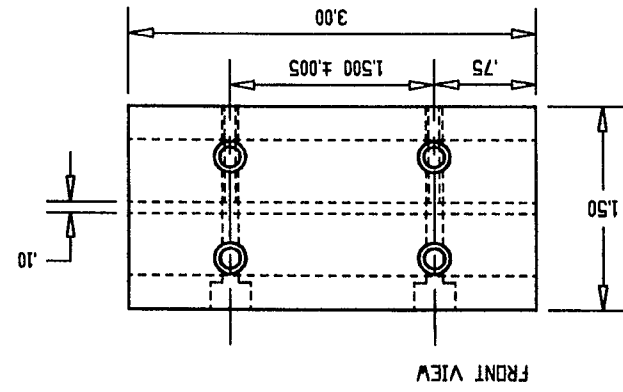
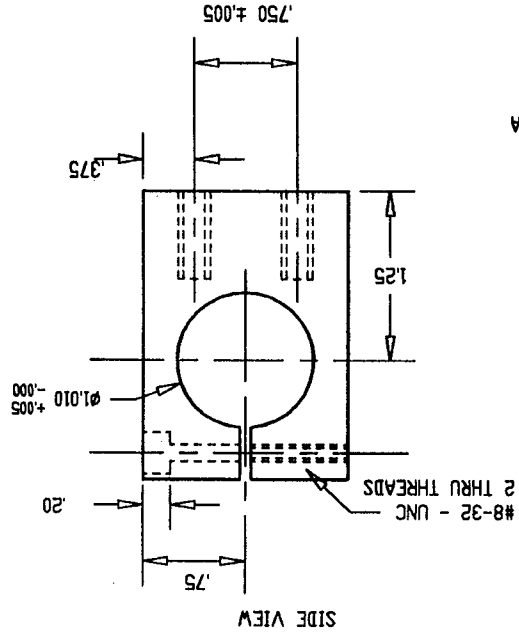


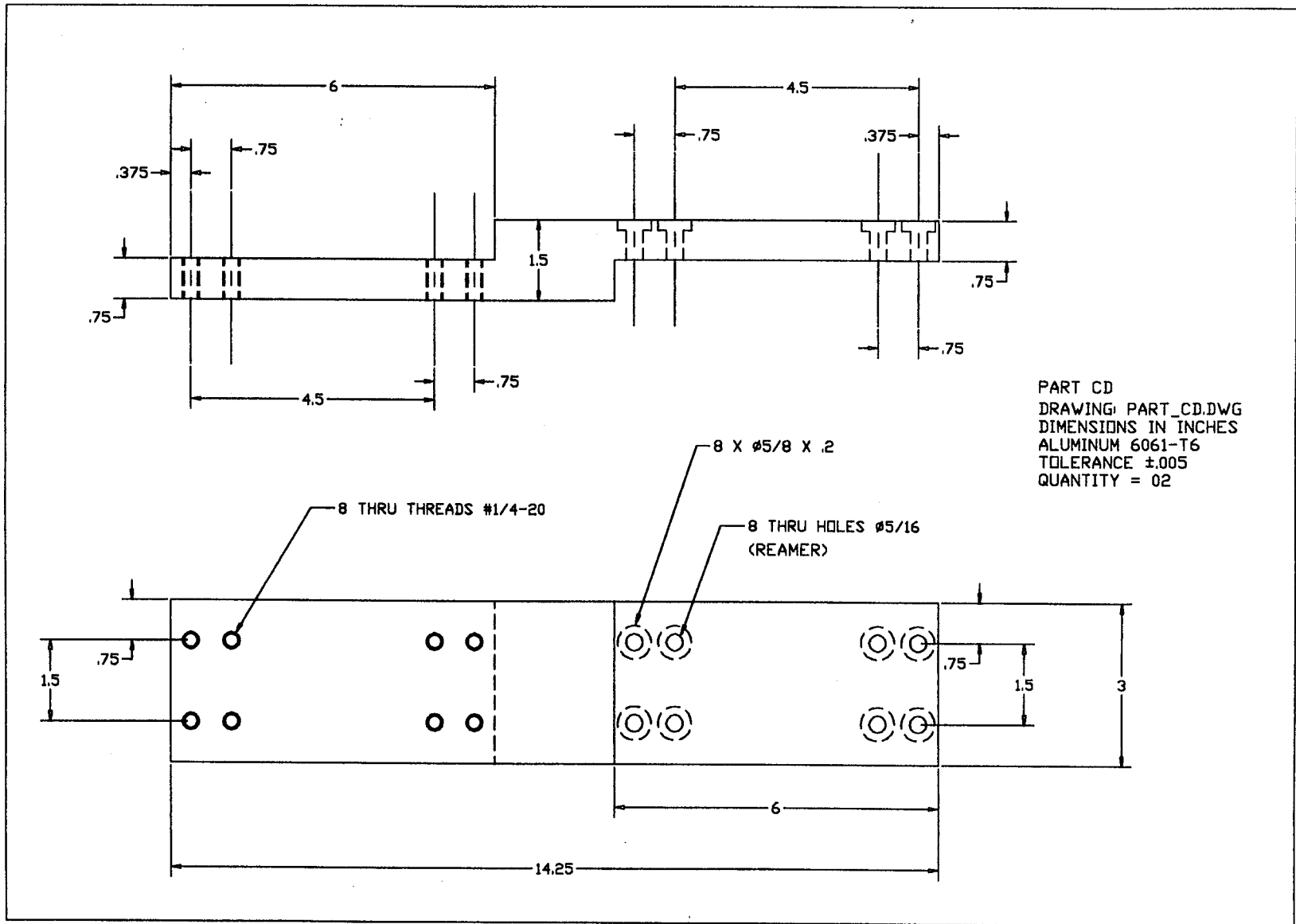


- NOTES:**
1. ALL DIMENSIONS IN INCHES
 2. ALUMINUM - JIG PLATE 1/2 IN. THICK
 3. TOLERANCE $\pm .010$ IN. WHEN NOT SPECIFIED
 4. QUANTITY = 4

PART A
A01
SCALE 1:1

NOTES:
1. ALL DIMENSIONS IN INCHES
2. ALUMINUM - 6061 - T6
3. TOLERANCE $\pm .010$ IN. WHEN NOT SPECIFIED
4. QUANTITY = 4

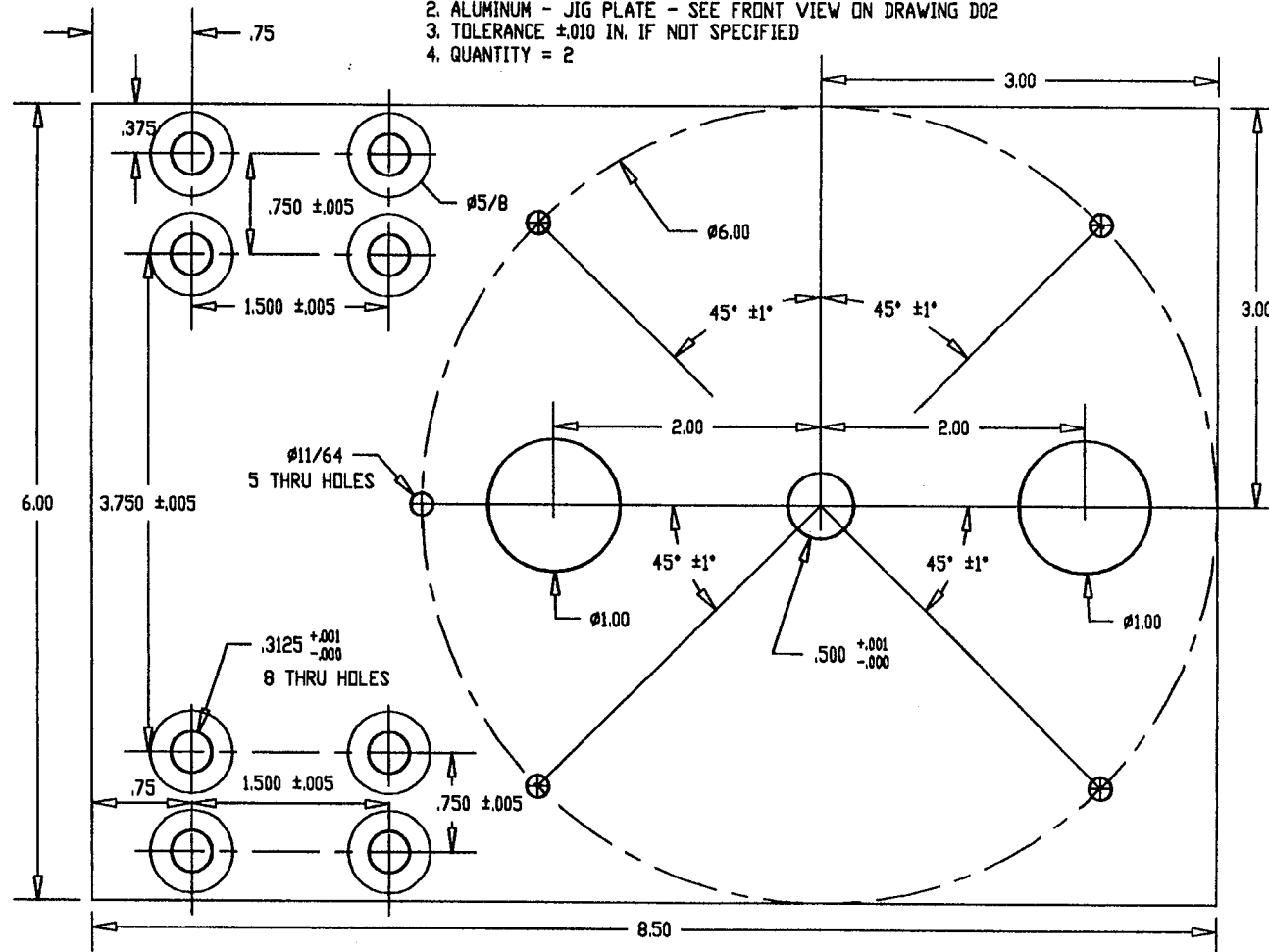




TOP VIEW

NOTES:

1. ALL DIMENSIONS IN INCHES
2. ALUMINUM - JIG PLATE - SEE FRONT VIEW ON DRAWING D02
3. TOLERANCE ± 0.010 IN. IF NOT SPECIFIED
4. QUANTITY = 2

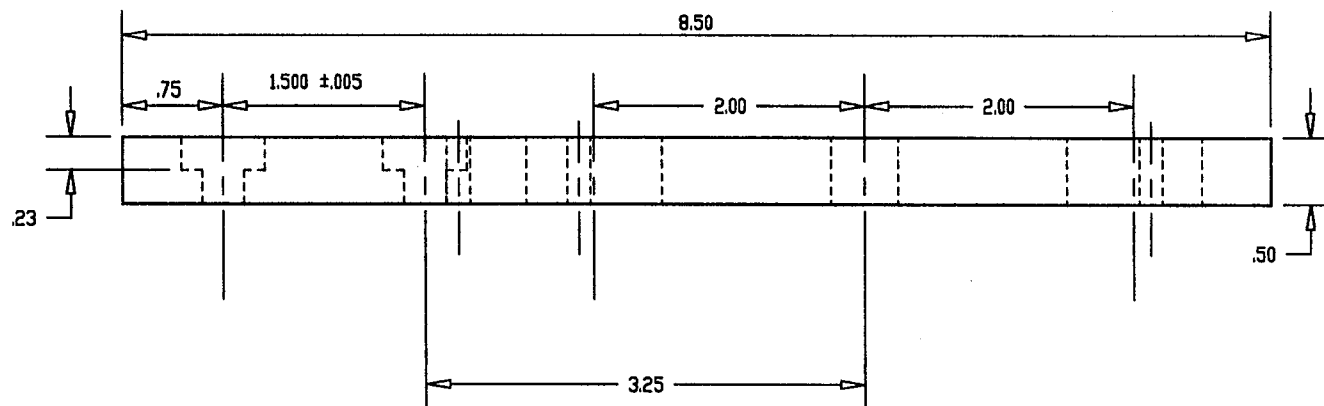


PART D
D01
SCALE 1:1

NOTES:

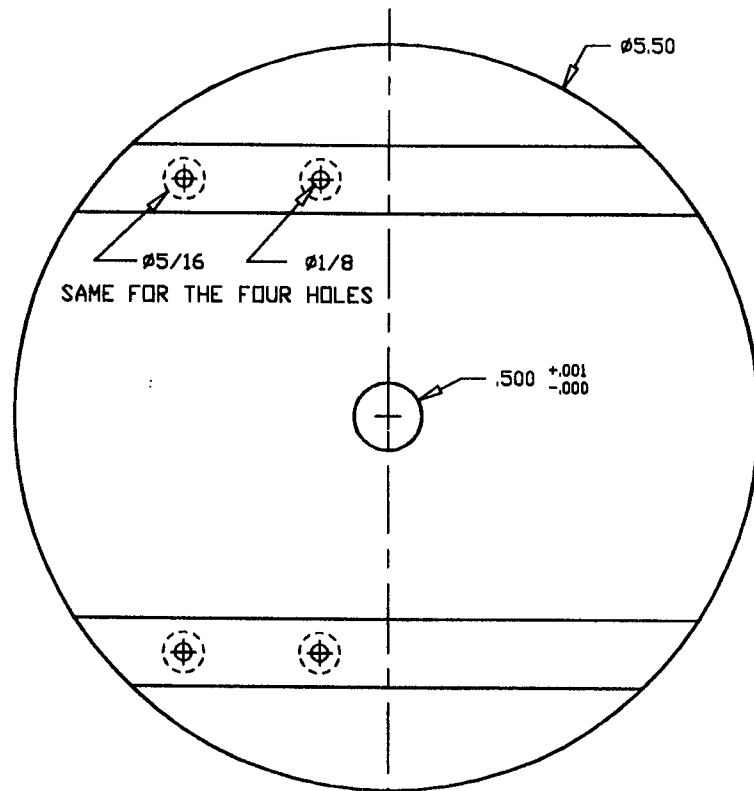
- NOTES:
1. ALL DIMENSIONS IN INCHES
 2. ALUMINUM - JIG PLATE
 3. TOLERANCE ± 0.010 IF NOT SPECIFIED
 4. QUANTITY = 2

FRONT VIEW

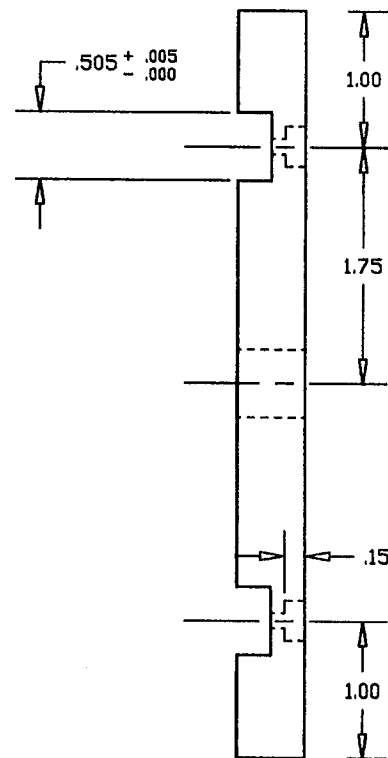


PART D
D02
SCALE 1:1

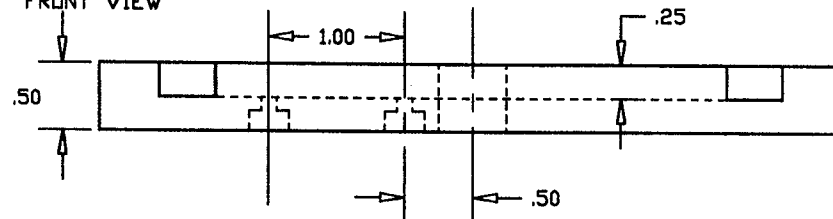
TOP VIEW



SIDE VIEW



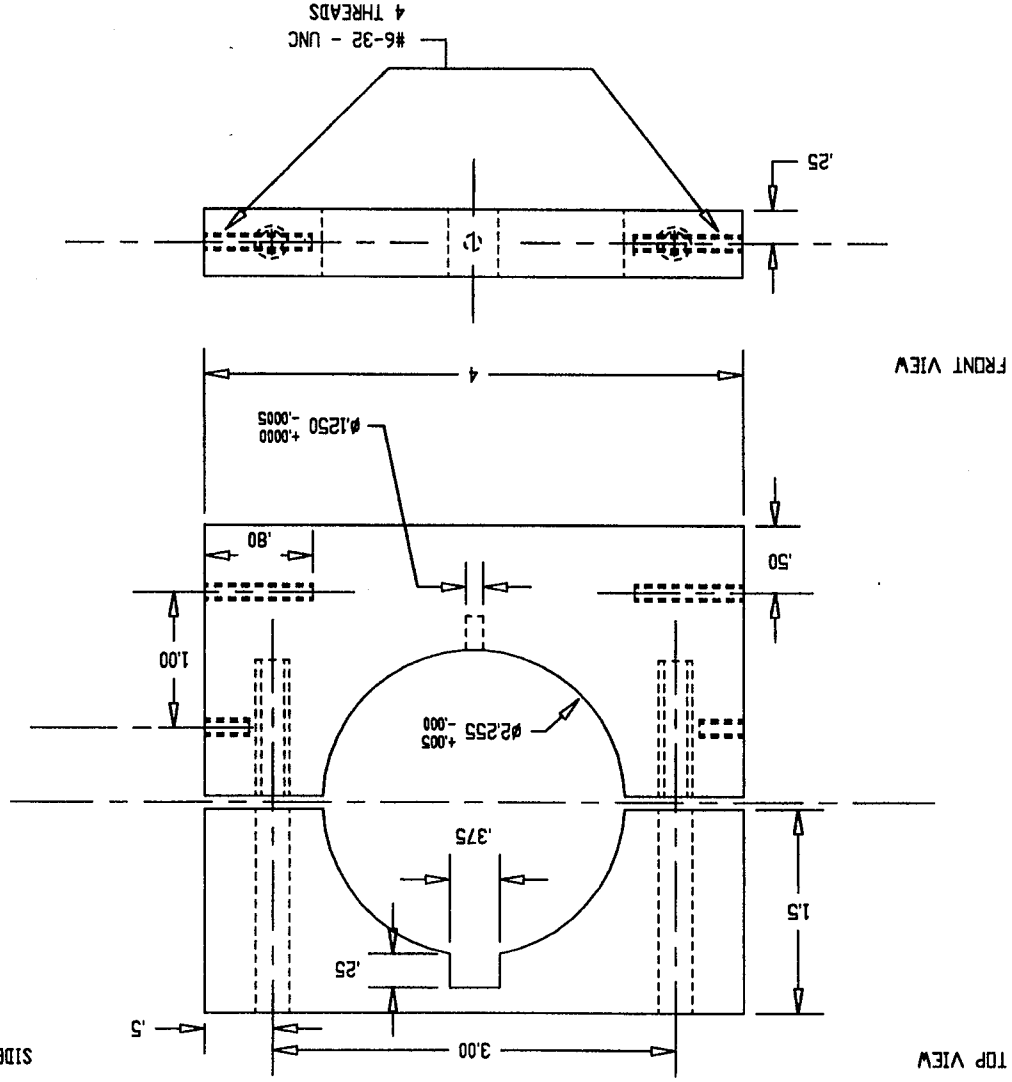
FRONT VIEW



NOTES:

1. ALL DIMENSIONS IN INCHES
2. ALUMINUM - JIG PLATE
3. TOLERANCE $\pm .010$ IN. IF NOT SPECIFIED
4. QUANTITY = 2

PART E
E01
SCALE 1:1

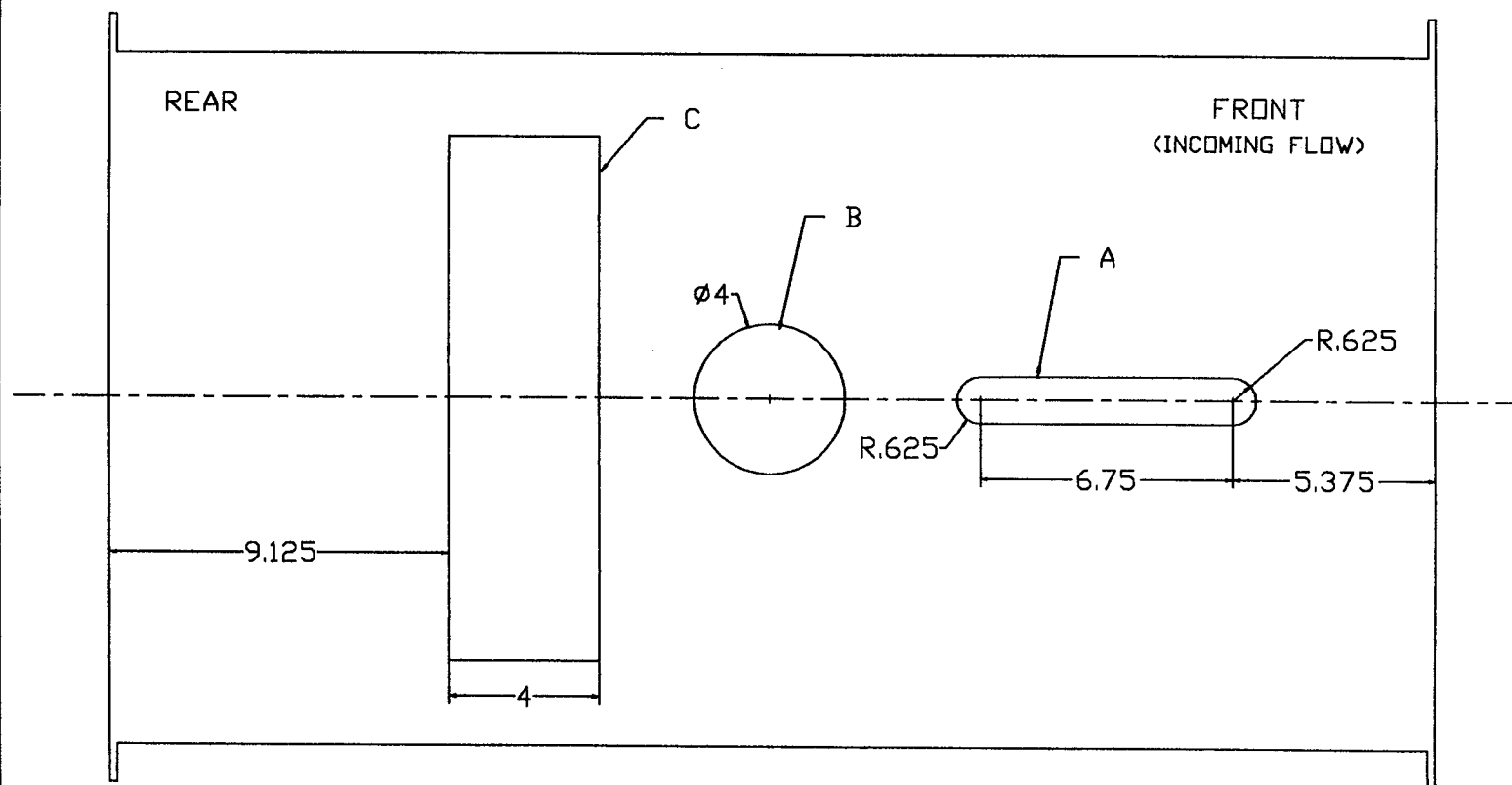


- NOTES:
1. ALL DIMENSIONS IN INCHES
 2. ALUMINUM - JIG PLATE
 3. TOLERANCE $\pm .010$ IN. IF NO SPECIFIED
 4. QUANTITY = 2
 5. FIT PART E

PART F
FOI
SCALE 1:1

TOP VIEW OF THE TEST SECTION BOTTOM WALL WITH CUT OUT DETAILS

1. CUTS A AND B ARE NOT USED AND ARE CLOSED
 2. CUT C ALLOWS THE ROLL SHAFT TO ENTER THE TEST SECTION
IT IS SHOWN AT ITS MAXIMUM SIZE AND IS PARTIALLY CLOSED
DURING EXPERIMENTS
- DIMENSIONS ARE IN INCHES. TOLERANCE ± 0.025



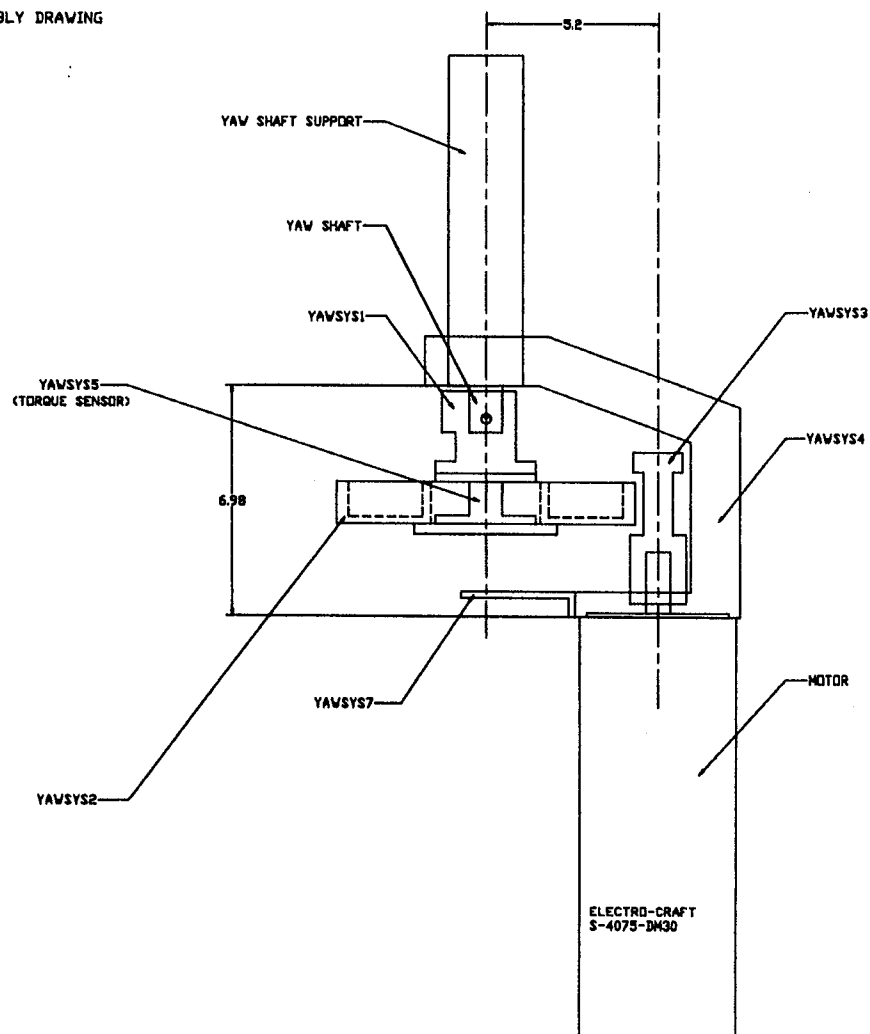
C.3 Active Cancellation Sub-system

The mechanical assembly drawing for the components of the active cancellation system is shown on Figure C.3. As seen, part YAWSYS1 connects to the yaw shaft and part YAWSYS3 to the yaw shaft support.

It is necessary to describe the location of some components not shown in the assembly drawing: The accelerometers, used to measure the angular acceleration about the γ -axis, are mounted inside the pockets of part YAWSYS2. The potentiometer, used to measure the γ angle, is mounted to part YAWSYS7 and has its axle connected to part YAWSYS2 which rotates with the yaw shaft. The 1/16 inch diameter steel cable used to connect parts YAWSYS2 and YAWSYS3 and form the 10:1 reduction.

A second assembly drawing which shows an alternate location for the accelerometers is presented in Figure C.4. It should be noted that this is an optional mounting configuration that, to date, has not been used and is included only for completeness.

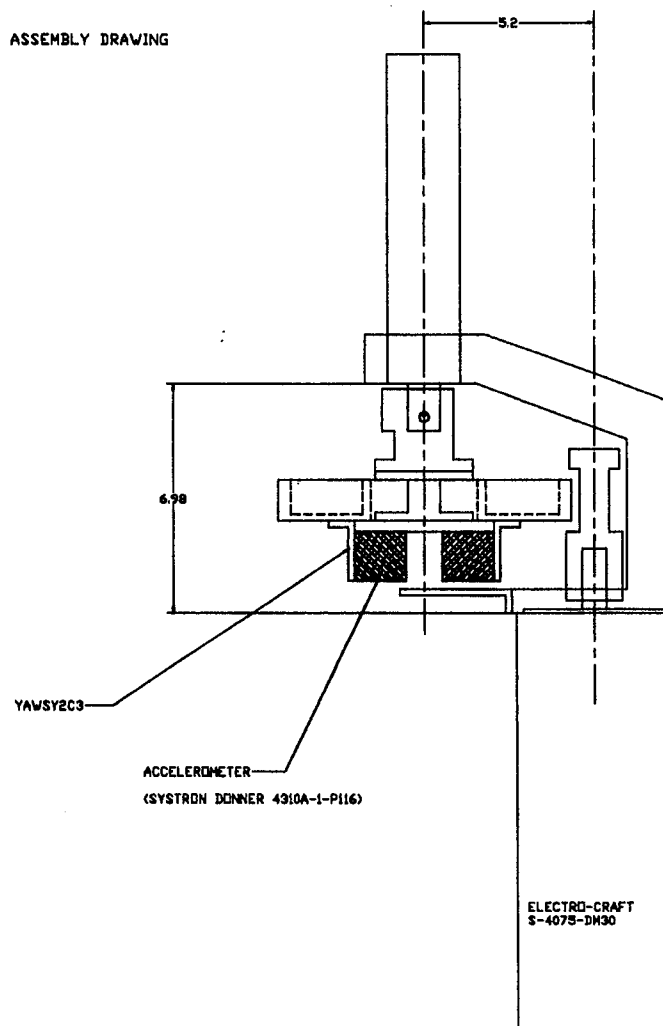
ACTIVE CANCELLATION SYSTEM ASSEMBLY DRAWING
DIMENSIONS IN INCHES



NELSON PEDREIRO
14 JAN 94
(415) 725-3297

Figure C.3: Active cancellation system assembly drawing.

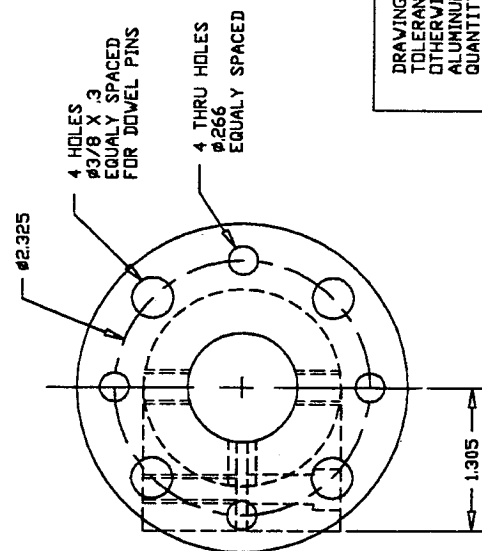
ACTIVE CANCELLATION SYSTEM ASSEMBLY DRAWING
DIMENSIONS IN INCHES



THE PREFERRED LOCATION FOR THE ACCELEROMETERS IS INSIDE THE POCKETS OF PART YAWSYS2. THEY ARE SHOWN HERE MOUNTED TO THE BOTTOM OF PART YAWSYS2 WHICH IS AN ALTERNATE LOCATION.

NELSON PEDREIRO
14 JAN 94
(415) 725-3297

Figure C.4: Alternate position for accelerometers.

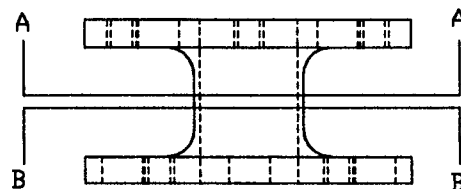
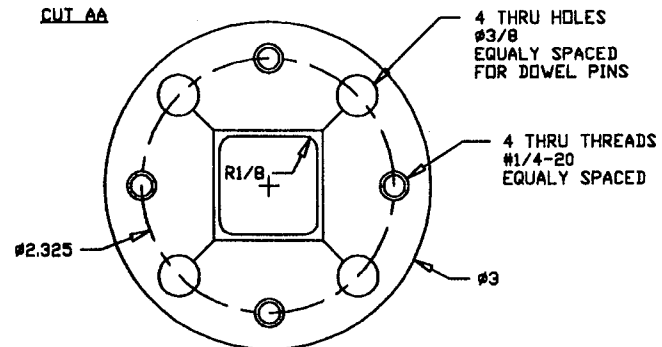


DRAWING: FAWSYS1B
TOLERANCES $\pm .005$ IN. UNLESS
OTHERWISE SPECIFIED
ALUMINUM 6061-T6
QUANTITY = 01

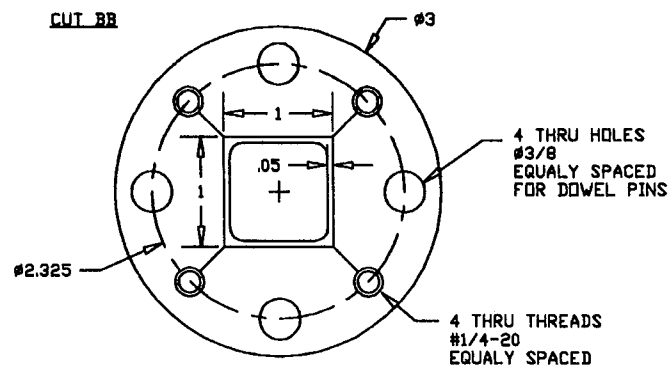
NELSON PEDREIRO (415) 725-3297

PART YAWSYS5

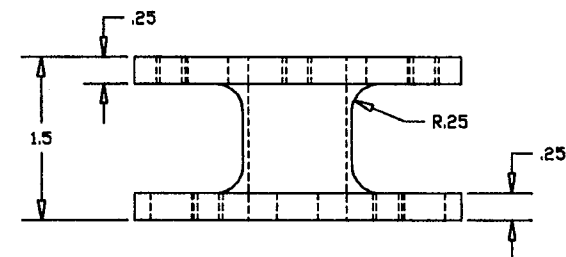
CUT AA



CUT BB



TORQUE SENSOR MECHANICAL COMPONENT

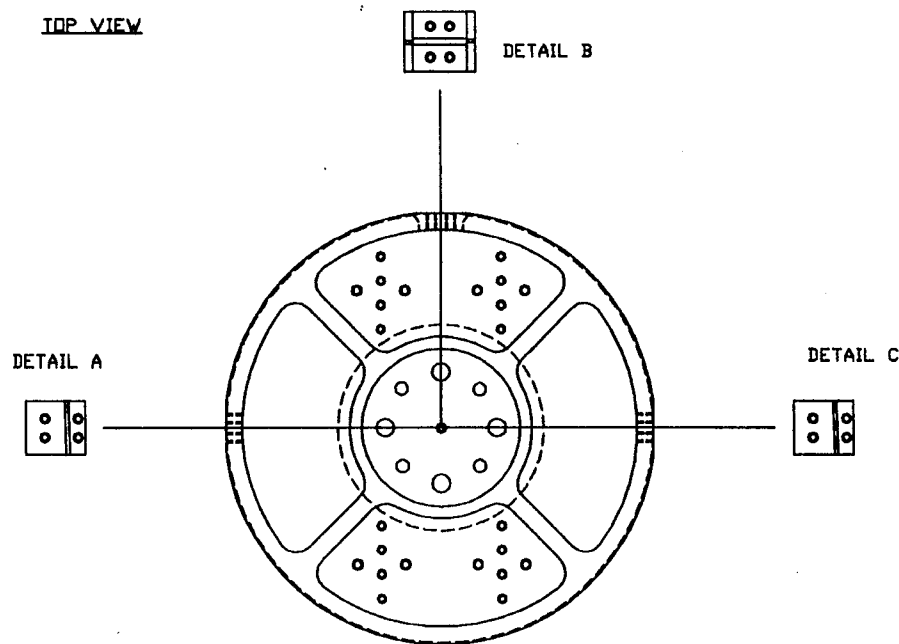


DRAWING: FAVSYS5B
TOLERANCES $\pm .005$ IN. UNLESS
OTHERWISE SPECIFIED
ALUMINUM 6061-T6
QUANTITY = 01

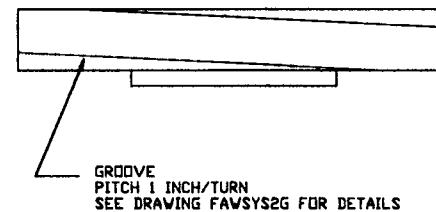
NELSON PEDREIRO (415) 725-3297

PART YAWSYS2: SEE ANEXED DRAWINGS FOR DIMENSIONS

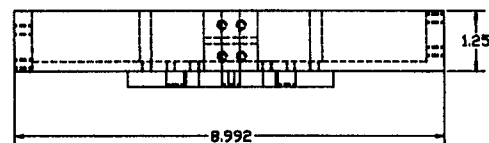
TOP VIEW



FRONT VIEW: ONLY CENTER LINE OF GROOVE IS SHOWN



FRONT VIEW: GROOVE NOT SHOWN

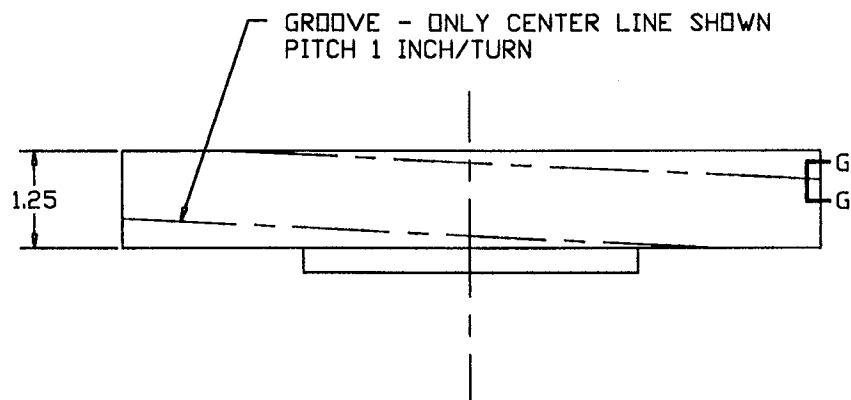


ANEXED DRAWINGS:

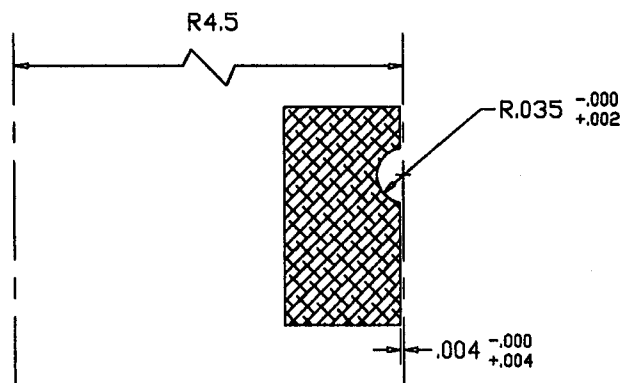
FAWSYS2G
FAWSYS2T
FAWSYS2F
FAWSYS2D
FAWSY2C1
FAWSY2C2

DRAWING: FAWSYS2B
DIMENSIONS IN INCHES
TOLERANCES ± 0.005 UNLESS
OTHERWISE SPECIFIED
ALUMINUM 6061-T6
QUANTITY = 01
NELSON PEDREIRO (415) 725-3297

FRONT VIEW: GROOVE DETAIL



CUT GG

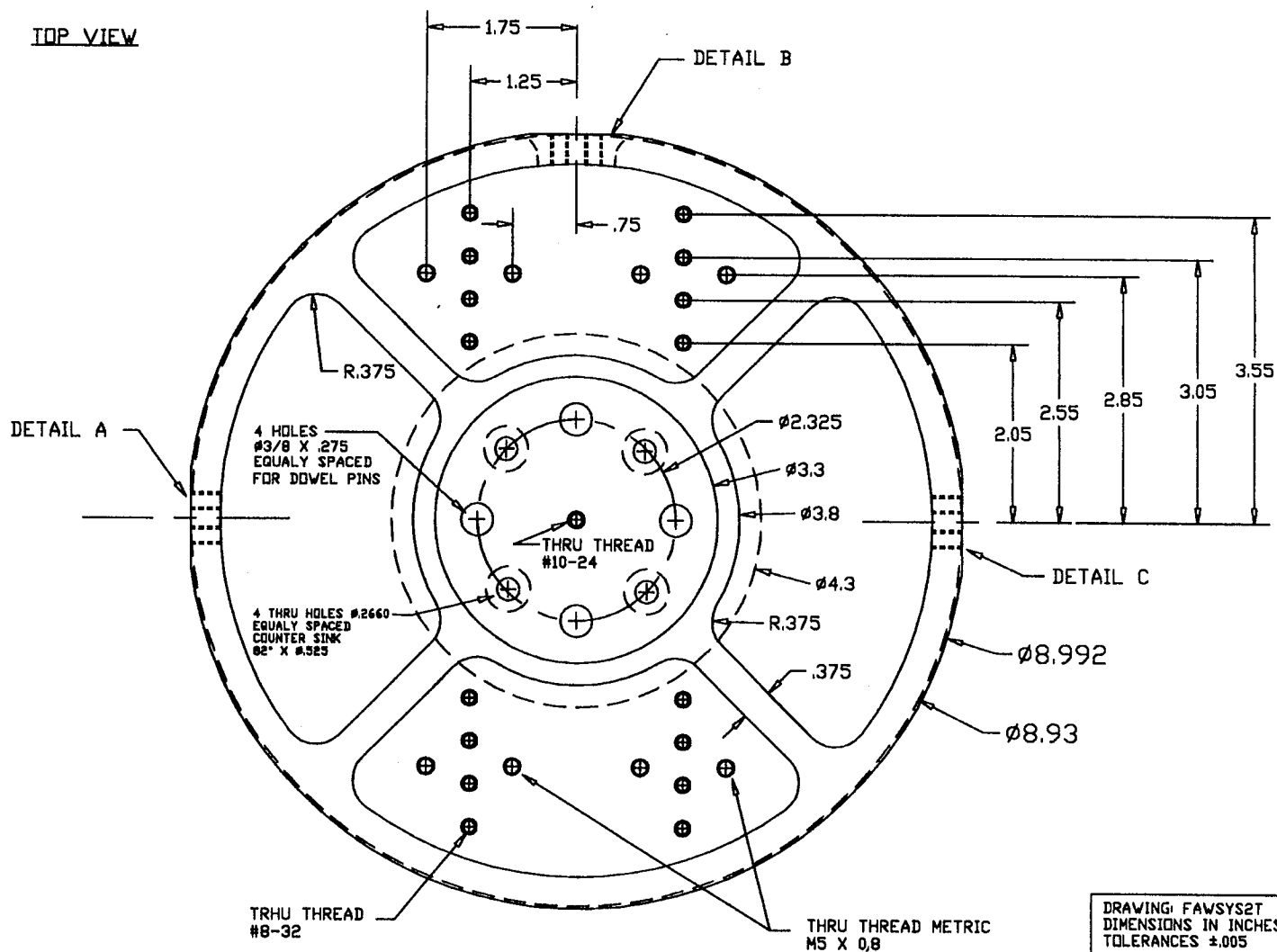


DRAWING: FAWSYS2G
DIMENSIONS IN INCHES
TOLERANCES $\pm .005$ UNLESS
OTHERWISE SPECIFIED

REFER TO DRAWING FAWSYS2B

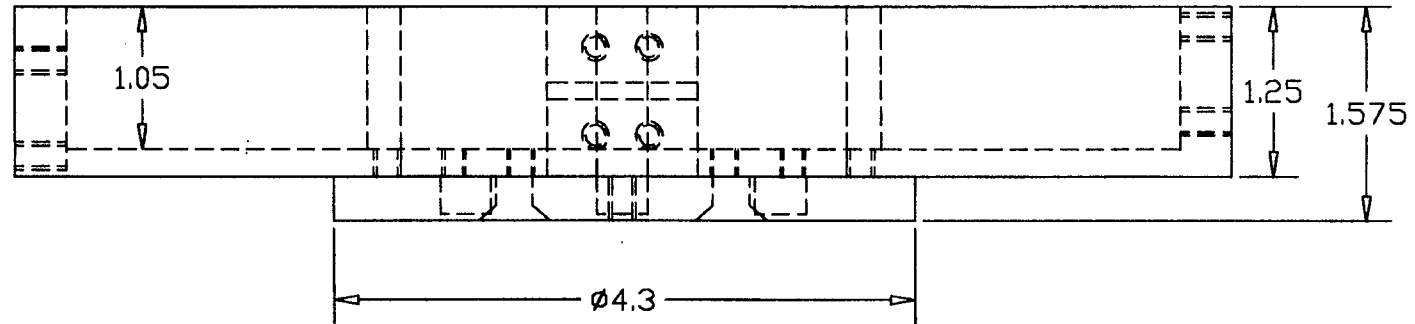
NELSON PEDREIRO (415) 497-2654

TOP VIEW



DRAWING: FAWSYS2T
DIMENSIONS IN INCHES
TOLERANCES ±.005
REFER TO DRAWING FAWSYS2B
NELSON PEDREIRO (415) 725-3297

FRONT VIEW: GROOVE NOT SHOWN

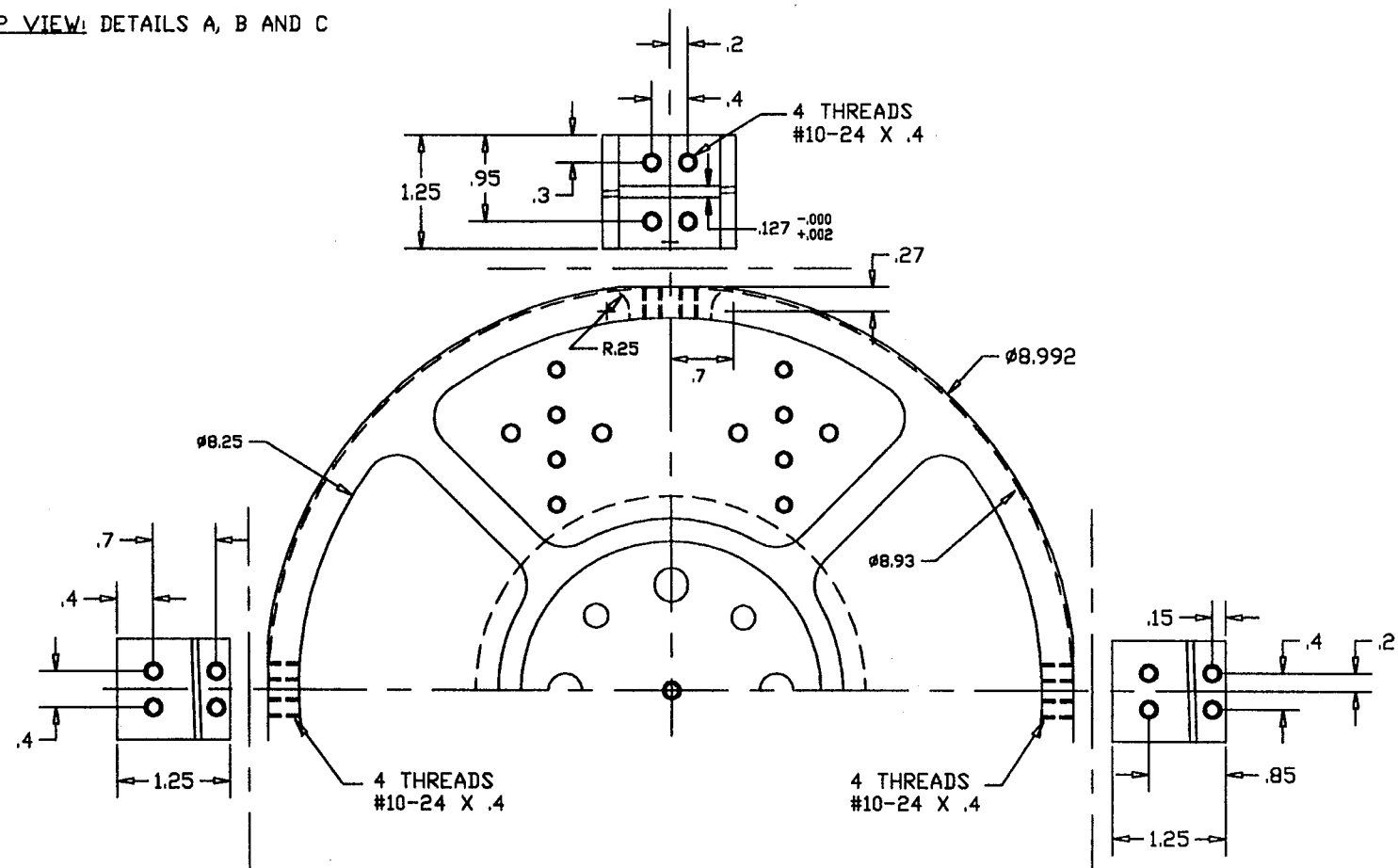


DRAWING: FAWSYS2F
DIMENSIONS IN INCHES
TOLERANCES ± 0.005 UNLESS
OTHERWISE SPECIFIED

REFER TO DRAWING FAWSYS2B

NELSON PEDREIRO (415) 725-3297

TOP VIEW: DETAILS A, B AND C



NOTE:
DETAILS A, B AND C ARE FLAT SURFACES TANGENT
TO CILINDER WITH Ø8.930 IN.

DRAWING: FAWSYS2D
DIMENSIONS IN INCHES
TOLERANCES $\pm .005$ IN.

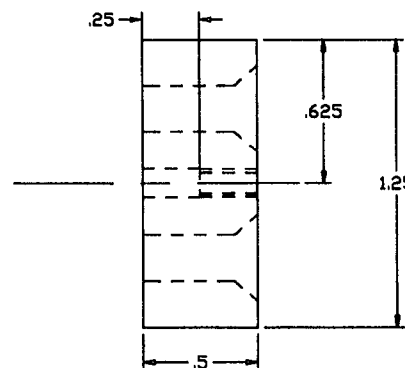
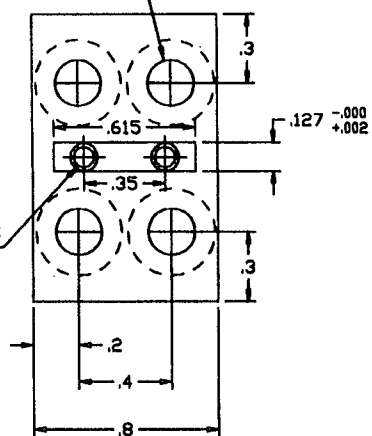
REFER TO DRAWING FAWSYS2B
NELSON PEDREIRO (415) 725-3297

PART YAWSYS2C1: FIT PART YAWSYS2B

WOODRUFF KEY ORDERED FROM BERG
STOCK NUMBER K1-12 (p.H537)

4 THRU HOLES ϕ .2010 (DRILL #7)
COUNTER SINK 82° X ϕ .375

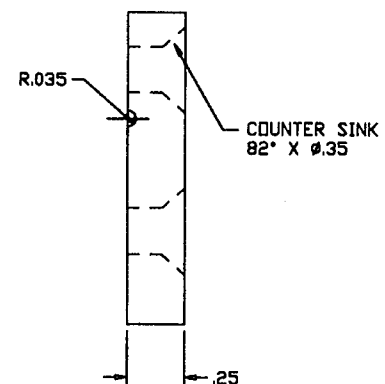
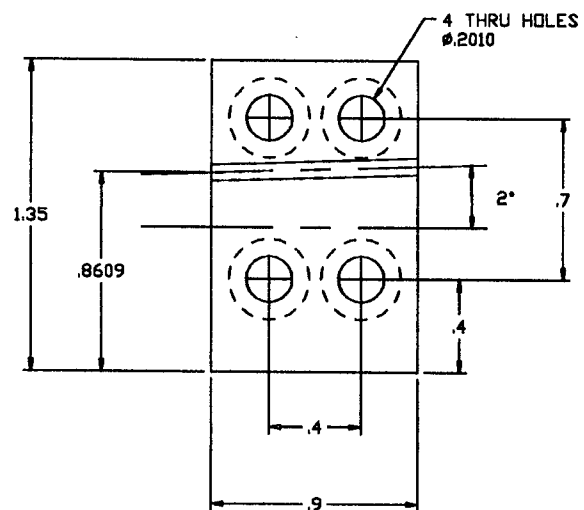
2 THRU THREADS
#4-40



DRAWING: FAWSY2C1
DIMENSIONS IN INCHES
TOLERANCES \pm .005 UNLESS
OTHERWISE SPECIFIED
ALUMINUM 6061-T6
QUANTITY = 01

NELSON PEDREIRO (415) 725-3297

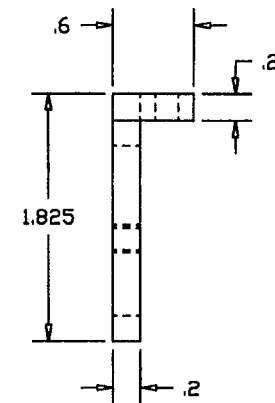
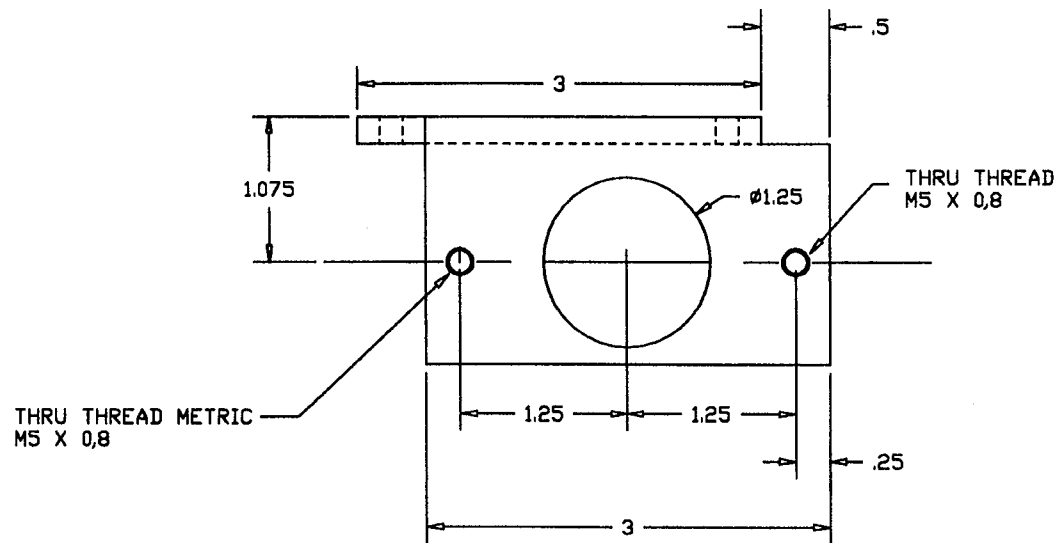
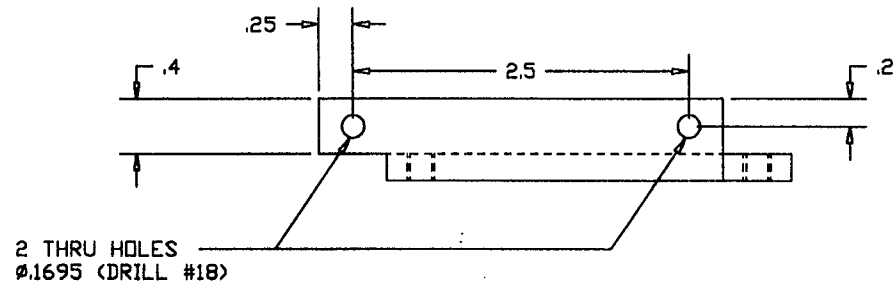
PART YAWSYS2C2: FIT PART YAWSYS2B



DRAWING: FAWSY2C2
DIMENSIONS IN INCHES
TOLERANCES ±.005 UNLESS
OTHERWISE SPECIFIED
ALUMINUM 6061-T6
QUANTITY = 02

NELSON PEDREIRO (415) 725-3297

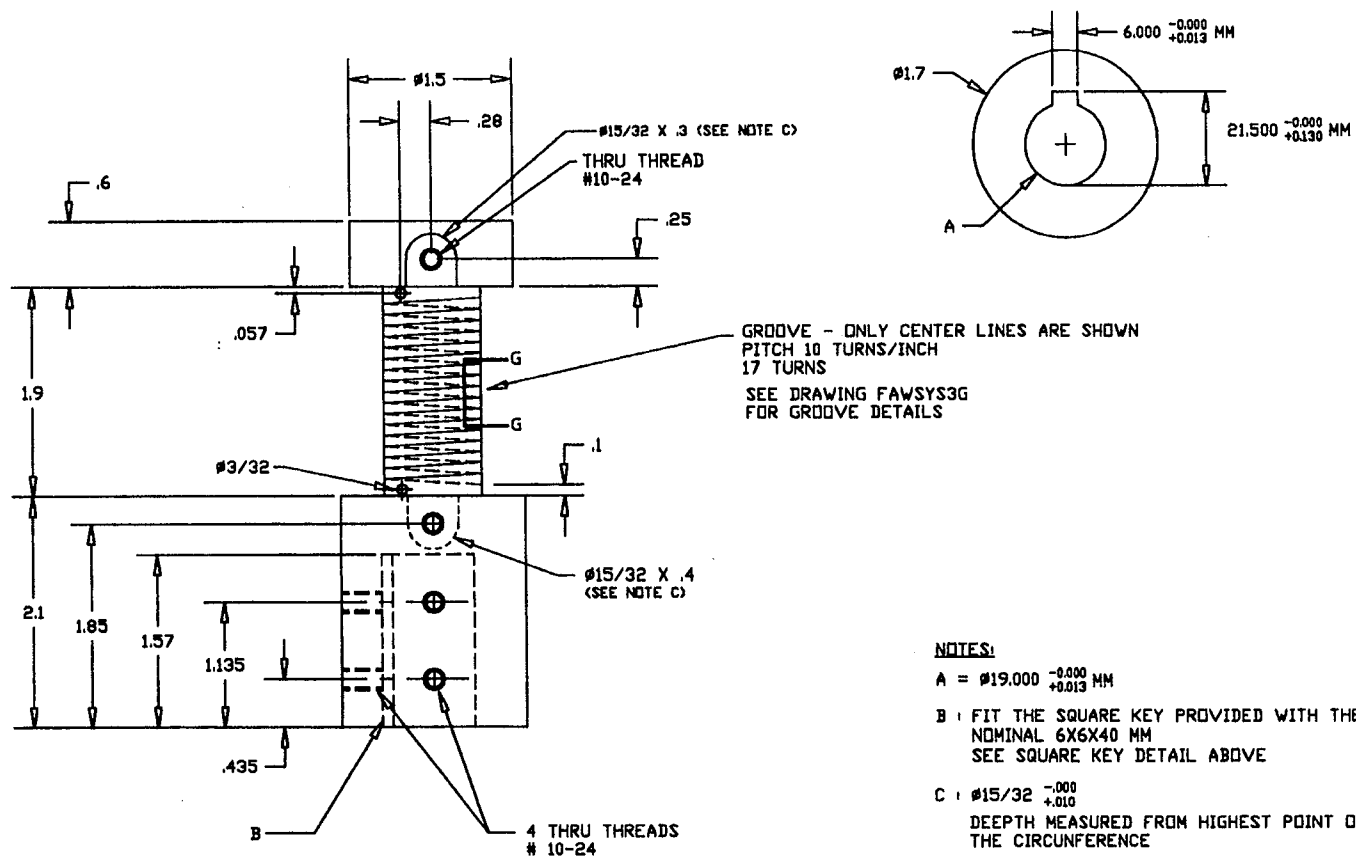
PART YAWSY2C3



DRAWING: FAWSY2C3
DIMENSIONS IN INCHES
TOLERANCES ±.005
QUANTITY = 02
FIT PART YAWSYS2 AND ACCELEROMETER
NELSON PEDREIRO (415) 725-3297

PART YAWSYS3

SLOT FOR SQUARE KEY



NOTES:

A = $\phi 19.000 \begin{smallmatrix} -0.000 \\ +0.013 \end{smallmatrix}$ MM

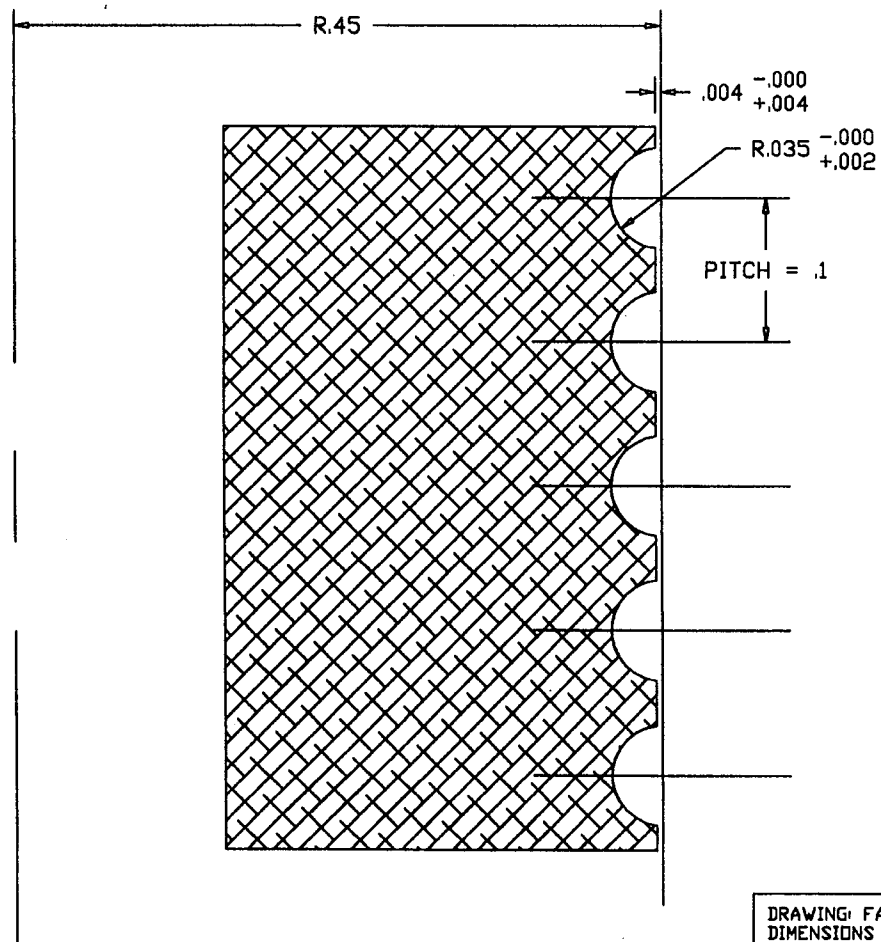
B : FIT THE SQUARE KEY PROVIDED WITH THE MOTOR
NOMINAL 6X6X40 MM
SEE SQUARE KEY DETAIL ABOVE

C : $\phi 15/32 \begin{smallmatrix} -0.000 \\ +0.010 \end{smallmatrix}$
DEPTH MEASURED FROM HIGHEST POINT ON
THE CIRCUMFERENCE

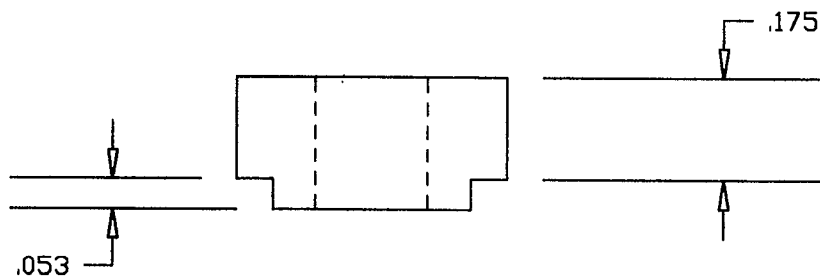
ANEXED DRAWINGS:
FAWSYS3C
FAWSYS3G

DRAWING: FAWSYS3B
DIMENSIONS IN INCHES UNLESS
OTHERWISE SPECIFIED
MM = MILLIMETER
TOLERANCES $\pm .005$ IN. IF NOT
OTHERWISE SPECIFIED
ALUMINUM 6061-T6
QUANTITY = 1
NELSON PEDREIRO (415) 725-3297

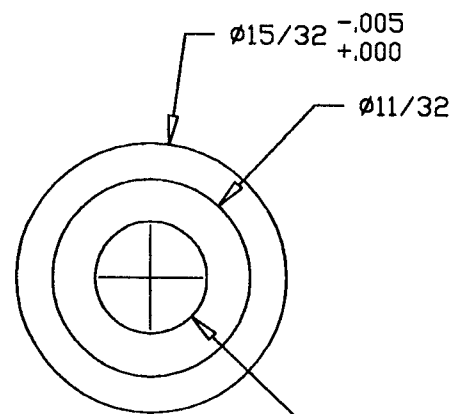
GROOVE DETAIL CUT GG FROM DRAWING FAWSYS3B



DRAWING: FAWSYS3G
DIMENSIONS IN INCHES
REFER TO DRAWING FAWSYS3B
NELSON PEDREIRO (415) 725-3297

NOTES:

1. ALUMINUM 6061-T6
2. FIT PART FAWSYS3B

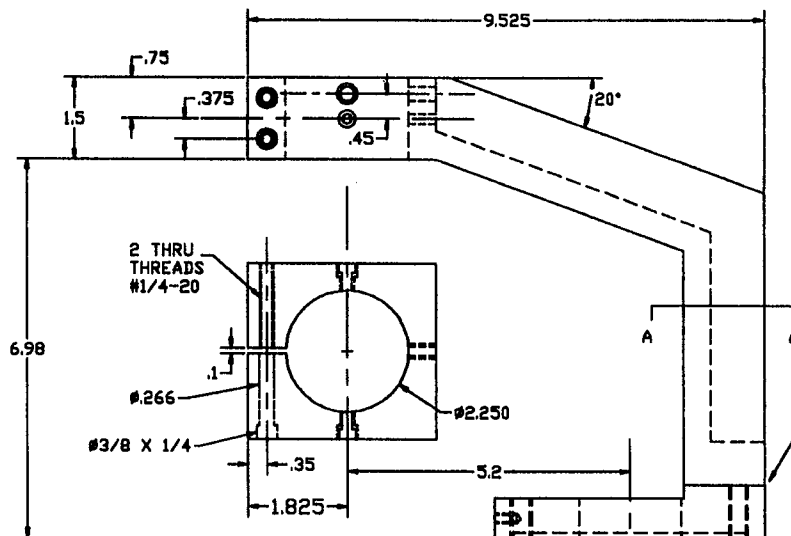


DRILL #9 CLOSE FIT
FOR 10-24 BOLT

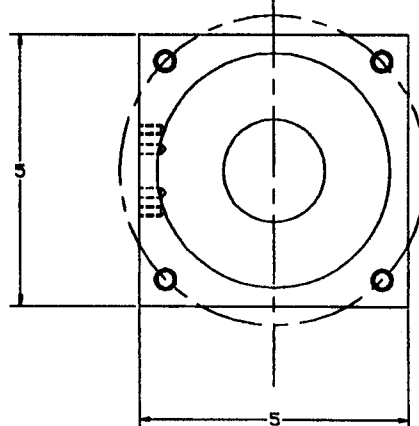
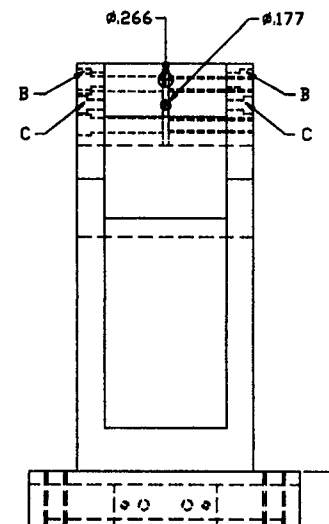
DRAWING: FAWSYS3C
DIMENSIONS IN INCHES
TOLERANCES $\pm .005$ IN IF NOT
OTHERWISE SPECIFIED
QUANTITY = 2

NELSON PEDREIRO (415) 725-3297

PART YAWSYS4



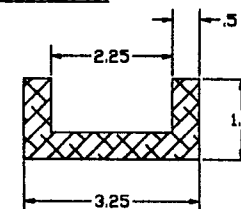
TWO PARTS
DETAILS OF
CONNECTION NOT
SHOWN.
SEE ANEXED
DRAWINGS



NOTES:

- B. 0.266 THRU
#3/8 X 1/4
- C. 0.177 THRU
#5/16 X .18

CROSS-SECTION AA



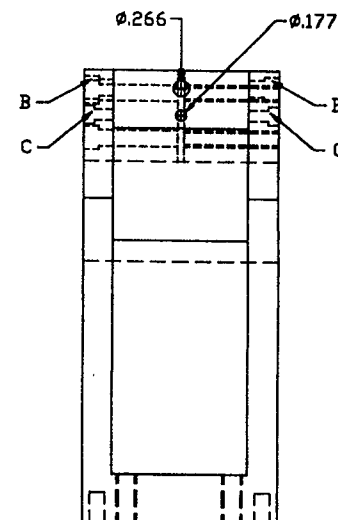
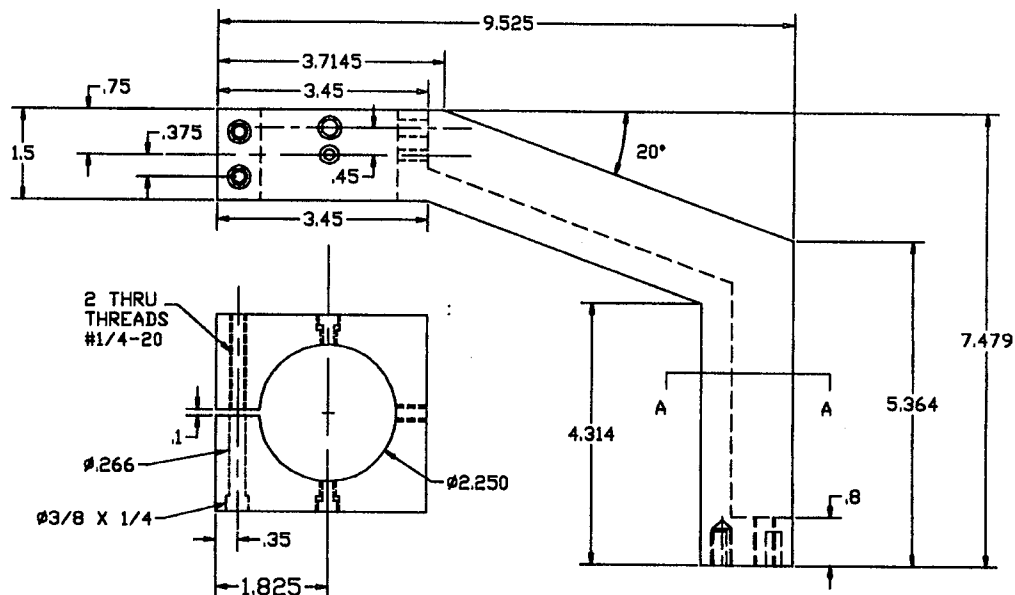
ANEXED DRAWINGS:

FAWSY4B1
FAWSY4B2
FAWSY4B3

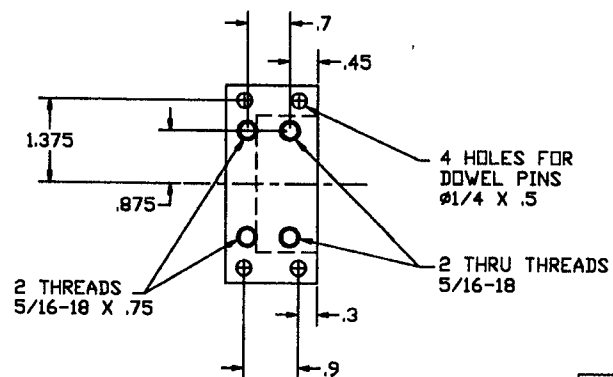
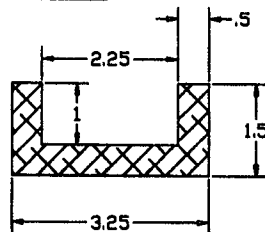
DRAWING: FAWSYS4B
DIMENSIONS IN INCHES UNLESS OTHERWISE SPECIFIED
TOLERANCES $\pm .005$ UNLESS OTHERWISE SPECIFIED
ALUMINUM 6061-T6
QUANTITY = 01

NELSON PEDREIRO (415) 725-3297

PART FAWSY4B1



CROSS-SECTION AA



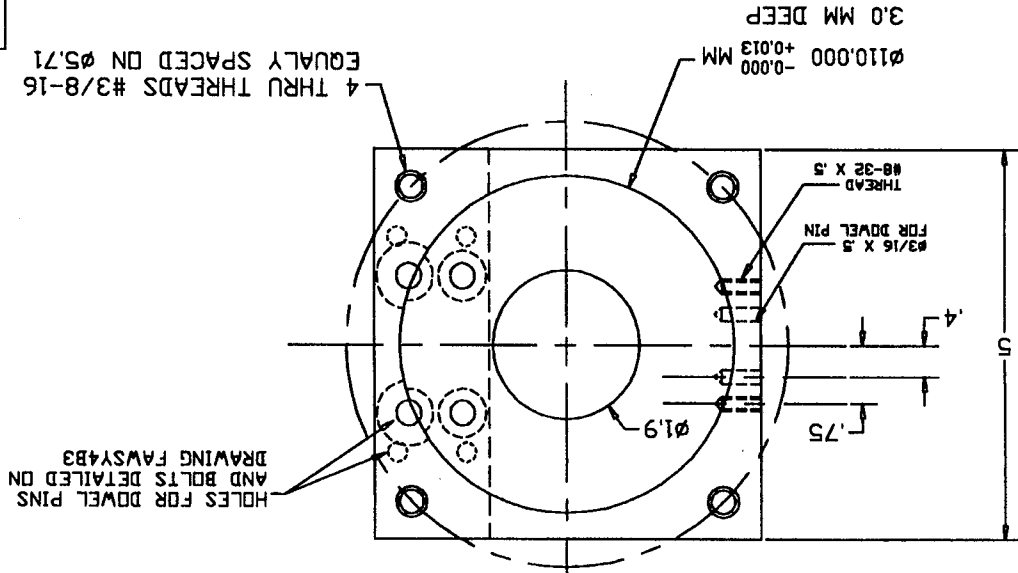
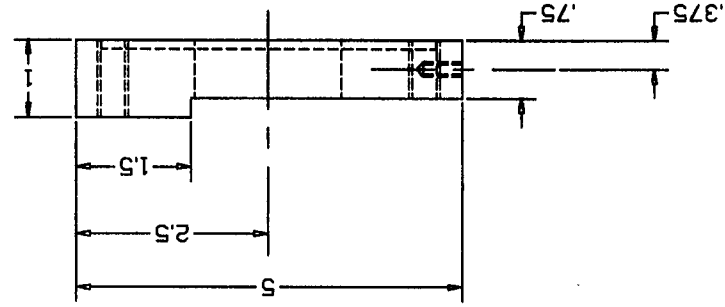
NOTES:

- B. $\varnothing .266$ THRU $\varnothing 3/8 \times 1/4$
- C. $\varnothing .177$ THRU $\varnothing 5/16 \times .18$

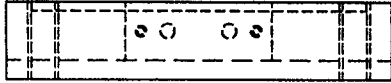
DRAWING: FAWSY4B1
 DIMENSIONS IN INCHES UNLESS OTHERWISE SPECIFIED
 TOLERANCES $\pm .005$ UNLESS OTHERWISE SPECIFIED
 ALUMINUM 6061-T6
 QUANTITY = 01

NELSON PEDREIRO (415) 725-3297

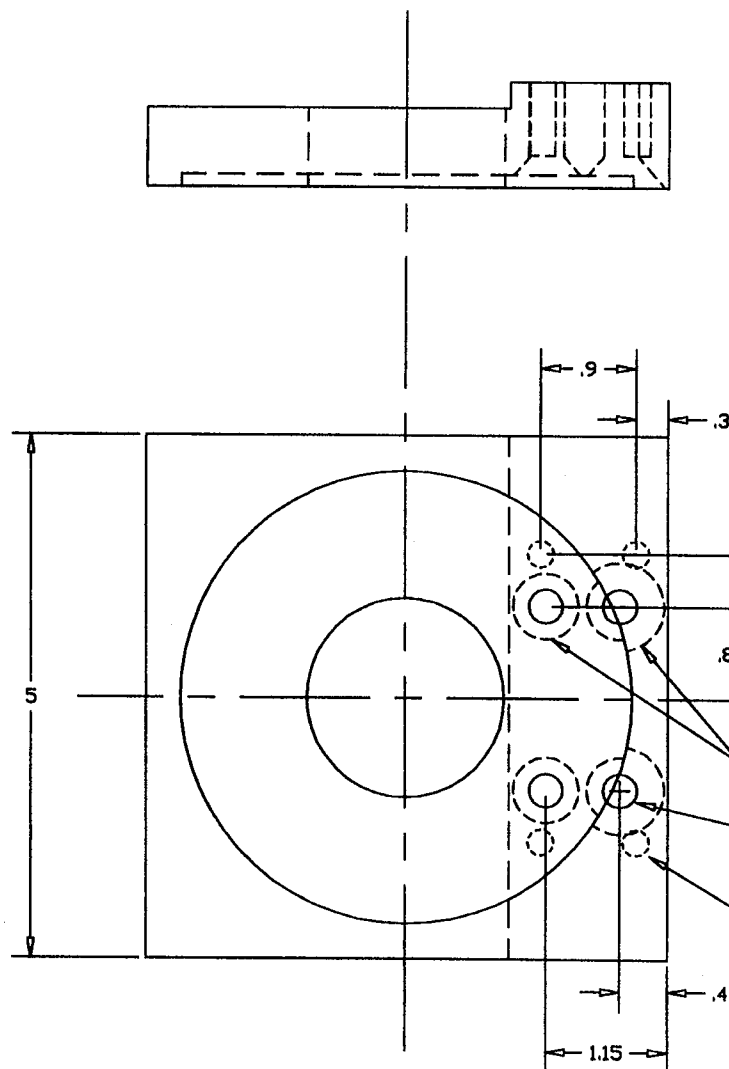
PART FAWSY4B2



HOLES FOR DOVEL PINS
AND BOLTS DETAILED ON
DRAWING FAWSY4B3



DRAWING FAWSY4B2
MM = MILLIMETER
DIMENSIONS IN INCHES UNLESS OTHERWISE SPECIFIED
TOLERANCES $\pm .005$ UNLESS OTHERWISE SPECIFIED
ALUMINUM 6061-T6
QUANTITY = 01
NELSON PEDREIRO (415) 725-3297



DRAWING: FAWSY4B3
 DIMENSIONS IN INCHES UNLESS OTHERWISE SPECIFIED
 TOLERANCES $\pm .005$ UNLESS OTHERWISE SPECIFIED
 ALUMINUM 6061-T6
 QUANTITY = 01

NELSON PEDREIRO (415) 725-3297

NOTES:

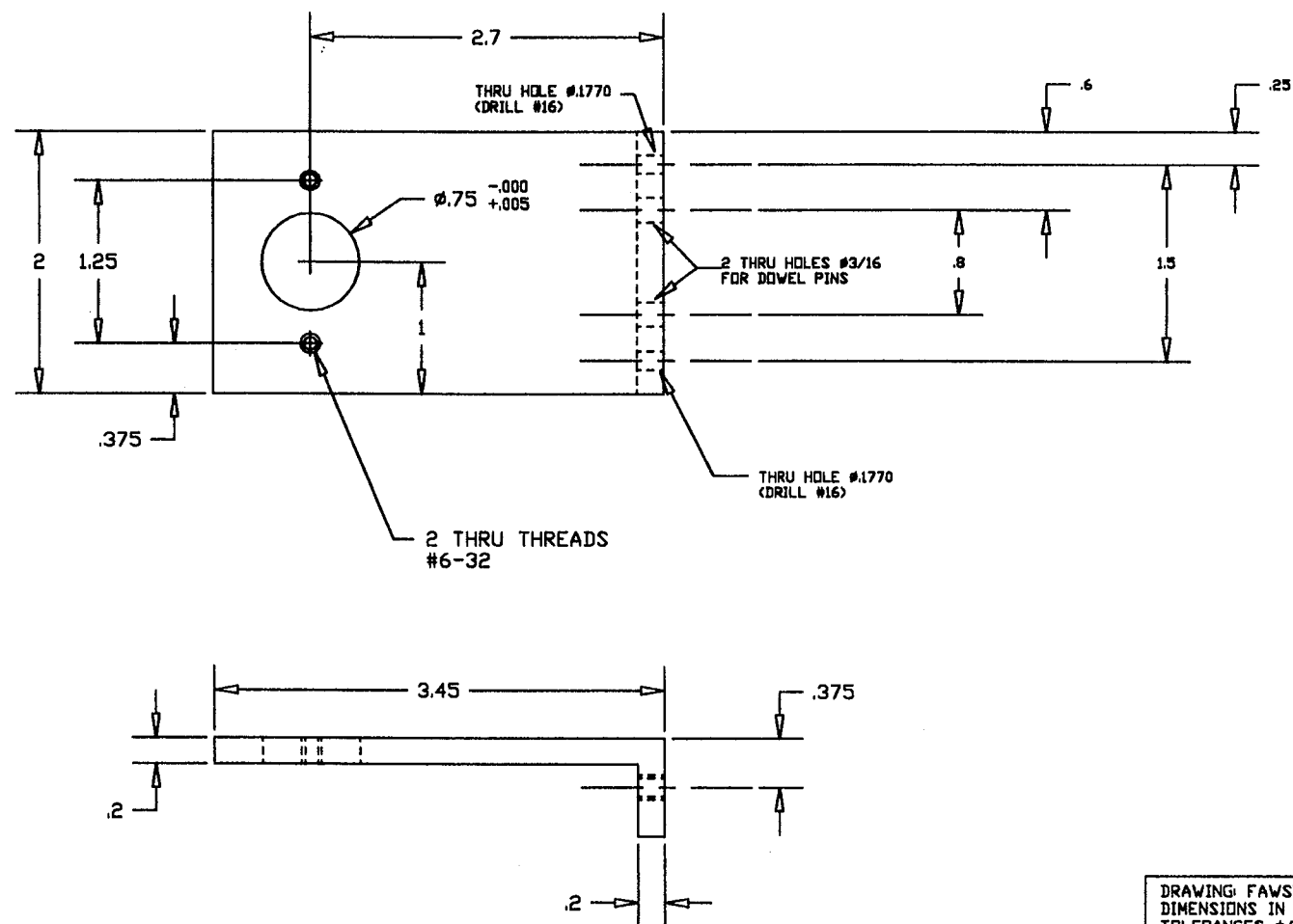
DETAILED DIMENSIONS FOR DOWEL PIN HOLES
 AND THRU HOLES FOR BOLTS FOR ASSEMBLY
 WITH PART FAWSY4B1.
 OTHER FEATURES NOT SHOWN FOR CLARITY.

COUNTER SINK FOR 5/16-18
 FLAT SOCKET HEAD 82°

4 THRU HOLES $\phi .323$ (DRILL P)

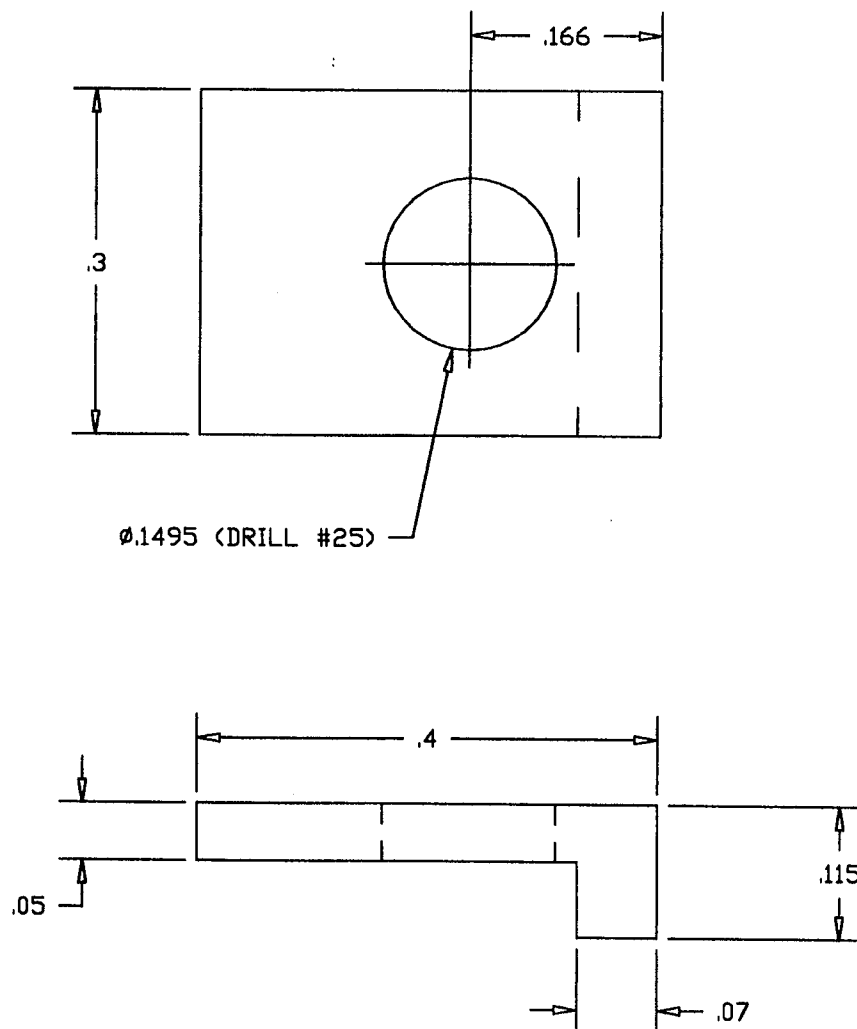
4 HOLES FOR DOWEL PINS
 $\phi 1/4 \times .7$

PART YAWSYS7



DRAWING: FAWSY7B1
 DIMENSIONS IN INCHES
 TOLERANCES $\pm .005$ UNLESS
 OTHERWISE SPECIFIED
 ALUMINUM 6061-T6
 QUANTITY = 01

NELSON PEDREIRO (415) 725-3297



DRAWING: FAWSY7B2
DIMENSIONS IN INCHES
TOLERANCES $\pm.005$ UNLESS
OTHERWISE SPECIFIED
ALUMINUM 6061-T6
QUANTITY = 02

NELSON PEDREIRO (415) 725-3297

D Listing of Computer Program

```

/*      program NO_GI9.C
This program implements the inertia and gravity moment cancelation.
The inner torque loop consists of a 2nd order (notch) compensation.


$$H(s) = K.b1.b2 / (ar^2 + ai^2) \cdot [s^2 + 2.ar.s + (ar^2 + ai^2)] / [s^2 + 2.(b1 + b2).s + b1.b2]$$


Discrete equivalent is obtained as follows:
Trapezoidal Integration     $s \leftarrow \frac{2}{T} \frac{(z-1)}{(z+1)}$ 

NOTE: It is important to consider the offset of the
torque sensor signal.

D/A Connections: Channel 1 connect to motor drive input
A/D Connections:
    Channel 0 - Torque sensor output signal
    Channel 1 - 'YAW' angle, Volts2
    Channel 2 - Angular Acceleration, acc in Volts

NOTES:
1. ACC is the sum of the signals from the two accelerometers.
The sum is done by an analog circuit. NOTE THAT NO ANALOG FILTER IS USED.
The signal ACC after read by the A/D converter in the computer
is filtered in this program by a 2nd order Butterworth filter:


$$F(s) = \frac{1}{(s/w)^2 + 2*ksi*(s/w) + 1}$$


where:  $w = 2*\pi*f$ 
 $f$  = cut off frequency in hertz
 $ksi = 0.707$ 

As used for the torque loop controller, a discrete equivalent is
obtained using Trapezoidal Integration.
287LAB assembly language I/O Subroutines
This 287LAB example uses the A/D and D/A capabilities of
the Data Translation DT2821-series Data Acquisition board.

Comments:
-Remember to use a Large memory model !!
-Store menu options under Options-Store options.
-Create a project file.

Nelson Pedreiro - 31MAR95
*/
#include <stdio.h>
#include <conio.h>
#include <math.h>
extern set_clock();
extern read_d2a();
extern write_d2a();

char *input;
static int      gain[3] = {1, 1, 1};
static int      num_of_chan = 3;
static float    ZERO = 0.0;
static float    V2RAD = 0.099702;
static float    PI = 3.141592654;
/* Constants                                     */
/* Kts torque sensor calibration, N.m/V          */
/* Ia inertia of the arm in 'yaw', Kg.m^2        */
/* Kaccf acceleration calibration, rad/s^2/V      */
static float    Kts = 6.125;
static float    Ia = 0.1589;
static float    Kaccf = 16.30;

```

```

int      sample_rate, error_flg, keypressed, exit_flg;
float    T, Vm, Vm_1, Vm_2, torque_signal, torque_offset, volts[3];
float    K, dK, ar, ai, b1, b2, cu_1, cu_2, c, c_1, c_2;
float    c0, c1, c2, d0, d1, d2;
float    KSAFE, Vm_out;
float    torque_error, torque_error_1, torque_error_2;
float    torque_cmd;
float    deadband_p, deadband_n;
float    Kg, dKg;
float    acc_offset, acc, acc_1, acc_2, ACCF, ACCF_1, ACCF_2;
float    ryaw, ryaw_1, ryaw_2, fyaw, fyaw_1, fyaw_2;
float    fn, wn, ksin, bn, acu_1, acu_2, ac, ac_1, ac_2;
float    f1, ksi1, w1, w1T, w1T2, af1, bf1, cf1, c1f1, c2f1;
float    f2, ksi2, w2, w2T, w2T2, af2, bf2, cf2, c1f2, c2f2;
float    Kiaux, Ki, alfa, dalfa;

/***** MAIN PROGRAM *****/
main()
{
    torque_offset = .108;          /* Torque offset in Volts = 0.100 */
    acc_offset = .000;             /* Angular Acceleration offset in Volts = .010 */

    torque_offset = .100;
    acc_offset = .012;

    deadband_p = 0.0;              /* Motor-Drive Dead-Band */
    deadband_n = 0.0;

    dalfa = .025;
    dKg = .01;
    dK = .0;
    sample_rate = 1500;
    T = 1.0/sample_rate;

    /* Define Torque Loop Parameters - Continuous *****/
    K = 10.0;
    ar = 14.5;
    ai = 182;
    b1 = 10;
    b2 = 600;
    /* Obtain Discrete Equivalent for Torque Loop *****/
    /* Auxiliary variables *****/
    c0 = 4-4*ar*T+(ar*ar+ai*ai)*T*T;
    c1 = 2*(ar*ar+ai*ai)*T*T-8;
    c2 = 4+4*ar*T+(ar*ar+ai*ai)*T*T;
    d0 = 4-2*(b1+b2)*T+b1*b2*T*T;
    d1 = 2*b1*b2*T*T-8;
    d2 = 4+2*(b1+b2)*T+b1*b2*T*T;
    /* *****/
    cu_1 = -d1/d2;
    cu_2 = -d0/d2;
    c = c2/d2*b1*b2/(ar*ar+ai*ai);
    c_1 = c1/d2*b1*b2/(ar*ar+ai*ai);
    c_2 = c0/d2*b1*b2/(ar*ar+ai*ai);
    /*****
    /* SPECIFY 2ND ORDER FILTER for YAW angle *****/
    f1 = 40.0;
    ksi1 = 0.707;

    w1 = 2.0*PI*f1;
    w1T = w1*T;
    w1T2 = w1T*w1T;
    af1 = 1.0+4.0*ksi1/w1T+4.0/w1T2;
    bf1 = 2.0-8.0/w1T2;
    cf1 = 1.0-4.0*ksi1/w1T+4.0/w1T2;
    c1f1 = -bf1/af1;
    c2f1 = -cf1/af1;
    *****/

```

```

/* SPECIFY 2ND ORDER FILTER for ANGULAR ACCELERATION*****/
f2=18.0;
ksi2=0.707;

w2=2.0*PI*f2;
w2T=w2*T;
w2T2=w2T*w2T;
af2=1.0+4.0*ksi2/w2T+4.0/w2T2;
bf2=2.0-8.0/w2T2;
cf2=1.0-4.0*ksi2/w2T+4.0/w2T2;
c1f2=-bf2/af2;
c2f2=-cf2/af2;
/*****/
/* Define Parameters for NOTCH Filter - Continuous *****/
fn = 33.0;
ksin = 0.07;
wn = 2*PI*fn;
bn = wn;
/* Obtain Discrete Equivalent for Filter *****/
ar = wn*ksin;
ai = sqrt(wn*wn-ar*ar);
b1 = bn;
b2 = bn;
/* Auxiliary variables *****/
c0 = 4-4*ar*T+(ar*ar+ai*ai)*T*T;
c1 = 2*(ar*ar+ai*ai)*T*T-8;
c2 = 4+4*ar*T+(ar*ar+ai*ai)*T*T;
d0 = 4-2*(b1+b2)*T+b1*b2*T*T;
d1 = 2*b1*b2*T*T-8;
d2 = 4+2*(b1+b2)*T+b1*b2*T*T;
/* *****/
acu_1 = -d1/d2;
acu_2 = -d0/d2;
ac = c2/d2*b1*b2/(ar*ar+ai*ai);
ac_1 = c1/d2*b1*b2/(ar*ar+ai*ai);
ac_2 = c0/d2*b1*b2/(ar*ar+ai*ai);
/*****/

exit_flg = 0;
set_clock(&sample_rate); /* Start the tick clock */
write_d2a(&ZERO,&ZERO);

do {
    system("cls");
    printf("\n\n SAMPLING FREQUENCY = %6.2d Hz \n",sample_rate);
    printf("\n\n Press:  Q ... to increase ALFA \n\n");
    printf("      A ... to decrease ALFA \n\n");
    printf("      P ... to increase Kg \n\n");
    printf("      L ... to decrease Kg \n\n");
    printf("\n      Z ... to set overall gain to ZERO \n\n");
    printf("      <ENTER> ... to exit program \n\n");

    printf("      Press 'G' to start. \n\n");
    input = getch();
    }while( toupper(input) != 'G');

printf(" PROGRAM RUNNING .... Press <ENTER> to exit. \n\n");
/* K=7 =====> Kg=.38 */
/* k=10 =====> Kg=.36 or .37 */

Kg=0.36;
alfa = 1.0;

Kiaux=la*Kaccf/Kts;
Ki = alfa*Kiaux;
ryaw_2 = 0.0;
ryaw_1 = 0.0;
fyaw_2 = 0.0;

```

```

fyaw_1 = 0.0;
ACCF_2 = 0.0;
ACCF_1 = 0.0;
acc_2 = 0.0;
acc_1 = 0.0;
Vm_2 = 0.0;
Vm_1 = 0.0;
torque_error_2 = 0.0;
torque_error_1 = 0.0;
KSAFE = 1.0;
do {
    printf("K = %5.2f   Kg = %6.3f   Alfa = %6.3f \n", K, Kg, alfa);
    /****** */
    do {
        read_a2d(&num_of_chan,gain,volts,&error_flg);
        torque_signal = volts[0];
        ryaw = -volts[1];
        acc = volts[2] - acc_offset;
/* 2ND ORDER BUTTERWORTH FILTER FOR YAW ANGLE */
/*   fyaw=(ryaw+2.0*ryaw_1+ryaw_2)/af1+c1f1*fyaw_1+c2f1*fyaw_2; */
        fyaw=ryaw;
/* 2ND ORDER BUTTERWORTH FILTER FOR ANGULAR ACCELERATION */
        ACCF=(acc+2.0*acc_1+acc_2)/af2+c1f2*ACCF_1+c2f2*ACCF_2;
/* NOTCH FILTER FOR ANGULAR ACCELERATION */
/*   ACCF = acu_1*ACCF_1 + acu_2*ACCF_2 + ac*acc + ac_1*acc_1 + ac_2*acc_2; */
        torque_cmd = -Ki*ACCF + Kg*sin(V2RAD*fyaw);
        torque_error = torque_cmd - (torque_signal - torque_offset);
        Vm = cu_1*Vm_1 + cu_2*Vm_2 + K*(c*torque_error + c_1*torque_error_1 + c_2*torque_error_2);
        Vm = KSAFE*Vm;
        if( fabs(Vm)-fabs(Vm_1) > 2 ) { Vm = Vm_1; }

        ryaw_2 = ryaw_1;
        ryaw_1 = ryaw;
        fyaw_2 = fyaw_1;
        fyaw_1 = fyaw;
        ACCF_2 = ACCF_1;
        ACCF_1 = ACCF;
        acc_2 = acc_1;
        acc_1 = acc;

        Vm_2 = Vm_1;
        Vm_1 = Vm;
        torque_error_2 = torque_error_1;
        torque_error_1 = torque_error;

        Vm_out = Vm;
        if(Vm>0.015) { Vm_out = Vm +deadband_p; }
        if(Vm<0.015) { Vm_out = Vm +deadband_n; }

/***** SAFETY CLAUSE *****/
        if( Vm_out > 2.0 ) {
            Vm_out = .1;
            printf(" Safety Clause - Output Exceeds 2V \n");
        }
        if( Vm_out < -2.0 ) {
            Vm_out = -.1;
            printf(" Safety Clause - Output Exceeds 2V \n");
        }

/***** SAFETY CLAUSE *****/
        if( fyaw > 6.0 ) {
            Vm_out = 0.0;
            KSAFE=0.0;
            printf(" Safety Clause - 'YAW' Angle Exceeds 6V \n");
        }
        if( fyaw < -6.0 ) {
            Vm_out = 0.0;

```

```

        KSAFE=0.0;
        printf(" Safety Clause - 'YAW' Angle Exceeds 6V \n");
    }

    write_d2a(&ZERO, &Vm_out);

    keypressed = kbhit();
    } while (keypressed==0 );
/*****

input = getch();
switch( toupper(input) ) {
    case 'Q':
        alfa = alfa + dalfa;
        Ki = alfa*Kiaux;
        break;
    case 'A':
        alfa = alfa - dalfa;
        Ki = alfa*Kiaux;
        break;
    case 'P':
        Kg = Kg + dKg;
        break;
    case 'L':
        Kg = Kg - dKg;
        break;
    case 'Z':
        K = 0.0;
        break;
    case 'r':
        exit_flg = 1;
        break;
}
} while( exit_flg == 0 );

write_d2a(&ZERO,&ZERO);

if(error_flg != 0) {
    printf("\n ***** SAMPLE RATE IS TOO FAST!!! *****");
    exit(1);
}

if(error_flg == 0) {
    printf("\n SAMPLE RATE IS OK");
}

}
/***** END OF MAIN PROGRAM *****/

```


References

- [1] Skow, A.M., Moore, W.A., and Lorincz, D.J., "Forebody Vortex Blowing - A Novel Control Concept to Enhance Departure/Spin Recovery Characteristics of Fighter and Trainer Aircraft", AGARD CP-262, No. 24, pp. 24-1 to 24-17, May 1979.
- [2] Ericsson, L.E. and Reding, J.P., "Alleviation of Vortex Induced Asymmetric Loads", Journal of Spacecraft and Rockets, Vol 17, Nov.-Dec. 1980, pp. 546-553.
- [3] Rao, D.M., Moskovitz, C., and Murri, D.G., "Forebody Vortex Management for Yaw Control at High Angles of Attack," Journal of Aircraft, Vol. 24, No. 4, p. 248-254, April 1987.
- [4] Ng, T.T., and Malcolm, G.N., "Aerodynamic Control Using Forebody Strakes," AIAA Paper 91-0618.
- [5] Adams, R.J., Buffington, J.M., and Banda, S. S., "Active Vortex Flow Control for VISTA F-16 Envelope Expansion," AIAA Paper 94-3681.
- [6] Mittelman, Z., and Kroo, I., "Unsteady Aerodynamics and Control of Delta Wings with Tangential Leading-Edge Blowing," AIAA Paper 89-3374.
- [7] Wood, N.J., Roberts, L., and Celik, Z.Z., "Control of Asymmetric Vortical Flows over Delta Wings at High Angles of Attack," Journal of Aircraft, Vol. 27, No. 5, May 1990.
- [8] Font, G.I., Celik, Z.Z., and Roberts, L., "A Numerical and Experimental Study of Tangential Jet Blowing Applied to Bodies at High Angles of Attack," AIAA Paper 91-3253.
- [9] Wong, G.S., "Experiments in the Control of Wing Rock at High Angles of Attack Using Tangential Leading Edge Blowing," Ph.D. Dissertation, Department of Aeronautics and Astronautics, Stanford University, 1992.
- [10] Celik, Z.Z. and Roberts, L., "Vortical Flow Control on a Wing-Body Combination Using Tangential Blowing," AIAA Paper 92-4430.
- [11] Celik, Z.Z., Roberts, L. and Pedreiro, N., "The Control of Wing Rock by Forebody Blowing," AIAA Paper 93-3685.
- [12] Celik, Z.Z., and Roberts, L., "Vortical Flow Control on a Delta Wing by Lateral Blowing," AIAA Paper 94-0509.
- [13] Hong, J.S., "A theoretical and Computational Study on the Effects of Leading Edge Lateral Blowing on Delta Wing Aerodynamics," Ph.D. Dissertation, Department of Aeronautics and Astronautics, Stanford University, 1994.
- [14] Celik, Z.Z., Roberts, L. and Pedreiro, N., "Dynamic Roll and Yaw Control by Tangential Forebody Blowing," AIAA Paper 94-1853.

- [15] Pedreiro, N., Rock, S.M., Celik, Z.Z. and, Roberts, L., "Roll-Yaw Control at High Angle of Attack by Forebody Tangential Blowing," AIAA Paper 96-0773.
- [16] Pedreiro, N., "Experiments in Aircraft Roll-Yaw Control Using Forebody Tangential Blowing," Ph.D. Dissertation, Department of Aeronautics and Astronautics, Stanford University (to be published).
- [17] Sensors Designer's Handbook and Catalog, New England Instrument, 245 Railroad Street, Woonsocket, RI 02895-1129, USA.
- [18] Kulite Semiconductor Strain Gage Manual, Kulite Semiconductor Products, Inc., One Willow Tree Road, Leonia, New Jersey 07605, USA.
- [19] Installation and Operations Manual for F/T, (Manual PN 9610-05-1001-09, Software version 4.25), Assurance Technologies, Inc. 503D Highway 70 East, Garner, North Carolina 27529, USA.
- [20] Electro-Craft[®] Servo Systems - BRU-200, BRU-500 Brushless Drives Instruction Manual, Reliance Motion Control, Inc., 6950 Washington Avenue South, Eden Prairie, Minnesota 55344, USA.
- [21] Ims, S.D., "Inertia Measuring System," ARL Memo 75, July 29 1991. Stanford Aerospace Robotics Laboratory.